The Dissertation Committee for Altan Ozkan
certifies that this is the approved version of the following dissertation:

Development of a Novel Algae Biofilm Photobioreactor for Biofuel Production

Committee:

Halil Berberoglu, Supervisor

Kerry Kinney

Lynn Katz

Mary Jo Kirisits

Desmond Lawler

Jerry Brand

Selim Cetiner

Development of a Novel Algae Biofilm Photobioreactor for Biofuel Production

by

Altan Ozkan, B.S., M.S.

DISSERTATION

Presented to the Faculty of the Graduate School of

The University of Texas at Austin

in Partial Fulfillment

of the Requirements

for the Degree of

DOCTOR OF PHILOSOPHY

THE UNIVERSITY OF TEXAS AT AUSTIN

August 2012

Acknowledgments

I gratefully acknowledge the financial support of the National Science Foundation (CBET-1125755) making this study possible. I would like to thank my advisor Dr. Halil Berberoglu for his encouragement, support, and guidance during my studies. I would like to thank Dr. Kerry Kinney and Dr. Lynn Katz for their support for my research. I would also like to acknowledge Dr. Lawler for all his assistance during my studies. Moreover, I would like to acknowledge my committee members Dr. Kirisits, Dr. Brand, and Dr. Cetiner for their valuable inputs to my research. I would like to acknowledge Dr. Poenie and his staff for their assistance with lipid extraction and analysis.

I would like to acknowledge the present and the past members of the Solar Energy and Biofuels Laboratory and my office mates Onur Taylan, Thomas Murphy, Angel Bolhouse, Edwin Peng, Akhil Kulkarni, and Andrew Gilbert for sharing their expertise and creating a great working atmosphere. Moreover, I would like to acknowledge the Environmental and Water Resources Engineering Program (EWRE) students for their assistance with my experiments and exchange of ideas especially Jinyong Choi and Fernendo Almada Calvo. I would like to thank John Lynk, Murat Ates, Anil Yuksel, Onur Nihat Demirer, and Ozgur Araz for their friendship during my stay in Austin. I would also like to acknowledge Tolga Alagoz, Gokcen Atilboz, Unal Sen, Serdar Surer,

and Ugur Sohmen for keeping in touch during my graduate studies.

I am grateful to my parents, my grandparents, and my brother Arcan for all their supports. Finally, I would like to acknowledge Saadet Ersungur for her assistance with the transcripts that I needed for my application to UT and for her patience for the past couple of years.

Development of a Novel Algae Biofilm Photobioreactor for Biofuel Production

Publication No. _____

Altan Ozkan, Ph.D.
The University of Texas at Austin, 2012

Supervisor: Halil Berberoglu

Algae are photosynthetic microorganisms that convert carbon dioxide and sunlight into biomass that can be used for biofuel production. Although they are usually cultivated in suspension, these microorganisms are capable of forming productive biofilms over substrata given the right conditions. This dissertation focuses on algal biofilms and their application in biofuel feedstock production. In particular it reports the construction and performance of an algae biofilm photobioreactor, the physico-chemical surface properties of different algal species and adhesion substrata, and cell-surface interactions based on experimental results and theoretical models.

A novel algae biofilm photobioreactor was constructed and operated (i) to demonstrate the proof of concept, (ii) to analyze the performance of the system, and (iii) to determine the key advantages and short comings for further research. The results indicated that significant reductions in water and

energy requirements were possible with the biofilm photobioreactor. Although the system achieved net energy ratio of about 6, the overall productivity was low as *Botryococcus branunii* is notoriously slow growing algae. Thus, further studies were focused on identification of algal species capable of biofilm growth with larger biomass and lipid productivities.

Adhesion of cells to substrata precedes the formation of all biofilms. A comprehensive study has been conducted to determine the interactions of a planktonic and a benthic algal species with hydrophilic and hydrophobic substrata. The physico-chemical surface properties of the algal cells and substrata were determined and using these data, cell-substrata interactions were modeled with the thermodynamic, Derjaguin, Landau Verwey, Overbeek (DLVO) and Extended Derjaguin, Landau Verwey, Overbeek (XDLVO) approaches and critical parameters for algal adhesion were identified. Finally, the adhesion rate and strength of algal species were quantified with parallel plate flow chamber experiments. The results indicated that both cell and substrata surface hydrophobicity played a critical role for the adhesion rate and strength of the cells and XDLVO approach was the most accurate model. Finally, based on these findings the physico-chemical surface properties of ten algal species and six substrata were quantified and a screening was done to determine algae species substratum couples favoring adhesion and biofilm formation.

Table of Contents

List of Tables

List of Figures

Chapter 1

Introduction

The present research aims at development of a novel algal biofilm photobioreactor for biodiesel production. In this section (i) the motivations for the development of the photobioreactor, (ii) the objectives of the current research, and (iii) organization of the document is presented.

1.1 Algal Biodiesel Production

Petroleum consumption accounts for about one third of the world's energy consumption [5]. General consensus indicates that the oil production will peak in between 2013 to 2020 and time periods as short as 35 years are being projected for depletion of reserves [5, 6]. In addition to problems associated with the limited quantity, petroleum consumption also accounts for one third of the CO_2 emissions related with energy production [7]. These emissions are considered to be one of primary reasons for increased atmospheric CO_2 levels [8]. Moreover, this increase is associated with detrimental environmental effects, as the atmospheric CO_2 absorbs the outbound radiation of the Earth and increases the global temperature [9].

Thus, alternative fuel sources are being investigated. Cultivation of oil

crops such as oil palm, jatropha, and soybean have received attention as carbon neutral biodiesel can be produced from these crops [2]. However, the areal lipid productivities of these crops are too low to replace the use of fossil based transport fuels. For instance, even the oil crop with the largest productivity requires 48% of the U.S. cropping area to completely replace transport fuel consumption of the U.S for the year 2007 [2]. Allocation of this cropping area competes for the cultivation of food crops resulting in shortage of food and increased food prices.

The use of algal lipids is considered to be a feasible alternative as the areal lipid productivity of these microorganisms is larger than the oleaginous crops. For instance, it is projected that using an area equivalent to 2.2% of the U.S. cropping area the algal lipid sufficient to sustain the transportation fuel needs of the U.S for the year 2007 can be produced [2]. Moreover, algae can sustain this productivity without the need for arable land or freshwater requirements [2, 10]. However, the commercial production of algal biodiesel has not been realized yet. One significant barrier to commerical production is that current technologies such as raceway ponds, flat plate and tubular photobiorectors cultivate the algae in suspension. These photobioreactors produce very dilute end products, i.e., suspensions with biomass concentrations ranging from 0.1 to 8 g L^{-1}, with large water and energy inputs [11]. For instance, these systems require 6000 L of water to produce 1 L of algal oil under most favorable conditions. Moreover, large energy inputs of up to 386 MJ per kg of algae cultivated is required to recirculate the algae suspensions within the

system to keep the cells suspended [1, 2]. Finally, the algal suspensions produced have to be processed using energy intensive harvesting and dewatering technologies as the extraction of algal metabolites requires production of algae cakes with solid contents ranging from 15 to 25% [12]. This study proposes the use of algal biofilms to overcome these drawbacks through production of highly concentrated algal output with minimal inputs of water and energy.

1.2 Objectives of the Present Study

The objectives of the current study are (i) to address the current challenges of algal biodiesel production through construction of a novel algal biofilm photobioreactor, (ii) to understand critical parameters controlling the adhesion of algae cells to substrata, and (iii) to use this information to determine algal species suitable for biofilm cultivation and associated substrata for growing biofilms on.

1.2.1 Reduction of water and energy requirement of algae cultivation using an algae biofilm photobioreactor

Development of an inexpensive, efficient, and scaleable photobioreactor system based on immobilized algae cultivation can significantly reduce the energy and water requirements of the process, bringing algae based biofuel production closer to being energetically, environmentally, and economically viable technology. The objective of this part of the study is to present the design and performance of an algal biofilm based photobioreactor that addresses these

issues. It provides a detailed analysis of the energy and water requirements of the system, identifies its key advantages as well as shortcomings requiring further research and development.

1.2.2 Selection of algal species capable of biofilm growth

- **Adhesion of Cells to Surfaces**

  The correct selection of algal species is critical for lipid productivity of any photobioreactor system. The biomass and lipid productivities of the previous photobioreactor experiment presented in Section 1.2.1 were smaller compared to the productivities reported in the literature as *Botryococcus braunii* is a notoriously slow growing algae. To the best of the author's knowledge other than the experiments conducted with *B. braunii*, there is no study in the literature that reports the cultivation of any axenic oleaginous algal biofilms. In this study the objective is to determine critical parameters controlling the adhesion of algae cells to substrata and biofilm formation through theoretical models and experiments.

- **Cell to Substrate and Cell to Cell Interactions of Algal Species**

  Based on the results from previous research this study uses theoretical models and aims at determining (i) algal species and substrata favoring cell adhesion and biofilm formation and (ii) algal species that can be used to promote attractive cell to cell interactions for bioflocculation based harvesting of algal suspensions.

1.2.3 Organization of the document

Chapter 2 provides the reader the background on (i) the current algae cultivation technologies, (ii) processes used for harvesting and dewatering of algal suspensions, (iii) previous research conducted on immobilized algae cultivation systems, (iv) models for cell to substrata and cell to cell interactions, and (v) limitations on productivity of algal biofilms. Chapter 3 presents the design, operation, and performance of a novel algae biofilm photobioreactor constructed. Chapter 4 presents an experimental study investigating the adhesion rate, density and strength of benthic and planktonic algae on hydrophilic and hydrophobic surfaces. Moreover, this chapter compares the experimental results with the predictions of thermodynamic, DLVO, and XDLVO models to assess their applicability in predicting algal attachment. In addition, Chapter 5 presents the physico-chemical surface properties of 10 algae species including fresh and saltwater green algae and diatoms and the interaction of cells with cells and cells with substrata with different surface properties based on thermodynamic models. Finally, Chapter 6 summarizes the conclusions of the study and presents recommendations for future work.

Chapter 2

Current State of Knowledge

This chapter presents background information on the current state of knowledge on algal biomass cultivation, harvesting as well as on algal biofilm research. A summary of the current algae cultivation methods is presented in Section 2.1. In Section 2.2, harvesting and dewatering technologies of algal suspensions are provided. The previous research performed on immobilized algae cultivation systems is summarized in Section 2.3. In Section 2.4, the steps of algal biofilm formation and previous research on algal adhesion are presented. Theoretical models on cell to substrata and cell to cell interactions are discussed in Section 2.5. Finally, Section 2.6 summarizes the main factors limiting the productivity of algal biofilms with an emphasis on mass and light transfer.

2.1 Current Algae Cultivation Technologies

The type of system used for cultivating algae depends on the requirements of the organism being cultivated and on the nature of the product being harvested. Most current technologies cultivate the algae as planktonic cells, suspended in liquid nutrient media. These include open systems such as race-

way ponds and closed systems such as flat panel and tubular photobioreactors (PBRs) which are being used for high value products such as β-carotene, astaxanthin, and C-phycocyanin which have prices ranging from \$310 to \$10,000 per kilogram [13]. In the case of biofuel production, strict limitations on the cost as well as the energy and water requirements are imposed due to (i) low value of biofuel as a product, (ii) biofuel production requiring larger than unity net energy ratio (NER) calculated as the ratio of the energy output from the system to the energy input required, and (iii) potentially large scale of operation.

A typical raceway pond is shown in Figure 2.1. These systems are constructed as artificial ponds having a depth of about 0.3 m [2]. The algae cultivated in these ponds are kept suspended through continuous agitation with a paddlewheel [2]. The main advantage of these systems is that they are relatively inexpensive to build and operate [14]. In raceway ponds, the maximum biomass concentration ranges from 0.1 to 0.5 kg m^{-3} while photosynthetic efficiency (defined as the ratio of the biomass energy produced over a given time period to the solar energy irradiated to the same area for the same duration) can range from from 1 to 4% [15, 16]. Moreover, areal biomass productivities ranging from 4 to 21 g m^{-2} day^{-1} have been reported for raceway ponds [17]. Due to low biomass concentration, these photobioreactors require large volumes of water [2]. Moreover, they require energy intensive harvesting and dewatering processes necessary for downstream processing of algae in the biorefinery [2, 18]. According to Gudin and Therpenier the harvesting costs

associated with algae biomass production are on the order of 20 to 30% of the total cost [19].

Another difficulty associated with open systems is the loss of water through evaporation. Evaporation losses as high as 10 L m^{-2} day^{-1}, amounting to about 410 kg water loss through evaporation per kg of algal biodiesel produced have been reported for raceway ponds [20, 21]. Although evaporation helps in buffering the temperature of the system, large volumes of fresh water has to be supplied to the ponds to keep the water chemistry and nutrient balance under control for maximum productivity [22]. Furthermore, increased use of fresh water not only increases the water intensity but also increases the auxiliary energy input for biofuel production.

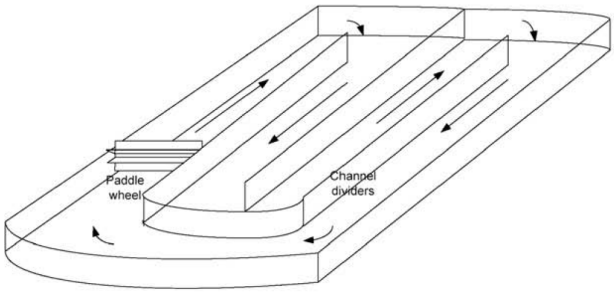

Figure 2.1: Schematic of a typical raceway pond used for algae cultivation [1].

To address some of these limitations, closed systems have been developed [14, 18]. The most common types of closed photobioreactors reported in the literature are tubular and flat panel types [23]. Figure 2.2 presents the schematics of typical tubular and flat plate photobioreactor systems. Tubular

photobioreactors cultivate algae by maintaining a turbulent flow in an array of tubes with diameters less than 10 cm. Use of tubes with small diameters is a strategy to match the depth of the algal suspensions with penetration depth of solar irradiance for optimized illumination within the system. Degassing zones are installed at least every 80 meters of tubing to (i) remove oxygen buildup, (ii) cool the algae suspensions, and (iii) add fresh nutrient medium [2]. Flat plate photobioreactors cultivate algae within narrow panels constructed from glass or plastic. The mixing within these systems is achieved using high gas flow rate inputs to the system [1]. The main advantage of this system is the absence of oxygen and carbon dioxide concentration gradients that develop along the flow line. It is also possible to find photobioreactors which have adopted different fermenter designs in research stage [23].

Biomass concentrations in the range from 2 to 8 kg m^{-3} are typical in closed photobioreactors [11]. Areal biomass productivities ranging from 13 to 47.7 g m^{-2} day^{-1}, and from 10.2 to 22.8 g m^{-2} day^{-1} have been reported for tubular and flat panel reactors respectively [13]. Moreover, photosynthetic efficiencies ranging from 1.3 to 6.9% have been reported for these reactors under outdoor conditions [24]. However, these systems are much more expensive to build and operate than open pond systems and require large amount of auxiliary energy input for cultivation of algae [1]. For instance in tubular PBRs, typical pumping energy inputs on the order of 350 to 400 MJ per kg of algae biomass is required [1, 25]. Flat panel reactors use gas flow for mixing within the system to ensure high mass transfer [25]. Although this high mass transfer

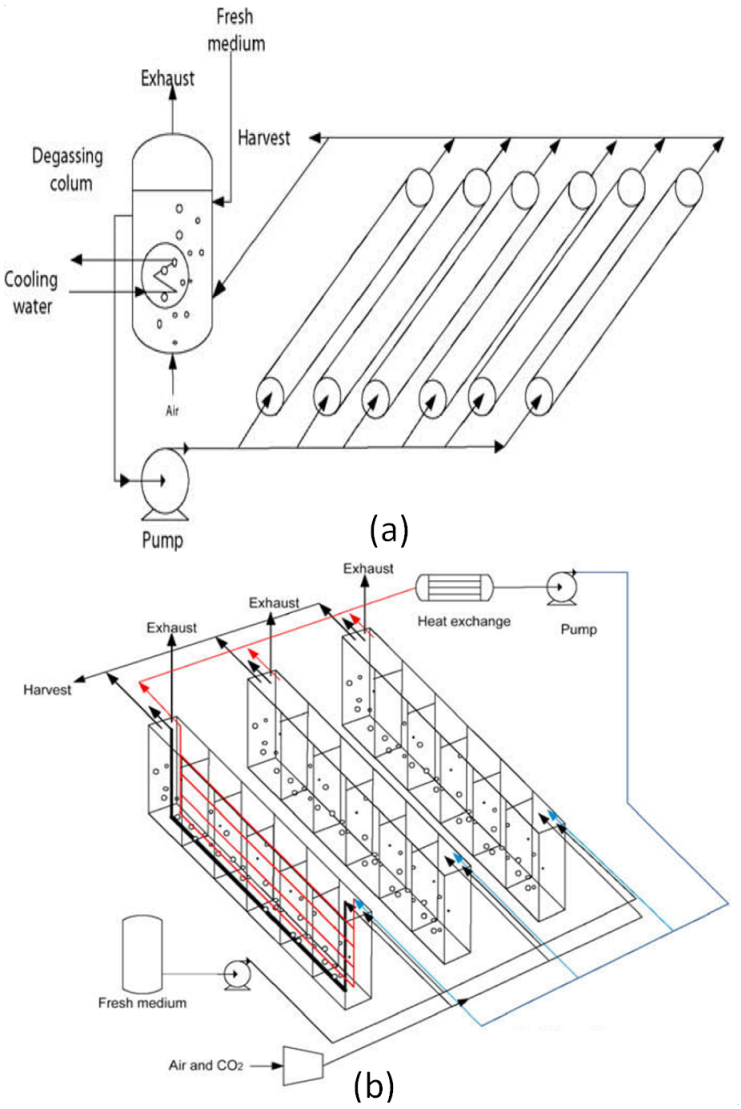

Figure 2.2: Schematic of typical (a) tubular and (b) flat plate photobioreactors used for algae cultivation [1].

increases the biomass productivity, an air pumping energy of 15 to 20 MJ is required per kg of algae biomass output which is about 15 times that required

for mixing in open ponds [1, 25]. A technical report by U.S. Department of Energy indicated that the capital cost associated with closed photobioreactors were 2 to 10 times that of open ponds which was about \$20 m^{-2} [26]. Moreover, it was reported that the production cost of algae ranged from \$8 to \$15 kg^{-1} dry algae biomass in open ponds whereas it was as large as \$50 kg^{-1} algae biomass in closed photobioreactors due to large operating costs [15, 27].

2.2 Harvesting and Dewatering of Algal Suspensions

As already discussed, current algal photobioreactors can be divided into two main groups, namely raceway ponds and closed photobioreactors. Raceway ponds are closed loop shallow channels with typical depths of 0.3 m. These ponds are mixed and recirculated with paddle wheels [2]. Biomass concentrations ranging from 0.1 g L^{-1} to 0.5 g L^{-1} are typical with these systems [15]. Closed photobioreactors use the same principle for cultivation of algae. Algae are recirculated using pumps within closed and controlled environments such as array of tubes, narrow panels and plastic sleeves [11]. This controlled environment results in higher biomass concentrations ranging from 2 g L^{-1} to 8 g L^{-1} [11]. From either the raceway ponds or closed photobioreactors, these outputs are very dilute considering that algal pastes with solid contents ranging from 15 to 25% are required for the extraction of algal metabolites such as lipids [12].

Technologies such as centrifugation, flocculation, filtration, gravity sedimentation, flotation, and electrophoresis are used to dewater algae suspen-

sions [12]. Centrifugal forces are used for algae recovery in centrifugation. Although this technology is reliable, high energy, on the order of 8 kWh m^{-3} (28.8 MJ m^{-3}), and capital intensities associated make it unfeasible for processing large volumes of dilute algae suspensions with low commercial value [12, 28].

Negative surface charge that is present over the algal cells is one of the main reasons that prevents the flocculation of algal cells [12]. In flocculation, inorganic and organic flocculants are added to algal suspensions to overcome this cell to cell repulsion [12]. Multivalent metal salts such as ferric sulfate, ferric chloride and aluminum sulfate are used as inorganic flocculants. These salts are added to neutralize the cellular surface charges. In addition to surface charge neutralization, at specific pH ranges these salts are also capable of forming polyhydroxyl complexes that aid in flocculation of algal cells [12, 28]. Organic flocculants such as chitosan, purifloc®, and zetag® have also been used for algal flocculation [12]. In addition to charge neutralization, these polymers create algal flocs by bridging algal cells. This bridging proceeds by adsorption of the same polymer over multiple cells at the same time. Although flocculation is a reliable technique, the cost of the flocculants can be high and the flocculants added have to be removed before reuse of the processed water for algae cultivation [12, 28].

Filtration is also studied for harvesting and dewatering of algae. Filtration systems are capable of providing a reliable means of algal harvesting and dewatering at the expense of considerable energy inputs, i.e., 0.1 to 2.06

kWh m^{-3} (0.36 to 7.41 MJ m^{-3}) [12]. Moreover, filters that are used have to be replaced periodically [12]. Gravity sedimentation is also studied for algal harvesting. The use of this process is advantageous as it requires low energy inputs. As gravitational sedimentation process is slow, large settling tanks may be required and the reliability of this system is low [12]. In flotation air bubbles are introduced to the algal suspension either through pressure variation or injection. These bubbles attach to the algal cells and carry them to the surface of the algal suspension. As this process requires a high energy input, on the order of 10 to 20 kWh m^{-3} (3.6 to 7.2 MJ m^{-3}), its use for algal harvesting and dewatering does not seem likely [12].

Electrophoresis techniques, namely electrolytic coagulation, flotation, and flocculation, are also investigated for algae harvesting [12]. In all of these techniques, a voltage is applied across the algae suspensions using electrodes. In electrolytic coagulation this voltage solubilizes reactive electrodes that are made up of metals such as iron or aluminum. The formed cations react with water to produce polymeric hydroxides. Consequently, the cations and hydroxides formed coagulate the algae cells. In electrolytic flotation inactive metals are used as cathodes and hydrogen bubbles are formed as water is split due to applied voltage. The formed bubbles attach over algal cells and carry them to the surface of the suspension. Finally, in electrolytic flocculation algal cells that are negatively charged move towards and contact the anode due to applied voltage. The surface charges over the algal cells are neutralized due to this contact and the cells flocculate. These electrophoresis techniques are

advantageous as they do not require addition of chemicals such as flocculants that may contaminate and limit the water reuse for algae cultivation. However, their applicability for algal harvesting might be limited as they require (i) considerable energy inputs ranging from 0.33 to 1.5 kWh m^{-3} (1.19 to 5.4 MJ m^{-3}) and (ii) periodic replacement of electrodes [12].

Due to cost, reliability, and energy intensity of these technologies harvesting and dewatering of algal suspensions are considered to be a major bottleneck for algal biofuel production [12]. For instance, Gudin and Therpenier estimated that 20 to 30% of the total cost of algae biomass production comes from harvesting and dewatering of algal suspensions [19]. Thus, alternative methods of algae harvesting are investigated. Gutzeit *et al.* developed a wastewater treatment technique based on the use of algal-bacterial flocs [29]. For the formation of these algal-bacterial flocs, *Chlorella vulgaris* and municipal wastewater treatment plant activated sludge were mixed and irradiated for a duration of two days. They investigated the use of these flocs for organic carbon and nutrient removal from wastewater streams. They achieved dissolved organic carbon, nitrogen, and phosphorus removals of 88%, 85%, and 50%, respectively, with a hydraulic retention time of two days. Moreover, they indicated that the use of these algal-bacterial flocs were advantageous for wastewater treatment as (i) algae supplied the oxygen requirements of bacteria which eliminated the need for aeration, and (ii) formed flocs were separable by gravity sedimentation. Oh *et al.* investigated the use of flocculant producing bacterial strains for flocculation of algal cells [30]. *Chlorella vulgaris*

was used as the model algal species. Flocculation efficiencies (defined as the ratio of the biomass recovered to the biomass that was already present) of 83% were achieved with the culture broth of *Paenibacillus sp.* AM49. Lee *et al.* studied the microbial flocculation of coccolithophorid alga *Pleurochrysis carterae* [31]. To test the efficiency of their method they (i) heterotrophically cultivated the bacteria that coexist with this algal strain separately, (ii) added this bacterial broth and carbon sources to algal suspensions cultivated, (iii) mixed these bacteria inoculated algal suspensions under dark conditions, and (iv) allowed the settling of the suspensions by gravity to test the recovery efficiencies and concentration factors. They achieved algae recovery efficiencies of about 90% and concentration factors of 240 with the addition of 0.1 g L^{-1} acetate, and a mixing duration of 24 hours. Jones *et al.* investigated the use of anion exchange resins for capturing algae cells and dewatering algae suspensions [32]. They achieved binding capacities of up to 37 mg of algae per gram of resin which corresponds to 93% efficient algae capturing from 1 L *Neochloris oleabundans* suspension with a concentration of 0.4 g L^{-1} with the addition of 10 g anion exchange resin. In addition to dewatering algae suspensions the use of the resins allowed the direct conversion of the algal lipids to biodiesel by exposing the captured cells to sulfuric acid and methanol mixture. Moreover, with this system the lipid content of the resin bound algae could be directly converted into biodiesel by exposing the resins to sulfuric acid and methanol. Finally Salim *et al.* studied the use of auto-flocculating algae as a flocculant [33]. They investigated the settling characteristics of *Chlorella*

vulgaris and *Neochloris oleoabundans*, non-flocculating algae, with and without the addition of flocculating algal species namely, *Ankistrodesmus falcatus*, *Scenedesmus obliquus*, and *Tetraselmis suecica* [33]. They reported that the addition of the flocculating algae increased the settling rate and biomass recovery efficiency of the non-flocculating algae. The authors also indicated that bioflocculation of algae may be a feasible option for pre-concentration of algal species as this method (i) is cost effective, (ii) does not require addition of flocculants or chemicals that might limit the reuse of water, and (iii) does not require any pretreatment before the extraction of algal lipids. However, this method required the addition of large amounts of flocculating algae to increase the recovery efficiency of the non-flocculating algae [33].

2.3 Research on Immobilized Algae Cultivation Systems

2.3.1 Immobilized algae cultivation systems for biofuel production

Cultivation of algae as benthic systems where cells are immobilized on surfaces has been attracting attention as these systems offer the potential to lower the energy and water requirements. Several research efforts can be found in the literature investigating immobilized algae cultivation systems in biofuel production as well as in environmental remediation applications. Akin *et al.* studied carbon dioxide sequestration using the green algae *B. braunii* immobilized on agar surfaces [34]. Using 10% by volume CO_2 enriched air and 0.24 mol L^{-1} $NaHCO_3$ as the carbon sources, oil contents ranging from

15 to 47% by dry cell weight were achieved. However, the authors did not report or compare the biomass production rates of suspended and immobilized cultivation systems. Balliez *et al.* reported an increase as large as 23% in lipid production of *B. braunii* cells immobilized in calcium alginate gels compared to cells suspended in liquid media [35]. However, biomass production rate was decreased by 21% in the log phase of growth. The decrease in biomass production was attributed to (i) a switch in metabolic activity from growth to hydrocarbon production as well as (ii) to steric stress on the encapsulated cells.

Moreover, a membrane photobioreactor was developed to mitigate CO_2 emissions from a fossil-fired power plant using a thermophilic cyanobacteria species [36]. The photobioreactor system consisted of vertically hung membranes contained in a closed chamber that were illuminated by optical fibers delivering light from solar collectors. Carbon dioxide from stacks was supplied to the chamber while the nutrient medium was delivered to the membranes using a drip system. The cyanobacteria grew on the membranes as immobilized cells and were washed off at the time of harvest. Biomass productivities up to 55 g m^{-2} day^{-1} were achieved with simulated flue gas emissions [36]. However, this cyanobacterium was not capable of accumulating appreciable amount of lipids. The economic analysis of the system indicated that the sophisticated solar collection system utilized made this reactor economically unfeasible either for carbon dioxide sequestration or for biofuel production [37].

Johnson and Wen investigated the use of *Chlorella* sp. biofilms to

produce biofuels [38]. The algae were cultivated on polystyrene foam immersed in dairy manure wastewater and agitated with a rocking shaker. The authors reported biomass yield as large as 25.65 g m^{-2} and biomass productivity of 2.57 g m^{-2} day^{-1}. This study gave encouraging results for the use of algal biofilms in biofuel production. However, it did not provide any energy or water use analysis of this method or offer a photobioreactor system that can potentially be implemented outdoors and scaled up. Cao *et al.* proposed the use of floating conveyor belts made out of laser textured stainless steel for cultivation of algal biofilms [39]. The authors reported better attachment of *Scenedesmus dimorphus* on microdimpled stainless steel surfaces compared to non-textured ones.

In a more recent study, Christenson and Sims [40] developed an algal biofilm reactor using cotton cords as immobilization surfaces and reported the operation under both indoor and outdoor conditions. The system consisted of a cotton cord wrapped around rotating drums that were partly submerged in wastewater. The authors reported a biomass production rate of 5.5 g m^{-2} day^{-1} for bench scale tests. Moreover, biomass and fatty acid methyl ester productivities of up to 31 g m^{-2} day^{-1} and 2.5 g m^{-2} day^{-1} were reported, respectively, for pilot scale tests under outdoor conditions. The system developed had a positive energy balance with a net energy output of up to 6.3 W m^{-2}. Finally, the system had a concentrated biomass harvest with a solid content ranging from 12 to 16%.

2.3.2 Immobilized algae cultivation systems for wastewater treatment

Eutrophication is excessive growth of autotrophs, such as cyanobacteria and algae, in natural waters due to elevated nitrogen and phosphorus levels that originate from urban, agricultural and industrial wastewater discharges. This excessive growth destroys the aquatic ecology, resulting in problems such as oxygen depletion, fish deaths, as well as odor and taste problems in water treatment [41, 42]. In current wastewater treatment systems, nitrogen and phosphorus are removed using biological and chemical methods. Current biological wastewater treatment systems use a mixed culture of bacteria to oxidize the nitrogen that is in form of ammonia to nitrate in aerobic conditions and then reduce it to nitrogen gas in anoxic environment [43]. Moreover, phosphate in wastewater is removed by inducing its storage as polyphosphate within bacteria by exposing the bacteria to sequential anaerobic and aerobic environments. Residual nitrogen and phosphorus are removed through processes such as filtration, reverse osmosis, electrodialysis, ion exchange, and chemical precipitation [43]. Algae have been studied as an environmental friendly, efficient, and alternative way of removing nutrients from wastewater streams and production of potentially valuable products [42, 44, 45]. Suspended, immobilized and biofilm growth of algae have been studied for nutrient removal from primary and secondary treated municipal wastewater, and wastewater with industrial origins [38, 44, 46–58].

Nutrient removal based on suspended algae cultivation has been stud-

ied both indoors at laboratory conditions and outdoors at ambient conditions. Various species of algae and mixed cultures have been tested for nutrient removal but *Chlorella* and *Scenedesmus* have been studied extensively since they are the dominant algal species at outdoor wastewater treatment ponds [45]. At laboratory scale, successful biomass production and nitrogen and phosphorus removal efficiencies above 90 % have been frequently reported [52, 58, 59]. An *et al.* reported biomass concentration of 7 g m^{-3} and hydrocarbon production of 0.85 g L^{-1} with *Botryococcus braunii* cultivated with piggery wastewater pretreated with acidogenic fermentation [60]. Ammonium and orthophosphate removal efficiencies of 96 and 99 %, respectively, and areal biomass productivities of 2.8 g m^{-2} d^{-1} have been achieved at outdoor conditions, resulting in a lipid production potential of 11000 L ha^{-1} $year^{-1}$ with piggery wastewater [58]. Lipid productivites of 9.2 to 17.78 tons ha^{-2} $year^{-1}$ have been reached with carpet mill effluents [52]. Phosphorus removal ranging from 94 - 97 % percent have been reported for hydraulic residence times (HRT) ranging from 2-6 days with high rate algal ponds (HRAP) at outdoors [45]. At ambient conditions using HRAP with CO_2 enrichment biomass productivites of up to 24.7 g m^{-2} d^{-1} have been reported with a HRT of 4 days [61].

Although successful studies have been done on wastewater treatment with suspended algae, the research on algal nutrient removal have been more focused on immobilized technologies [60, 62–65]. The reason behind this interest is the requirement of capital and energy intensive harvesting systems required to capture the biomass grown [46]. Moreover, this type of growth

may fail to meet effluent criteria such as chemical oxygen demand (COD) since each gram of algae in the effluent is equivalent to 1.25 g COD [46, 66]. Thus, immobilization methods such as covalent coupling, adsorption, and entrapment have been tested to produce effluents free of algal cells. Compared to suspended growth, nutrient removal efficiencies that are comparable or superior have been reported for algae grown immobilized compared to that grew in suspension [54, 67, 68]. Ruiz-Marin *et al.* reported nitrogen removal efficiencies of 90 % with *Scenedesmus obliquus* and *Chlorella vulgaris* immobilized in alginate and higher nitrogen and phosphorus uptakes were achieved with algae immobilized compared to free algae [54]. Lau *et al.* studied nutrient removal from primary effluent with suspended algae and algae immobilized in alginate and carrageenan [67]. Compared to algae cultivated in suspension they reported log phase growth rates that are higher or comparable with immobilized algae. Nitrogen and phosphorus removal efficiencies were 95 % and 99 %, respectively, with immobilized algae while the same numbers were 50 % with algae grown in suspension. Chevalier and de la Noue *et al.* reported similar nitrogen and phosphorus uptakes from secondary effluent with immobilized and free *Scenedesmus* [68]. Although successful results have been reported with immobilized algae in laboratory conditions, considering the volume of wastewater to be treated the cost of immobilization agents, such as alginate and carrageenan, makes them economically unfeasible [45].

Considering the cost prohibitive nature of cell immobilization, natural adhesion and biofilm formation capabilities of algae have been tested as

an alternative way of growing algae and nutrient removal [55]. Craggs *et al.* successfully operated an algal biofilm photobioreactor with treatment efficiencies of up to 100 % for both nitrogen and phosphorus with primary effluent [46]. The reactor studied were inoculated with endemic monocultures and the system was unialgal at ambient conditions after an experimental duration of four months. Algal biofilm cultivation system that has been most extensively studied is the algal turf scrubber (ATS). ATS consists of (1) a surface for formation and growth of algal biofilm, and (2) a wave surge bucket that flows the wastewater over the biofilm surface at high velocity [49]. Craggs *et al.* achieved mean and maximum algal biomass productivities of 35 g m^{-2} d^{-1} and 60 g m^{-2} d^{-1}, respectively, with ATS at ambient conditions with secondary effluent from an evaporation pond [50]. Under laboratory conditions biomass productivity of 5 g m^{-2} d^{-1} was reported with dairy manure using ATS [69]. With a similar study Wilkie and Mulbry reported a biomass productivity up to 5.5 g m^{-2} d^{-1} at indoor conditions with a nitrogen uptake of 1430 kg ha^{-1} $year^{-1}$ [49]. Based on the uptake rates achieved, algae require 26% and 23% the area that conventional plant based systems require for the same nitrogen and phosphorus removal, respectively [49]. Kebede-Westhead *et al.* reported an increase of biomass productivity from 7.6 to 19.1 g m^{-2} d^{-1} by adjusting the nitrogen loading rates and incident light over the algal biofilm [69]. Although, at ambient conditions biomass productivities of up to 25 g m^{-2} d^{-1} have been reported with a pilot scale unit, cost analysis of the system indicates that ATS is too costly just for animal feed production purposes [47].

However, the cost of nitrogen removal with ATS was below the cost associated with the upgrade of existing wastewater treatment plants [47]. A study that has been done to investigate the lipid production of the ATS indicated that the fatty acid content of the biofilm grown ranged from 0.6 to 1.5% and its utilization for biomass production was economically unfeasible [70].

2.3.3 Immobilized algae cultivation systems for heavy metal removal and recovery

Toxic heavy metals are discharged to aquatic environments in effluents of both industrial and urban origin [71]. Since these metals are not biodegradable, they get accumulated in organisms and their concentrations increase as they go up in the food chain [72]. Thus, treatment technologies such as chemical precipitation, adsorption, ion exchange, and osmosis have been used for removal of these metals from water streams [71]. However, there are numerous disadvantages associated with these technologies such as being energy intensive and cost prohibitive, and formation of toxic sludge that may require special disposal [71, 72]. Moreover, in addition to these disadvantages they are ineffective or expensive for when the heavy metal concentration is in the range of 10-100 mg L^{-1} [71].

Algae are known for their high capacity to remove heavy metals from aqueous solutions through the adsorption of the metals to the functional groups that are present over their cell walls such as hydroxyl, phosphoryl, amino, and carboxyl groups [71]. Thus algae have been studied as an economical alter-

native for heavy metal removal [71–73]. In addition to adsorption over the cell wall, algae also remove heavy metals through their uptake into the cell. However, more than 80% of the removal is associated with the adsorption and the significance of the adsorption is larger for short term contact of heavy metals and algae cells [71]. One of the challenges associated with the use of algae is the challenge of removing heavy metal containing algal cells from the treated water streams. For this reason different systems such as gel entrapment, encapsulation, biomass cross-linking have been tested to immobilize these cells to surfaces [72]. However, use of these systems have disadvantages such as increased limitations of mass transfer, cost, and loss of biological activity [71, 72]. Use of natural biofilm formation capacity of algae might offer the solutions to these problems. Moreover, due to increased pH values in algal biofilms heavy metals can also be removed from the liquid phase by precipitation [74]. Thus, in addition to adsorption algal biofilms may lead to heavy metal removal through precipitation [74]. Due to these advantages algal biofilm based heavy metal removal offer high potential [71].

2.4 Algal Adhesion and Biofilm Formation

Although biofilm formation characteristics depend on the type of organism, as well as environmental, interfacial and physiological factors, the sequence of events in the formation of all biofilms is the same [3, 75]. This sequence can be grouped in two parts (1) initial attachment, and (2) deliberate secondary adhesion [3].

Initial adhesion of cells is preceded by adsorption of organic and inorganic aqueous molecules to the solid surface forming a conditioning film [3, 76]. Cells can either actively move towards the conditioned surface by motility or they can be transported by gravity or advection. Once transported, cells can spontaneously adsorb on the surface. This initial, often reversible, adhesion of cells to a surface is followed by a committed secondary adhesion through the production of adhesive EPS resulting in an irreversible adhesion [3, 77]. Once the deliberate attachment is established, EPS also provides a three dimensional hydrated matrix that cements the growing algae cells, forming the biofilm [77]. EPS mainly consist of polysaccharides and proteins [77]. The binding strength of the EPS comes from the presence of various functional groups that interact with functional groups of other EPS molecules through hydrogen bonding, electrostatic interactions, and van der Waals interaction [77].

Studies in the literature mostly focus on the effects of surface energy on adhesion density and adhesion strength of diatoms [75, 78–83]. Although not universal, a general trend is that higher adhesion density is observed over hydrophobic surfaces [75, 80–83]. Li *et al.* studied the adhesion of the diatom *Nitzschia closterium* on self-assembled monolayers (SAMs) of hydrophobic methyl (CH_3-SAM) and hydrophilic carboxylic (COOH-SAM) end groups on glass [75]. Attachment density of this diatom was higher on surfaces with more hydrophobic groups which had smaller free energy. However, percent removal of adhered cells under shear stress was higher for hydrophobic sur-

faces indicating a weaker adhesion strength. In a similar study Finlay *et al.* examined the adhesion of the diatom *Amphora coffeaeformis* on SAMs formed from alkanethiols terminated with different mixtures of methyl (CH_3) or hydroxyl (OH) groups [78]. They reported that there was no significant effect of surface wettability on cell adhesion. They explained this indifference by the presence of extracellular polymeric substances (EPS) that covered the cells adhering them to surfaces. Becker *et al.* investigated the EPS production, adhesion strength and density of *Amphora coffeaformis* over surfaces with different surface energy. They reported that adhesion strength and density did not follow any trend with surface energy properties. However, higher adhesion density was attained with higher EPS production. Moreover, EPS production and adhesion strength increased with time [79]. Schilp *et al.* investigated the adhesion of *Navicula perminuta* on SAMs of varying surface energies prepared with hexa(ethylene glycols) with different alkoxyl end group terminations [81]. They reported an increase in adhesion density of cells with decreasing surface wettability, i.e., increasing surface hydrophobicity. The adhesion strength of cells was independent of the surface wettability. This higher adhesion density was proposed to be due to easier exclusion of water from hydrophobic adhesion surfaces [83].

2.5 Models on Cell to Substrata and Cell to Cell Interactions

Understanding cell to cell and cell to substrata interactions of algal species may offer improvements in design and performance of both suspended and attached growth of algae. In planktonic photobioreactors, cell to cell interactions can be used for selection of target and harvesting species to improve bioflocculation based harvesting. In biofilm photobioreactors based on cell to substrata interactions, algal species and substrata favoring adhesion can be determined.

2.5.1 Characterization of surface energy and surface energy parameters of algal cells and substrata

The results from contact angle measurements and known surface tension properties of three probe liquids are used to calculate the surface energy parameters of the algal mats and the adhesion substrata based on the extended Young's equation according to [84],

$$cos\theta = -1 + \frac{2(\gamma_{sr}^{LW}\gamma_{l}^{LW})^{1/2}}{\gamma_l} + \frac{2(\gamma_{sr}^{+}\gamma_{l}^{-})^{1/2}}{\gamma_l} + \frac{2(\gamma_{sr}^{-}\gamma_{l}^{+})^{1/2}}{\gamma_l} \qquad (2.1)$$

where θ is the measured contact angle, γ_{sr}^{LW} is the apolar surface energy component, γ^- and γ^+ are the electron donor and acceptor parameters, respectively, while subscripts sr and l refer to the surface and probe liquid, respectively. Contact angle of the apolar liquid, diiodomethane, is used to quantify the apolar surface energy component γ_{sr}^{LW} as γ_l^- and γ_l^+ are both equal to zero for this

probe liquid. Moreover, the contact angles measured with the other two probe liquids, water and formamide, are used to solve for the other two unknown surface energy parameters, γ_{sr}^{+} and γ_{sr}^{-}. Polar surface energy component (γ_{sr}^{AB}) of the surface is calculated based on the calculated γ_{sr}^{+}, γ_{sr}^{-} as,

$$\gamma_{sr}^{AB} = 2\sqrt{(\gamma_{sr}^{+}\gamma_{sr}^{-})} \tag{2.2}$$

The total surface energy γ_{sr} is calculated based on γ_{sr}^{AB}, γ_{sr}^{LW} as,

$$\gamma_{sr} = (\gamma_{sr}^{AB} + \gamma_{sr}^{LW}) \tag{2.3}$$

When a contact angle drop of a probe liquid is placed over a surface with large surface energy, the vapor of the liquid may condense over the surface around the droplet and may influence the contact angles measured [84, 85]. In this study these effects, spreading pressure effects, are ignored since for surfaces with surface energy below 100 mJ m^{-2} this effect is negligible and the surface energy of all the surfaces studied were below this value [84, 85]. Finally, hydrophilicity and hydrophobicity of surfaces are determined based on the free energy of cohesion (ΔG_{coh}) according to,

$$\begin{aligned}\Delta G_{coh} = &-2(\sqrt{\gamma_{sr}^{LW}} - \sqrt{\gamma_{l}^{LW}})^2 \\ &-4(\sqrt{\gamma_{sr}^{+}\gamma_{sr}^{-}} + \sqrt{\gamma_{l}^{+}\gamma_{l}^{-}} - \sqrt{\gamma_{sr}^{+}\gamma_{l}^{-}} - \sqrt{\gamma_{sr}^{-}\gamma_{sr}^{+}})\end{aligned} \tag{2.4}$$

While a negative ΔG_{coh} indicates hydrophobicity where surface-surface interactions are stronger than surface-water interactions, a positive value indicates hydrophilicity [86].

2.5.2 Thermodynamic approach

Either for a cell to substrata or a cell to cell system, the thermodynamic model depends on the calculation of change in total interfacial free energy for prediction of attractive or repulsive interaction. For cell substrata interaction the change in total free energy (ΔG_{adh}) of a substrate, microorganism, and liquid system is calculated based on formation and removal of interfaces according to [3],

$$\Delta G_{adh} = \gamma_{ms} - \gamma_{ml} - \gamma_{sl} \tag{2.5}$$

where γ_{ms} is the microorganism-substrate, γ_{ml} is the microorganism-liquid, and γ_{sl} is the substrate-liquid interfacial free energy in J m^{-2} [87]. Moreover, similarly for a cell to cell system, the change in total interfacial free energy before and after the cell-cell adhesion or coaggregation (ΔG_{co-agg}) is quantified according to [3],

$$\Delta G_{co-agg} = \gamma_{m_1 m_2} - \gamma_{m_1 l} - \gamma_{m_2 l} \tag{2.6}$$

where γ_{m1m2} is the microorganism-microorganism, and $\gamma_{m_1 l}$ and $\gamma_{m_2 l}$ are the microorganism-liquid interfacial free energy [3]. This model suggests that cell-cell and cell-substrata adhesions are thermodynamically favorable if the total interfacial energy of the system decreases after the adhesion, i.e., if ΔG_{adh} or ΔG_{co-agg} are less than zero [87]. Moreover, the interfacial free energy between two identical cells, same species, or substrata is equal to zero. By calculating

ΔG_{adh} or ΔG_{co-agg} for these identical systems free energy of cohesion (ΔG_{coh}) is quantified and as already discussed based on this quantified parameter the surface hydrophobicity or hydrophilicity can be determined.

The interfacial free energies that are required to quantify ΔG_{adh} and ΔG_{co-agg} are calculated with Lifshitz-van der Waals-acid base (LW-AB) approach using (i) the surface energy parameters of the algal cells and adhesion substrates presented in Section 2.5.1 and (ii) surface tension properties of probe liquids [3, 88, 89].

Using this approach, γ_{sl},γ_{sm}, γ_{ml}, $\gamma_{m_1m_2}$, γ_{m_1l} and γ_{m_2l} are calculated using the van der Waals component of surface free energy, and the electron donating and accepting parameters of the substratum, microorganism, and the probe liquids. For instance γ_{sl} is calculated as,

$$\gamma_{sl} = (\sqrt{\gamma_s^{LW}} - \sqrt{\gamma_l^{LW}})^2 + 2(\sqrt{\gamma_s^+\gamma_s^-} + \sqrt{\gamma_l^+\gamma_l^-} - \sqrt{\gamma_s^-\gamma_l^+} - \sqrt{\gamma_s^+\gamma_l^-}) \quad (2.7)$$

Similarly, γ_{sm} and γ_{ml} are calculated and these interfacial free energies are substituted into Equation (2.6) to calculate the free energy of adhesion ΔG_{adh} and $\gamma_{m_1m_2}$, γ_{m_1l}, and γ_{m_2l} are calculated to quantify ΔG_{co-agg}. The total free energy of adhesion or co-aggregation can also be considered as the sum of Lifshitz-van der Waals and acid-base components as,

$$\gamma = \gamma^{AB} + \gamma^{LW} \quad (2.8)$$

where the AB component is calculated using the electron donor and acceptor

parameters as,

$$\begin{aligned}\Delta G_{adh}^{AB} &= 2(\sqrt{\gamma_m^+}-\sqrt{\gamma_s^+})(\sqrt{\gamma_m^-}-\sqrt{\gamma_s^-})-2(\sqrt{\gamma_m^+}-\sqrt{\gamma_l^+}) \\ &\quad (\sqrt{\gamma_m^-}-\sqrt{\gamma_l^-})-2(\sqrt{\gamma_s^+}-\sqrt{\gamma_l^+})(\sqrt{\gamma_s^-}-\sqrt{\gamma_l^-}) \qquad (2.9)\end{aligned}$$

In addition, LW component of surface free energy of microorganism, liquid, and substrate are taken into account to calculate LW component of the change in free energy as,

$$\Delta G_{adh}^{LW} = -2(\sqrt{\gamma_m^{LW}}-\sqrt{\gamma_l^{LW}})(\sqrt{\gamma_s^{LW}}-\sqrt{\gamma_l^{LW}}) \qquad (2.10)$$

Finally, to calculate ΔG_{co-agg}^{AB} and ΔG_{co-agg}^{LW}, surface energy parameters of the substrata should be substituted with those of the second microorganism and Equations (2.9) and (2.10) should be used.

2.5.3 Derjaguin, Landau, Verwey, Overbeek (DLVO) approach

In the DLVO approach, microbial adhesion is described as a balance between van der Waals (LW) and electrostatic (EL) interaction energy [3]. LW forces originate from instantaneous asymmetrical distribution of electrons in molecules and it is usually attractive [90]. Electrostatic interactions are the result of the coulombic interactions between the cell and the surface. This latter is usually repulsive as both the algal cell and substrates usually carry a negative charge [91]. The total interaction energy G_{TOT} is a function of the distance between the cells or cell and substrata and defined as,

$$G^{TOT}(d) = G^{LW}(d) + G^{EL}(d) \tag{2.11}$$

where G^{LW} and G^{EL} are the Lifshitz-van der Waals and the electrostatic interaction energy, respectively. While a negative G^{TOT} indicates adhesion, a positive sign indicates repulsive interaction between the cells or the cell and the substrate. The magnitude of the total interaction and the separation distance associated determines how reversible the adhesion is. An interaction energy scale of kT in joules, where k is the Boltzman constant and T is the temperature of the cell and the medium, is commonly used for comparison of the interaction energy between microorganism-microorganism or microorganism-substrate with that of the thermal energy of the microorganism [3]. For cell to substrata interactions Lifshitz-van der Waals component of free energy (G^{LW}) is defined as,

$$G^{LW}(d) = -\frac{A}{6}\left[\frac{a}{d} + \frac{a}{d+2a} + ln\left(\frac{d}{d+2a}\right)\right] \tag{2.12}$$

where a is the radius of the algal cell in m, d is the separation distance in m, and A is the Hamaker constant given as [3],

$$A = -12\pi d_0^2 \Delta G_{adh}^{LW} \tag{2.13}$$

where d_0 is minimum separation distance between two surfaces equal to 1.57×10^{-10} m [3]. For cell to cell interactions the van der Waals interaction is calculated as,

$$G^{LW}(d) = -\frac{Aa_1a_2}{6d(a_1+a_2)} \tag{2.14}$$

where a_1 and a_2 are the radius of the algal cells in m, and A is the Hamaker constant for the cell-cell system calculated based on ΔG^{LW}_{co-agg} using Equation (4.4) [3]. Finally, electrostatic component of free energy, G^{EL}, between the cell and the surface is defined as [3],

$$G^{EL}(d) = \pi\varepsilon a(\psi_m^2+\psi_s^2)\left[\frac{2\psi_m\psi_s}{\psi_m^2+\psi_s^2} ln\frac{1+e^{-\kappa d}}{1-e^{-\kappa d}} + ln(1-e^{-2\kappa d})\right]$$

where ε is the permittivity of water equal to 6.88×10^{-10} F m^{-1}, ψ_m and ψ_s are the surface potential of algal cells and substrate in V, respectively, and κ^{-1} is the double layer thickness in m which is given by [3],

$$\kappa = \left[\frac{e^2}{\varepsilon kT}\sum_i z_i^2 n_i\right]^{1/2} \tag{2.15}$$

where e is the electron charge equal to 1.6022×10^{-19} C, z_i is the charge number for ions of species i, and n_i is the concentration of ions of species i in the solution # of ions m^{-3}. Similarly, the electrostatic interaction between two algal cells is calculated as,

$$G^{EL}(d) = \frac{\pi\varepsilon a_1a_2(\psi_{m_1}^2+\psi_{m_2}^2)}{(a_1+a_2)}\left[\frac{2\psi_{m_1}\psi_{m_2}}{\psi_{m_1}^2+\psi_{m_2}^2} ln\frac{1+e^{-\kappa d}}{1-e^{-\kappa d}} + ln(1-e^{-2\kappa d})\right]$$

Finally, to quantify the surface potential of the algal cells the following relation is used,

$$\psi = \zeta(1 + \frac{v}{a})e^{\kappa v} \tag{2.16}$$

where v is the thickness of hydration layer associated with the algal cells in m. Its value changes inversely with the ionic strength of the medium and it varies between 3×10^{-11} m to 5×10^{-11} m [89]. In this study a value of 5×10^{-11} m and 3×10^{-11} m were used for the measurements performed in BG-11 and ASP-M, respectively, based on their ionic strengths.

2.5.4 Extended Derjaguin, Landau, Verwey, Overbeek (XDLVO) approach

Based on Van Oss's studies, acid-base interactions are added to the van der Waals and electrostatic interactions that are considered in DLVO approach [92]. AB forces originate from electron transfer interactions between polar components of the cell and the surface. AB interactions can be attractive (hydrophobic attraction) or repulsive (hydrophilic repulsion) based on the hydrophobicity of the interacting surfaces [92]. The acid-base interaction component of the free energy for a cell-substrata system is defined as [3],

$$G^{AB}(d) = 2\pi a\lambda\Delta G^{AB}_{adh}e^{[(d_0-d)/\lambda]} \tag{2.17}$$

where $\Delta\ G^{AB}_{adh}$ is the polar free energy change in the system given by Equation (2.9) and λ is the correlation length also known as the gyration radius of water

molecules in a solution. For hydrophilic interaction λ is equal to 0.6 nm and for hydrophobic interaction the same parameter ranges from 1 to 2 nm as water molecules have a larger gyration radius around hydrophobic surfaces [3, 90, 93]. A value of 1.5 nm is adapted for this study for the hydrophobic attraction since modeling based on this correlation length could explain the adhesion characteristics of algae-substrata interactions better. The acid base interaction between two algal cells is calculated as [94],

$$G^{AB}(d) = 2\pi \frac{a_1 a_2}{a_1 + a_2} \lambda \Delta G^{AB}_{co-agg} e^{[(d_0 - d)/\lambda]} \tag{2.18}$$

The total interaction energy between the cell and the substratum determines the strength and rate of adhesion. For instance, the type of adhesion that occurs due to presence of an attractive energy minimum at a distance from the substratum surface is called adhesion at secondary minimum. This type adhesion is considered to be weaker and more reversible compared primary adhesion where the cell and the substratum interaction results in adhesion at the substratum surface [91].

2.6 Factors Limiting the Productivity of Algal Biofilms

The mass and light transfer are the main parameters that affect the growth and productivity of algal biofilms [95]. This section provides background on their importance and means of optimization of these phenomena for maximizing productivity.

2.6.1 Mass transfer limitations

In biofilm photobioreactors the nutrient solution is flowed over the photosynthetic biofilm for delivering nutrients to the cells. Due to the no slip condition, flow velocity becomes zero on the biofilm surface and the hydrodynamic boundary layers form [96]. This induces the formation of a concentration boundary layer that reduces the nutrient flux to the biofilm. Figure 2.3 shows the flow velocity and the nutrient concentration profiles that are developed over the biofilm surface.

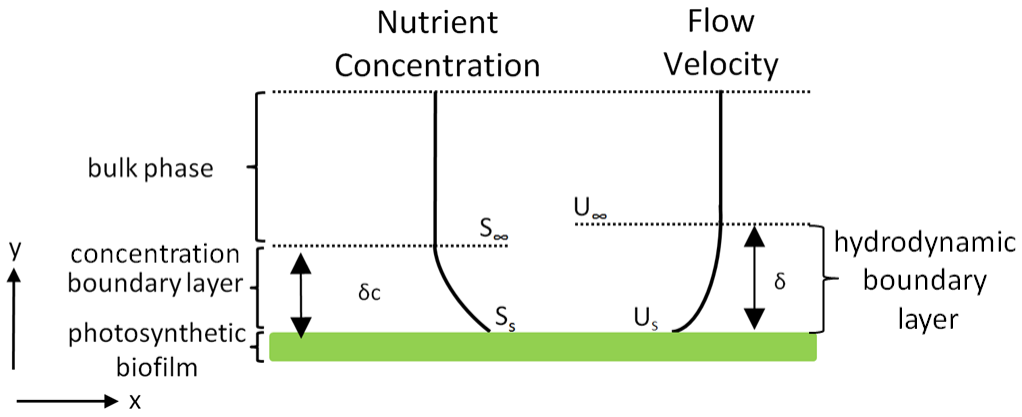

Figure 2.3: Nutrient concentration and flow velocity profiles near a biofilm surface.

While the transport of nutrients is convection dominated in the bulk liquid phase, the scale of advective mass transport decreases within the hydrodynamic boundary layer with reduced flow velocity, and the transport becomes diffusion dominated. As the cells consume the nutrients faster than nutrients are transported by diffusion, their concentration decreases near the biofilm

surface, resulting in microbial processes becoming diffusion limited [97, 98]. Assuming a linear concentration profile within this boundary layer, the flux of nutrients, j_i, can be calculated as [99],

$$j_i = D_i \frac{S_{\infty i} - S_{si}}{\delta_c} \tag{2.19}$$

where D_i is diffusivity in $m^2\ s^{-1}$ of the nutrient i in water, δ_c is the thickness of the diffusion boundary layer in m, and S_{si} and $S_{\infty i}$ are the concentrations of species i in kg m^{-3} on biofilm surface and in bulk phase, respectively. In order to increase the flux of nutrients to the biofilm, the diffusivity of the nutrients can be increased through (1) increased temperature which increases the diffusion coefficient, (2) increased bulk nutrient concentration, and (3) reduced boundary layer thickness through increased flow velocity in the bulk phase [96]. Considering narrow optimum temperature ranges of algal growth, temperature adjustment is not a feasible option for increasing the nutrient flux. However, bulk flow velocity of nutrient solution and concentrations of its constituents can be varied. Through increased flux of nutrients to the biofilm layer, higher photosynthetic rates can be attained, increasing biofuel production rate [99].

For instance, in a study by Sperling and Grunewald decrease of flow velocity from 45 cm s^{-1} to 2 cm s^{-1} resulted in decreases in biomass growth and phosphate uptake rates of about 48% and 64%, respectively, with thermophilic benthic algae [100]. Whitford and Schumaher reported that phosphorus uptake rates were directly proportional to flow velocity up to 40 cm s^{-1} with

Spyrogyra and *Oedogonium* [101]. Similarly, higher phosphorus uptake rates were also reported by Lock and John up to a velocity of 5.4 cm s^{-1} with a river periphyton composed of a mixed biofilm community of photosynthetic and heterotrophic bacteria as well as fungi [102]. Furthermore, Whitford and Schumacher reported about 10 times increase in phosphorus uptake rate and about 70 times increase in respiration rate with flow velocities of 18 cm s^{-1} and 15 cm s^{-1}, respectively, compared to stagnant conditions with periphyton [103]. McIntre reported an increase of biomass production rate of periphyton community with increased current velocity. In addition, they reported diatom dominance at high and filamentous green algae dominance at low flow velocities within the periphyton [104]. The dominance of diatoms at high shear stress was explained by high skin friction coefficient of filamentous algae resulting in higher shears experienced causing erosion [105]. The authors stated that periphyton dominated with green filamentous algae had a more open matrix compared to that dominated by diatoms leading to better diffusion of nutrients [105]. Moreover, due to this higher diffusivity the effect of velocity on green algae growth was lower compared to diatoms [105]. In addition to the effects on algal growth, the flow velocity is also important for adhesion rate of cells on a surface. In general, less algal adhesion has been reported with higher flow velocities [106–109]. Poff *et al.* studied the effects of algal deposition on ceramic tiles in Colorado river and reported up to 40 times increase in biomass deposition on tiles exposed to a flow velocity of less than 1 cm s^{-1} and velocity of 14 to 20 cm s^{-1} compared to tiles exposed to higher velocities [106].

Similarly, Lam and Lowe reported 2 times larger adhesion density of diatoms with a flow velocity of 15 cm s^{-1} compared to 40 cm s^{-1} [109]. Studies that combine the initial adhesion and algal growth reveal that, although higher cell adhesion rates are achieved at lower velocities, their subsequent growth rates are lower under this environmental condition. Thus, high flow velocity lead to a lower initial adhesion but larger subsequent growth rates of the cells [108]. In contradiction to these studies, Johnson and Wen reported that *Chlorella sp.* could not firmly attach on substrates under static conditions where rocking shaking movement was necessary for the formation of the biofilm [38].

Furthermore, Marks and Lowe studied the effects of nutrient concentration on lake periphyton and reported that nutrient enrichment resulted in algal biovolume increases of up to five times [110]. In a study by Peterson *et al.*, phosphorus enrichment resulted in about 30 times increase in the chlorophyll content of river periphyton [111]. Lohman *et al.* reported chlorophyll and biomass content increases of 5 and 4 times, respectively, with the enrichment of nitrate and phosphate in a stream periphyton [112]. Finally, Hillebrand *et al.* reported an increase in algal biomass productivity in both freshwater and marine periphyton with nitrogen and phosphorus enrichment [113].

2.6.2 Light transfer limitations

Algae use the energy from sunlight to convert inorganic carbon into organic molecules. As depicted in Figure 2.4, the rate of this conversion depends on the intensity of light that the microorganisms receive. The figure indicates

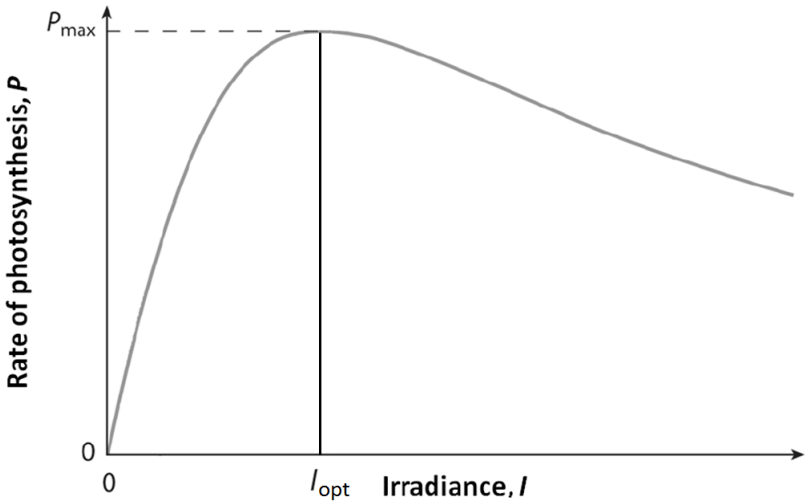

Figure 2.4: Typical photosynthetic saturation curve for algae [2].

that photosynthesis rate increases linearly at low intensities and at large intensities due to over excitation and oxidative damage that are exerted on photosynthetic apparatus the rate of photosynthesis decreases [2, 114]. The irradiation that the algae biofilm receive is essential as the biomass productivity is linearly related with photosynthesis and the light intensity decreases across the biofilm thickness exponentially [115, 116]. This exponential decrease can create large light intensity variations across the biofilm that while the algae cells on top can be photoinhibited the cells on the bottom of the biofilm can be photolimited [115, 117, 118]. Due to steep changes in light intensity within the biofilm, light intensities that are larger than those used in suspended algae cultivation can increase the overall photosynthesis rate of biofilm PBR systems [119]. For instance, Revsbech *et al.* studied the rate of photosynthesis of

a mixed culture microbial mat and found that the rate of oxygen generation increased from 0.860 to 21.803 mmol m^{-2} h^{-1} with an increase of irradiance from 36 to 1800 μmol m^{-2} sec^{-1} (8 to 378 W m^{-2}), respectively [120]. Solar irradiance of up to about 2000 μmol m^{-2} sec^{-1} (420 W m^{-2}) is typical at noon time [121]. Moreover, Wootton and Power reported a linear increasing trend in the rate of photosynthesis with increasing irradiance up to 1750 μmol m^{-2} sec^{-1} (367.5 W m^{-2}) with river periphyton [122]. Zippel *et al.* studied the growth of photosynthetic biofilms under different irradiance and reported that (i) the lag phase of growth decreased from 21 to 5 days, and (ii) biomass productivity increased from 0.23 g m^{-2} day^{-1} to 1.83 g m^{-2} day^{-1} with an increase of irradiance from 15 to 120 μmol m^{-2} sec^{-1} (3 to 25 W m^{-2}). Moreover, in a similar study Staal *et al.* reported an increase of about 1.5 times in the growth rate of phototrophic biofilms with similar increase in the intensity of light [95]. Also, Kuhl *et al.* reported the effect of irradiance on photosynthetic rate of a cyanobacterial biofilm. The authors indicated that (i) a 6.5 times increase in the rate of photosynthesis and (ii) an 85% increase in the depth of the photic zone were achieved with an increase in irradiation intensity from 16 to 200 μmol m^{-2} sec^{-1} (3 to 42 W m^{-2}) [118]. As opposed to these studies Boston and Hill reported a decrease in the rate of photosynthesis with irradiance exceeding 400 μmol m^{-2} sec^{-1} (84 W m^{-2}) with a stream periphyton [123]. Moreover, Graham *et al.* reported photoinhibition with irradiance exceeding 1500 μmol m^{-2} sec^{-1} (315 W m^{-2}) with benthic *Spirogyra* [124]. Finally, Hill *et al.* studied the light limitation in benthic algae in streams and

reported that irradiance above 350 μmol m^{-2} sec^{-1} (74 W m^{-2}) resulted in photoinhibition [125].

The irradiation magnitude and spectral quality are critically important for the cultivation of algal biofilms as (i) biomass productivity is directly proportional to the rate of photosynthesis and (ii) the light intensity is attenuated exponentially across the biofilm . Indeed the intensity of light can decrease by two orders of magnitude within a photosynthetic biofilm thickness of 1 mm . Due to this gradient at high irradiance while the cells on top of the biofilm are photoinhibited, the cells at the subsurface can be exposed to optimum or limited irradiances [119]. Thus, when the whole biofilm community is considered irradiances much larger than typically used in planktonic systems can result in increase in the total rate of oxygen production [119].

Chapter 3

Reduction of Water and Energy Requirement of Algae Cultivation Using an Algae Biofilm Photobioreactor

3.1 Introduction

Cultivation of algae is a promising method for producing renewable hydrocarbon feedstock for biofuel production as (i) select algae species can produce about two orders of magnitude more oil per acre than from soybeans, (ii) algae cultivation does not require arable land, and (iii) can use marginal sources of water not suitable for drinking or irrigation [2]. However, a cost effective algae cultivation technology that can be scaled up to sizes large enough to make a significant contribution in reducing our dependence on foreign oil has yet to be realized [2, 28, 126]. In part, this stems from cultivation of dilute biomass concentrations in conventional systems, such as raceway ponds as well as flat plate and tubular photobioreactors (PBR), where algae cells are suspended in the liquid phase [11, 23, 127]. These technologies require (i) in excess of 6000 gallons of water to cultivate 1 gallon of algae oil, (ii) a large amount of energy for pumping and circulating a dilute algae suspension as large as 385.71 MJ per kilogram of cultivated algae, and (iii) energy intensive dewatering and biomass concentration processes for downstream use of the

biomass resulting in energy requirements of up to 82 MJ per kilogram algae biomass produced [1, 2, 12, 28]. To address these challenges, this chapter reports the design, operation, and performance of a novel photobioreactor based on algal biofilm cultivation that reduces the water and energy requirements of algae cultivation for economic and sustainable biofuel production.

3.2 Materials and Methods

3.2.1 Inoculum preparation

In this study the green alga *Botryococcus braunii* (LB 572) was employed due to its capability to produce biofilms and capacity to accumulate hydrocarbons [2]. The strain was obtained from UTEX culture collection at the University of Texas at Austin. The inoculum was cultivated in the autotrophic nutrient medium BG-11 due to its superiority over BBM, BBMa, and modified Chu13 media in terms of biomass and lipid productivity [128]. The culture was continuously sparged with air containing 1% by volume CO_2 and illuminated with fluorescent light bulbs (Home Light Cool White Plus, Philips, Netherlands) at 100 μE m^{-2} s^{-1} (21 W m^{-2}) in the photosynthetically active radiation (PAR) measured with a quantum sensor (LI-COR, Model LI-190SL; LICOR Inc., Lincoln, NE, USA).

3.2.2 Photobioreactor construction and operation

Figure 3.1 shows the schematic of the algae biofilm photobioreactor. The system consists of (i) a biofilm growth surface, (ii) a nutrient medium

recirculation system, and (iii) an illumination system. The biofilm growth surface was an 8 mm thick concrete layer (Commercial Grade Quikrete Quick Settling Cement, ATL, USA) over a wood support plate and had an active cultivation area of 0.275 m^2. The initial pH of the concrete was 13 which served to sterilize the immobilization surface. In order to decrease the surface pH to a more favorable level for algal growth, the concrete surface was carbonated with 1.9 M $NaHCO_3$ solution. At the completion of the carbonation the surface pH was stabilized at 8.3.

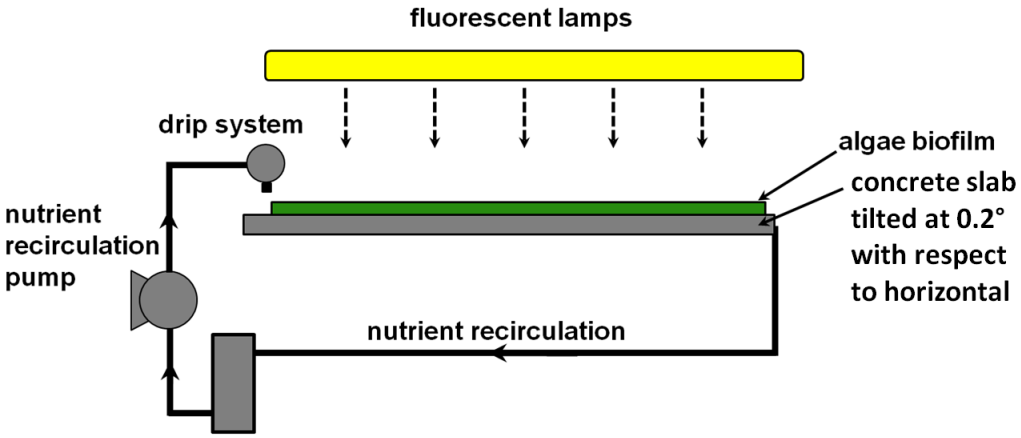

Figure 3.1: Schematic of the algae biofilm photobioreactor system.

The nutrient medium BG-11 was delivered by dripping nozzles (Adjustable Dripper, DIG Irrigation Products, CA, USA) located above the concrete surface at a total rate of 150 mL min^{-1}. The growth surface was tilted by 0.2^o with respect to the horizontal to enable the flow of nutrient medium over the algae biofilm by gravity. At the end of the growth surface the nutrient medium was collected and delivered to the reservoir by gravity. Finally,

the medium was pumped to the dripping system located 3.6 cm above the reservoir using a peristaltic pump (Master Flex L/S 7524-40 and HV-0701452, Cole-Parmer Instrument Company, IL, USA). During the operation of the photobioreactor, the liquid volume over the growth surface as well as the liquid volume in the rest of the system was 300 mL each giving a total volume of 600 mL. The growth surface was illuminated with four 32 W fluorescent lamps (Philips, Home Light Cool White Plus, Netherlands) providing 55±3 μE m^{-2} s^{-1} (11.55±0.63 W m^{-3}) irradiation in the PAR measured with a quantum sensor (LI-190SL, LI-COR Inc., NE, USA). Spectral irradiance of the fluorescent bulbs was measured using a lock-in amplifier (SR830, Stanford Research Systems, CA, USA) and a monochromator (Cornerstone 260, Newport, CA, USA). Figure 3.2 shows the normalized spectral irradiance of the fluorescent light bulbs over the spectral range from 400 to 700 nm. The normalization was performed with respect to the maximum irradiance at the wavelength of 543 nm. The results indicated that the fluorescent bulbs had major peaks at 435, 490, 545, 585, and 615 nm in PAR.

The carbonated concrete surface was inoculated with 500 mL of *B. braunii* culture during its exponential growth phase at a concentration of 0.50 kg m^{-3} giving an initial inoculation of 0.90±0.01 g m^{-2}. In order to promote cell attachment, nutrient media was not circulated for 5 days and the cells were allowed to settle and attach on concrete. The biofilm photobioreactor was operated for 35 days under continuous illumination. Moreover, samples from the biofilm were taken at regular intervals and observed under optical microscope

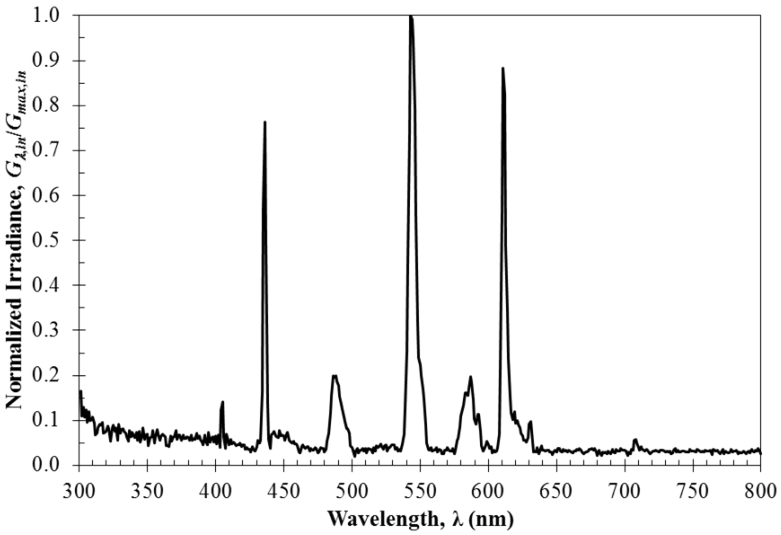

Figure 3.2: The spectra of the irradiance provided by the fluorescent light bulbs normalized by its maximum value G_λ/G_{max}.

(Eclipse 80i, Nikon, Japan) to check for contamination by other species. Over the course of experiments no contamination of the culture was observed. Figure 3.3 shows the micrograph of an algae biofilm sample indicating the densely packed *B. braunii* cells in the biofilm containing oil droplets.

3.2.3 Biofilm thickness, direct harvest biomass density measurement and areal biomass productivity

At the end of the 35^{th} day, the algae biofilm was divided into 9 subsections and biomass was harvested from the concrete surface by gentle mechanical scraping with a squeegee. This method does not incorporate any contaminating chemicals, such as flocculants, thus eliminates any additional purification process. During scraping care was taken to ensure that the har-

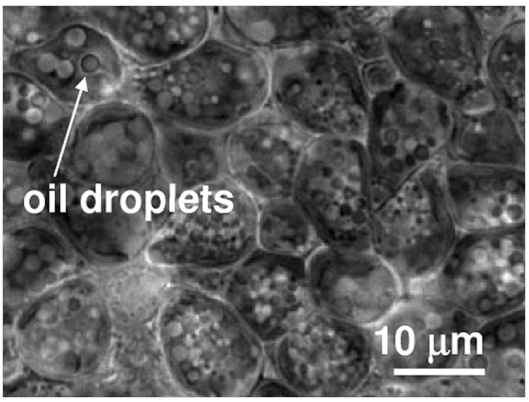

Figure 3.3: Bright-field optical micrograph of *B. braunii* biofilm.

vested biomass was free from contaminations thus no further purification was necessary. The biomass and lipid productivities of each area was determined individually to evaluate the variation in performance across the bioreactor. Figure 3.4 shows the picture of the biofilm photobioreactor before and after harvest. First the volume of the direct harvest V_H was quantified using a pipette. Using the total volume of the harvest and the cultivation surface area A_S the algal biofilm thickness t_b was estimated as $t_b = V_H/A_S$. Then, the biomass was dried in pre-weighed aluminum weighing boats at 60^{o}C in a vacuum oven (Isotemp Vacuum Oven, Model 280A, Fisher Scientific, NH, USA). The dry biomass was weighed using an analytical scale (Model AB135-S/FACT, Mettler Toledo, Switzerland) over time to ensure the weight did not vary. Using the dry weight W_{dry}, the biomass density of the direct harvest X_H was estimated as $X_H = W_{dry}/V_H$.

Moreover, the areal productivity R_A was estimated as the ratio of the

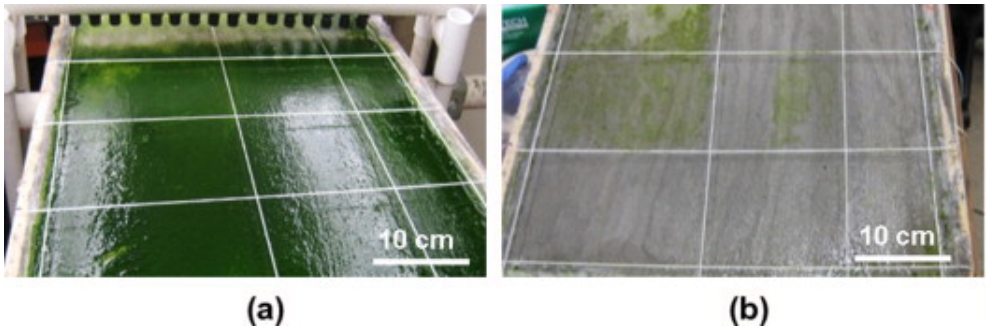

Figure 3.4: (a) Biofilm photobioreactor cultivating algae, (b) biofilm photobioreactor after harvesting the algal biofilm.

net dry biomass weight produced over the total cultivation surface area, W_{net} over the entire cultivation period Δt as, $R_A = W_{net}/(A_S \cdot \Delta t)$.

3.2.4 Lipid extraction and analysis

To determine the neutral lipid content of the cultivated algae, part of the dried biomass was weighed and homogenized in mortar and pestle with gas chromatography grade n-hexane (H307-4, Fisher Chemical, PA, USA) for 15 minutes and the supernatant obtained from centrifugation was dried under nitrogen flow according to Rao *et al.* [129]. The weight of the extracted lipids was determined gravimetrically using the analytical balance to obtain the weight fraction of neutral lipids x_L. In addition, using the remaining part of the biomass total lipids, both polar and nonpolar, were extracted by Folch method and quantified gravimetrically [130].

3.2.5 Light to biomass and neutral lipid energy conversion efficiency

The light to biomass energy conversion efficiency η_B is computed according to,

$$\eta_B = \frac{W_{net} E_B}{G_{in} A_s \Delta t} \tag{3.1}$$

where E_B is the heating value of the dry biomass equal to 28.3 MJ kg^{-1} dry weight for *B. braunii* [131], G_{in} is the irradiation, and Δt is the total duration of the experiment. Finally, the light to neutral lipid energy conversion efficiency η_L of the system was estimated as,

$$\eta_L = \frac{x_L W_{net} E_L}{G_{in} A_s \Delta t} \tag{3.2}$$

where x_L is the mass fraction of neutral lipids in the biomass, and E_L is the heating value of the algal lipids equal to 37.5 MJ kg^{-1} [132].

3.2.6 Net energy ratio

The net energy ratio of the photobioreactor system was quantified according to

$$NER = \frac{W_{net} E_B}{E_{aux}} \tag{3.3}$$

where E_{aux} is the auxiliary energy input associated with pumping and dewatering and does not include energy associated with the light input as ultimately sun is envisioned as the light source.

3.3 Results and Discussion

Table 3.1 summarizes the key system parameters obtained for cultivating *B. braunii* in the algal biofilm photobioreactor. It indicates that the algal biofilm grew to an estimated thickness of 278±21μm over the 35 day cultivation period yielding a net dry biomass yield of 24.94±2.07 g m^{-2}. This corresponds to a light to biomass energy conversion efficiency of 2.02±0.17%. Moreover, the direct harvest from the biofilm photobioreactor yielded a biomass concentration of 96.4±6.8 kg m^{-3}. Based on the lipid extraction and analysis, 9.81±0.81% of the dry biomass was neutral lipids which corresponds to a light to neutral lipid energy conversion efficiency of 0.26±0.03%. In addition, based on Folch extraction, the total lipid content of the biomass was 26.8±2.05% by weight. Finally, during the operation of the photobioreactor, a total of 32.29±0.47 kJ of energy was used in the nutrient recirculation, and an evaporative loss rate was 1.09±0.05 L m^{-2} day^{-1} for the system.

Table 3.1: Parameters on start up, cultivation, and harvest of the biofilm

Parameter	Value and uncertainty
Irradiance (W m^{-2})	11.55 ± 0.63
Ambient temperature (^{o}C)	25 ± 1
Total liquid volume of the system (L)	0.60 ± 0.01
Total area of the system (m^2)	0.275 ± 0.010
Total duration of the experiments (days)	35.0 ± 0.5
Evaporative loss rate (L m^{-2} day^{-1})	1.09 ± 0.05
Total pump energy used (70% pump efficiency) (kJ)	32.29 ± 0.47
Net biomass yield (g m^{-2})	24.94 ± 2.07
Total lipid fraction of the biomass (Folch method) (%)	26.80 ± 2.05
Biomass thickness at the time of the harvest (μm)	278 ±21
Initial biomass inoculation (g m^{-2})	0.90 ±0.01

Based on these results the productivity, energy and water use of the biofilm photobioreactor were estimated. Table 3.2 summarizes these results and compares them with those of a raceway pond, flat-plate and tubular photobioreactors. Due to lack of consistent set of data for these photobioreactors cultivating *B. braunii*, the comparison is given with respect to systems cultivating *Nannochloropsis sp.* reported by Jorquera *et al.* [1]. The results indicate that the areal productivity of the biofilm photobioreactor was 0.71±0.06 g m^{-2} day^{-1} which was 1/15 and 1/35 times as much as that achieved in open pond and closed photobioreactor cultivating *Nannochloropsis*, respectively, and about one quarter of the highest areal biomass productivity reported for *B. braunii* cultivated in suspension at a lab setting [1, 133]. The reasons for the observed low areal productivity can be attributed to (i) *B. braunii* being a notoriously slow grower with a doubling time ranging from 40 h to 6 days compared with *Nannochloropsis sp.* having a doubling time of about 29 h [134], (ii) to low irradiation used in this experimental system having a magnitude of only 11.55 W m^{-2} compared with the outdoor systems cited receiving daily irradiation of 109.5 W m^{-2}, and (iii) to mass transport limitations of the biofilm [126, 135, 136]. Indeed, the light to biomass energy conversion efficiency of the algal biofilm photobioreactor in this study was 2.02±0.17% based on PAR which was comparable with those of other systems. For instance, areal biomass productivities corresponding to 2% solar energy conversion efficiency under outdoor conditions are on the order of 30 to 40 g m^{-2} day^{-1} [137]. It should be noted that photosynthesis is light limited

Table 3.2: Comparison of the performance of the current system with those of raceway ponds, flat plate, and tubular PBRs reported in the literature.

	Race. ponds	Fl.-pl. PBR	Tubul. PBR	B.film PBR[e]
Biomass concentration (g L^{-1})	0.35[a]	2.7[a]	1.02[a]	96.4
Neutral lipid content (%)	29.6[b]	29.6[b]	29.6[b]	9.81
Areal biomass productivity (g m^{-2} day^{-1})	11[a]	27[a]	25[a]	0.71
Energy input per kg of biomass (MJ kg^{-1})	9.18[a,c]	16.96[a,c]	385.71[a,c]	4.71
NER on biomass (direct harvest)	3.44[a]	1.86[a]	0.08[a]	6.01
NER on biomass including dewatering with tangential flow filtration to produce an algae cake ready for lipid extraction.	1.06[d]	1.61[d]	0.08[d]	6.00

[a] Based on data compiled by Jorquera *et al.* [1].
[b] Based on lipid content reported by Rodolfi *et al.* [138].
[c] Based on energy requirement for 24 h of daily pumping within the system as suggested by Chisti [2].
[d] Based on Uduman *et al.* for calculation of dewatering energy requirement [12].
[e] Results obtained in this study.

at low and light inhibited at large intensities [2]. The incident light intensity and spectral quality are critically important for the cultivation of algal biofilms as (i) biomass productivity is directly proportional to the rate of photosynthesis and (ii) the light intensity is attenuated exponentially across the biofilm [115, 116, 119]. Indeed the intensity of light can decrease by two orders of magnitude within a photosynthetic biofilm thickness of 1 mm [115, 117, 118]. Due to this gradient at high irradiance while the cells on top of the biofilm are photoinhibited, the cells at the subsurface can be exposed to optimum or limited irradiances based on thickness of the biofilm [119, 139]. Thus, when the whole biofilm community is considered, irradiances much larger than typically used in planktonic systems can result in increase in the total rate of photosynthesis

[119, 139]. For instance, Dodds *et al.* studied the rate of photosynthesis of a mixed culture algal biofilm collected from a river and reported increases in overall photosynthesis rate with increasing irradiance of up to 6000 μE m^{-2} s^{-1} (1260 W m^{-2}) [139]. For comparison it should be noted that solar irradiance goes up to about 2000 μE m^{-2} s^{-1} (420 W m^{-2}) at noon time [121]. Thus it is expected that under larger irradiance, the algal biofilm photobioreactor productivity can be further increased. To circumvent any possible photo-oxidative damage to the cells, the cultivation surface can be corrugated to work with reflected light over larger surface area rather than with direct irradiation. This strategy will not only minimize photoinhibition, but also (i) increase the surface to volume ratio for O_2 desorption and (ii) increase the biofilm growth area per reactor footprint increasing areal productivity.

One of the reasons for the lower productivity of the current system compared to suspended systems is the mass transport limitation. Due to no slip condition for fluid flow over the biofilm surface, hydrodynamic and concentration boundary layers form [96]. These boundary layers reduce the nutrient flux from the liquid phase to the biofilm resulting in diffusion dominated nutrient transport [97, 98]. To increase the mass transfer of nutrients the bulk flow velocity of nutrient solution and concentration of its constituents can be increased. Indeed, increases in biological activity and growth rate have been reported for increased flow velocities and nutrient concentrations in mixed culture benthic algae [100–103, 110, 111, 113].

Temperature is another critical parameter significantly affecting the

biomass productivity of algae cultivating systems. The thermal effects including culture temperature and evaporative losses in algae bioreactor have recently been reported by Murphy and Berberoglu [140]. The authors reported that biofilm photobioreactors are more prone to culture temperature fluctuations as these systems contain significantly smaller quantities of water than planktonic systems which help buffering the system temperature [140]. To reduce these fluctuations, the authors suggested using selective covers that are transparent in PAR while opaque in infrared radiation or increasing thermal capacitance of the system.

Based on the neutral lipid fraction of the biomass, the areal lipid productivity was estimated to be 277±32 L ha^{-1} $year^{-1}$, corresponding to a light to lipid energy conversion efficiency of 0.26±0.05%. The reason behind the low productivity is the combination of low biomass productivity combined with relatively low neutral lipid content of *B. braunii*. Thus, in future systems a strain capable of benthic growth with higher biomass and neutral lipid productivities should be investigated. Moreover, nitrogen starvation and other nutrient stresses can more easily be imposed in the benthic system to further increase the lipid productivity as the biomass is decoupled from the nutrient medium.

The water requirement of the biofilm photobioreactor was 1618 L kg^{-1} biomass produced. This is encouraging when compared to that of an open pond system which is 2857 L kg^{-1} [1]. In the biofilm system more than 95% of the water requirement was due to the evaporative losses. This can be

attributed to the large surface to volume ratio of these photobioreactors which is on the order of 550 m^2 m^{-3} compared to open ponds which have 6.67 m^2 m^{-3} [11]. While evaporation is undesirable as it increases the fresh water and auxiliary energy inputs for biofuel production, it is critical for buffering the temperature of the system. To decrease the evaporative losses and maintain optimal temperature ranges within the system, the PBR can be closed with a transparent film capable of blocking infrared radiation.

Finally, the biofilm photobioreactor required 4.71±0.62 MJ of energy per kg dry biomass produced. This corresponds to a net energy ratio (NER) of 6.01±0.49. To bring this achievement in perspective let us consider the energy requirements of raceway ponds, flat plates and tubular photobioreactors which are 9.18, 16.96, and 385.71 MJ kg^{-1}, respectively corresponding to a NER of 3.44, 1.86, and 0.08, respectively, based on 24 hours of daily pumping [1, 2]. It should be noted that these NER values only take into account the energy required for biomass cultivation and exclude those of harvesting. The direct algal biomass harvest from the biofilm photobioreactor in this study yielded a concentration of 96.4 kg m^{-3}, which is about 275, 35 and 95 times as concentrated as the biomass concentration of the direct harvest from a raceway pond, flat plate and tubular photobioreactor systems, respectively [1]. For downstream processing, the harvest needs to be concentrated to an algae cake with a solid content of 15 to 25% by weight [12]. To achieve this concentration tangential flow filtration or centrifugation are being used which require an energy input of 2 and 8 kWh m^{-3} of algae suspension processed, respectively

[12]. To produce a kilogram of algae cake using tangential flow filtration, 2.86, 0.37, 0.98 m^3 of suspension has to be treated requiring an energy input of 21, 2.7, 7.1 MJ for raceway ponds, flat plate and tubular photobioreactors, respectively. On the other hand, the dewatering of the biomass harvested from the biofilm PBR requires only 0.075 MJ of additional energy which is about 0.3% of the dewatering energy requirement of the raceway pond harvests. When filtration based harvesting and dewatering are included in the system boundaries of NER calculation, the NER of raceway ponds, flat plate and tubular photobioreactors, decrease to about 1.06, 1.61, and 0.08, respectively, for algal biomass production. Thus, open ponds and tubular photobioreactors consumes more or similar amounts of energy compared to the energy output from these systems. However, even with the additional harvest energy requirement, the NER for the biofilm photobioreactor is equal to 6.00±0.56. These results indicate that even at a biomass productivity of 0.7 g m^{-2} day^{-1} attained with the current system, the net energy output is equal to that from an open pond with a productivity of 9.3 g m^{-2} day^{-1} indicating the importance of biomass harvest concentrations.

Finally, algal biofilm photobioreactors are not mature technologies but hold potential to be further developed for achieving energy and water efficient algae cultivation targeted for biofuel production. To optimize the productivity and performance of these systems (i) light, mass, and thermal energy transport in these systems should be investigated to identify and mitigate the major bottlenecks through system design, (ii) species capable of benthic growth that have

higher biomass and lipid productivities should be identified and incorporated, (iii) biofilm photobioreactors with proper corrugation maximizing photon use should be designed, and (iv) strategies for minimizing evaporative losses and contamination should be developed. Moreover, to bring these systems closer to practical implementation, pilot scale biofilm photobioreactors should be tested under outdoor conditions, and life cycle analysis of these systems should be conducted for assessing their energy, economic, and environmental impacts.

3.4 Conclusion

The novel algae biofilm photobioreactor reported in this study was capable of producing direct algal harvest density of 96.4 kg m^{-3} which is approximately 35 times as concentrated than the highest reported direct harvest, making the downstream process integration easier and less energy intensive. Moreover, the system achieved a net energy ratio of 6.00 while that of open ponds was 1.06. Also, the light to biomass conversion efficiency was 2.02% comparable with that of planktonic systems. Finally, the system is open for further improvement through research on thermal management, mass and light transfer optimization as well as algal species selection.

Nomenclature

A_s	cultivation surface area, m^2
G_{in}	the incident light energy, W m^{-2}
t_b	algal biofilm thickness, μm

V_H	volume of the direct algal biomass harvest, m^3
E_{aux}	auxiliary energy input for pumping and dewatering, MJ
E_B	heating value of algal biomass, MJ kg^{-1}
E_L	heating value of algal neutral lipids, MJ kg^{-1}
R_A	areal biomass productivity, kg m^{-2} day^{-1}
W_{dry}	total dry weight of biomass harvested, kg
W_{net}	net dry weight of biomass produced, kg
X_H	density of direct algal biomass harvest, kg m^{-3}
x_L	the mass fraction of neutral lipids in the biomass

Greek symbols

Δt	total duration of experiments, days
η_B	light to biomass energy conversion efficiency, %
η_L	light to lipid energy conversion efficiency, %

Chapter 4

Algal Adhesion to Surfaces

4.1 Introduction

Microalgae are a diverse group of unicellular or multicellular photosynthetic microorganisms having sizes ranging from 2 to 140 μm [141, 142]. These microorganisms are capable of forming highly productive biofilms over surfaces [77]. Unintended formation of algal biofilms is undesirable such as (i) on ship hulls as biofilms increase drag and decrease fuel efficiency of transportation, (ii) on cooling-heating systems as they increase pressure drop and decrease thermal efficiency, and (iii) in photobioreactors they cause biofouling lowering the performance of these systems [2, 15, 83, 143]. On the other hand, algal biofilms are complex biological systems where their optimized formation and cultivation offers unique advantages in wastewater treatment and biofuel production technologies [46, 47, 144–147]. In wastewater treatment, algal biofilms offer higher quality effluent compared to suspended cell cultivation since the effluent is free of algal cells [46]. In biofuel production, cultivation of algae as biofilms reduces the requirement for the volume of water and the associated pumping power as well as producing concentrated biomass, thus minimizing the need for energy and capital intensive harvesting and dewatering technologies [147].

The studies reported in the literature on algae substrate interactions are concentrated on the effects of substrate surface energy and exclude the effects of algal surface properties on adhesion of cells. To the best of our knowledge, there is no comprehensive study that takes into account the surface properties of both the algae and the adhesion substrate. This chapter addresses this gap in the literature (i) by reporting a complete set of physico-chemical surface properties of both algae and substratum surfaces obtained from experimental measurements, (ii) by modeling surface interactions through thermodynamic, Derjaguin, Landau, Verwey and Overbeek (DLVO), and extended DLVO (XDLVO) models and (iii) by validating the results of model predictions with experimental data. To identify critical parameters controlling algal adhesion, glass and indium tin oxide (ITO) were chosen as adhesion substratum with large and small surface energy, respectively. Moreover, *C. vulgaris* and *B. sudeticus* were chosen as representative planktonic and benthic algal species to quantify their surface properties and compare their interactions with different adhesion substrata.

4.2 Materials and Methods

4.2.1 Algae culturing and sample preparation

Chlorella vulgaris (UTEX 2714) and *Botryococcus sudeticus* (UTEX B 2629) were obtained from the Culture Collection of Algae at the University of Texas at Austin, UTEX. The algae were cultivated as batch cultures in BG-11 nutrient medium [148] supplied with 2.5 vol.% CO_2 under continuous

irradiation of 125 μE m^{-2} sec^{-1} (26.25 W m^{-2}). Algal cultures in log-phase of growth were harvested with centrifugation at 3000 rpm (1962 g) for 5 minutes and washed twice and re-suspended in phosphate buffered saline (PBS) containing 1.62 mM KH_2PO_4, 6.49 mM K_2HPO_4, and 1.35 mM NaCl. PBS prepared had a pH of 7.559 $\pm$0.019 (Accumet AB15 Plus, Fisher Scientific, USA), a conductivity of 1.777$\pm$0.026 mS cm^{-1} (Con 2700, Oakton, USA), and an ionic strength of 19.60 mM. The PBS was prepared to match the pH and ionic strength of BG-11. Before further experiments *B. sudeticus* suspensions were passed through a syringe needle with an opening diameter of 0.34 mm multiple times to break the flocs that were present within the suspension. This process ensured that a homogenous size distribution was obtained for the experiments.

Surface free energy of algal cells were quantified based on the method described by Busscher *et al.* [149]. In this method, algae mats were prepared on 0.45 μm mixed cellulose acetate filters (Nalge Nunc International, USA) by filtering algae suspensions that were washed twice with deionized water. The average mat thickness obtained in this study was about 200 μm over the filter surface. The algal mat thicknesses were determined based on the images obtained with the goniometer. The prepared algal mats were placed over 1% agar (weight to volume) prepared with 10% (volume to volume) glycerol in water until experimentation to keep the mats moist.

4.2.2 Characterization of morphological properties of algal cells

Morphological properties of algal cells were quantified based on their images obtained with an inverted microscope (Nikon Ti-E, Nikon, USA). The major and minor diameters of the cells were determined using the image analysis software ImageJ [150]. Also, the equivalent spherical diameters were determined for the cells such that the volume of the equivalent sphere was the same as that of the ellipsoidal cell with the specified major and minor diameters. Finally, the circularity of cells were determined according to [150],

$$Circularity = 4\pi \frac{A_{cell}}{P_{cell}^2} \tag{4.1}$$

where A_{cell} and P_{cell} are the imaged area and the perimeter of the cell [150]. A circularity of one indicates that the cell is perfectly spherical [150].

4.2.3 Adsorption surface preparation

Glass (Fisherfinest Premium Microscope Slides, Fisher Scientific, USA) and indium tin oxide (ITO) coated glass (CG-40IN-1115, Delta Technologies, USA) were selected as hydrophilic and hydrophobic surfaces, respectively. Microscope glass slides were cleaned in hydrochloric acid for 5 hours. Cleaned slides were rinsed with deionized (DI) water and cleaned in ultrasonic bath with 1% Alconox (Alconox Inc., Alconox, NY) solution, ethanol, and acetone for 10 minutes each, and air dried after rinsing with DI water. ITO coated

glass surfaces were cleaned in the ultrasonic bath with 1% Alconox solution for 10 minutes. After sonication and rinsing with DI water, ITO coated glass surfaces were air dried.

4.2.4 Contact angle measurements for algal cells and adhesion substrates

Surface energy of algal cells and adhesion substrates were quantified based on contact angle measurements made with the sessile drop technique using water, diiodomethane and formamide as the reference liquids [149]. Contact angles of all the probe liquids were measured using a goniometer (Model 190 CA, Rame-Hart, USA). Successive droplets of deionized water with 5 μL volume were placed over the mats until contact angle measurements were stabilized. After stabilization, contact angles of all the probe liquids were determined. The results presented are the average of at least 14 measurements performed with each probe liquid which resulted in standard deviations of at most 9%.

4.2.5 Zeta potential measurements

Algal suspensions with cell number concentrations of 2.5×10^{10} m^{-3} were used for the zeta potential measurements. Electrophoretic mobility measurements of algal cells were conducted with a Zeta meter (ZetaCompact, CAD, France) at a voltage of 80 V. Using the mobilities measured, zeta potential, ζ, of cells were determined with Smoluchowski's equation [151]. To quantify the zeta potential of glass, streaming potential measurements were

made with glass slides using an electrokinetic analyzer (SurPASS, Anton Paar GmbH, Austria). Moreover, to quantify the zeta potential of ITO, streaming current measurements were made with ITO coated glass slides. Streaming current measurements were conducted with ITO to ensure that surface conductivity of this surface was taken into account for the quantification of its zeta potential [152]. The Fairbrother-Mastin approach was used for calculation of the zeta potential of these substrata based on the streaming potential and current measurements performed [153, 154].

4.2.6 Adhesion density and strength measurements

A parallel plate flow chamber was constructed for measuring the adhesion density and strength of algal cells over different substrates. Figure 4.1 shows the side and top view of the flow chamber. A 0.75 mm thick spacer made of polydimethylsiloxane (PDMS) (Sylgard 184 Silicone Elastomer Kit, Dow Corning, USA) was sandwiched between a transparent polycarbonate sheet on top and test surface on the bottom to create the flow chamber. The length, width and height of the chamber were 50.8 mm, 26.0 mm, and 0.75 mm, respectively. Two fluidic adapters were placed at the inlet and outlet of the flow chamber for flowing the algae suspension. The fluid introduced at the inlet was slowly expanded at an angle of 15^o to ensure laminar flow.

Figure 4.2 presents the setup used for the adhesion tests. A syringe pump (NE-1000, New Era, USA) was used to deliver the algae suspensions from the reservoir to the flow chamber by pulse free suction. The algae sus-

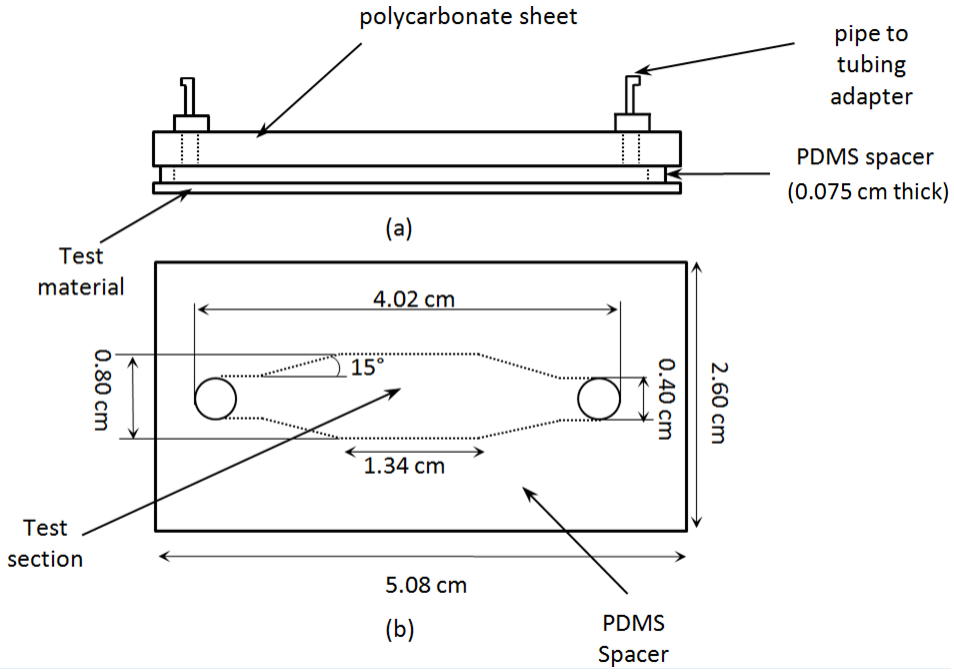

Figure 4.1: (a) Side and (b) top view of the parallel plate flow chamber.

pension inside the reservoir was constantly stirred at 120 rpm using a magnetic stirrer (Isotemp, Fisher Scientific, USA) to ensure homogeneity. Algal suspensions with cell number concentrations of $9.47 \pm 0.12 \times 10^{12}$ m^{-3} were delivered to the chamber at a rate of 0.450 ± 0.05 ml min^{-1} for 5 minutes. The required cell number densities were obtained by measuring the optical density of each sample at 750 nm in a 1 cm path length cuvette using a spectrophotometer (Genesys 20, Thermo Scientific, USA) and by counting the number of cells using a hemocytometer (Bright-line, Hausser Scientific, USA). For each adhesion experiments a total of at least 2000 cells were counted to ensure repeatability of cell number densities. After five minutes of operation, pump was stopped

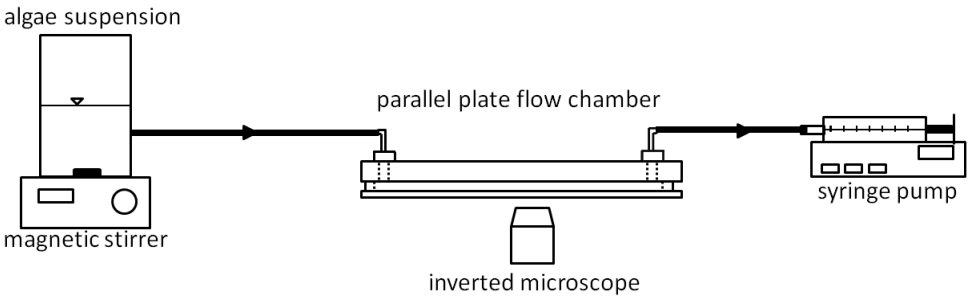

Figure 4.2: Schematic of the experimental setup used for cell in-situ attachment and detachment quantification.

and the cells were left undisturbed for two hours. Reynolds number, Re, and wall shear rate, $\dot{\gamma}$, over the test section were 0.97±0.01 and 10.13±0.10 s^{-1}, respectively, during the flow of the algal suspension. The temperature of the algal suspensions were 20±1 ^{o}C. The attachment surface was imaged with an inverted microscope (Nikon Ti-E, Nikon, USA) equipped with a digital camera (DS-QI1, Nikon, Japan) and a 10X objective (Nikon Fluor 10X, Nikon, USA) for *in situ* enumeration of attached cells. A surface area of 0.541 mm^{-2} was imaged every minute during the flow of the algal suspension. The images were processed using the image analysis software ImageJ to quantify the number of attached cells and the adhesion density as a function of time [150]. The cells that remained attached after 5 minutes of washout with a shear rate of 10 s^{-1} were considered to be adhered and the experiments were continued until the adhesion densities were saturated. Results presented are the average of at least duplicate experiments performed.

After the cell density saturates in order to quantify the adhesion strength

the flow inside the chamber was increased stepwise from 4.50 to 31.50 ml min^{-1} with increments of 2.25 ml min^{-1} which corresponds to Re and $\dot{\gamma}$ ranging from 9.71 to 67.99 and from 101.27 s^{-1} to 708.86 s^{-1}, respectively. In addition to wall shear rate, the net force due to lift and drag forces acted on cells were also calculated based on equations provided by Busscher and van dar Mei [155]. Before these desorption experiments, the algal suspension in the reservoir was replaced with PBS to avoid the effects of suspended cell-attached cell collisions on desorption kinetics. Each of the flow rates were maintained for a duration of 1 minute and the adhesion area was imaged at the end of each flow duration to quantify the number of cells still attached on the substrate.

4.2.7 Lift and drag forces acting on the cells

A cell that is adhered over a substrata within a parallel plate flow chamber experiences lift and drag forces due to fluid flow [155]. The lift force is due to variation of flow velocity around the adhered cell. This force desorbs the cells since it acts in the opposite direction of the adhesive cell-surface interactions [155]. The lift force acting on a spherical cell is defined as [155],

$$F_L = 81.2\eta r^2 (\frac{\dot{\gamma}\rho}{\eta})^{1/2} v(a) \tag{4.2}$$

where η and ρ are the viscosity in Pa s and the density in kg m^{-3} of the fluid, respectively, a is the cell radius in m, $\dot{\gamma}$ is the wall shear rate in s^{-1}, $v(a)$ is the flow velocity over the substrata at a vertical distance equal to the radius of the cell in m s^{-1}. The wall shear rate is calculated as [155],

$$\dot{\gamma} = \frac{6Q}{b^2 w} \tag{4.3}$$

where Q is the volumetric flow rate in $m^3\ s^{-1}$, b is the depth and w is the width of the parallel plate flow chamber in m. For fully developed laminar flow in a rectangular channel, the velocity profile can be given as [155],

$$v(c) = 6\frac{Q}{bw}\frac{c}{b}(1 - \frac{c}{b}) \tag{4.4}$$

where c is the vertical distance from the substratum surface in m. Viscous drag acts in the same direction as the flow and can desorb the cells through rolling [155]. The drag force is usually larger than the lift force and is given as [155],

$$F_D = 1.7009(6\pi\eta r v(a)) \tag{4.5}$$

where $v(a)$ is the flow velocity over the substrata at a vertical distance equal to the radius of the cell in $m\ s^{-1}$.

4.3 Results and Discussions

4.3.1 Properties of algal species and substrates

Table 4.1 presents the morphological properties of the algal species studied. The results indicate that both species have circularity close to one, 0.93 and 0.94 for *C. vulgaris* and *B. sudeticus*, respectively, indicating that

these species can safely be approximated as spheres. Moreover, *C. vulgaris* and *B. sudeticus* have equivalent spherical diameters of 5.34 μm and 4.48 μm, respectively. These equivalent spherical diameters were used as the size parameters of algal cells in the subsequent modeling studies.

Table 4.1: Shape and size parameters of *C. vulgaris* and *B. sudeticus*

Species	Major dia.(μm)	Minor dia.(μm)	Equivalent Sph. Dia. (μm)	Circularity
C. vulgaris	5.62±1.15	5.08±0.70	5.34±0.97	0.93±0.06
B. sudeticus	4.48±1.43	4.17±1.46	4.32±1.44	0.94±0.02

Table 4.2 summarizes the experimentally measured surface properties, including the total surface free energy (γ), the free energy of cohesion (ΔG_{coh}), and the surface potential (ψ) of glass, ITO, *C. vulgaris*, and *B. sudeticus* surfaces. Based on the free energy of cohesion the table indicates that glass and *C. vulgaris* have hydrophilic, ITO and *B. sudeticus* have hydrophobic surfaces. Moreover, all hydrophilic surfaces have a larger surface free energy compared to hydrophobic surfaces. The LW component of surface free energy of glass is larger than that of ITO indicating larger LW interaction for glass. Bayoudh *et al.* reported similar values for the surface energy properties of the ITO [156].

All surfaces analyzed in this study had negative surface potentials. The surface potential of *B. sudeticus* and *C. vulgaris* were calculated using Equation (2.16) using the zeta potentials quantified experimentally. The results indicated that *B. sudeticus* had a larger surface potential compared to *C. vul-*

Table 4.2: Physico-chemical surface properties of the algal species and substrata.

	Surface energy components, free energy of cohesion (mJ m^{-2}), and surface potential (ψ) (mV)						
Surface	${\gamma_s}^{LW}$	${\gamma_s}^{AB}$	${\gamma_s}^{-}$	${\gamma_s}^{+}$	γ	ΔG_{coh}	ψ
Glass	47.1	9.0	54.7	0.4	56.1	32.0	- 35.49
ITO	34.2	0.7	4.2	0.0	34.9	-64.4	-0.79
C. vulgaris	37.8	5.1	41.2	0.2	42.9	20.8	-25.56
B. sudeticus	28.3	0.2	2.8	0.0	28.5	-69.0	-38.95

garis. Moreover, ITO had a surface potential close to zero. Noting that the pH of the PBS used for the experiments was about 7.6, this result is in agreement with the data reported in the literature where ITO's isoelectric point, i.e., the pH at which ITO's surface potential goes to zero, is between pH 7 and 8 [157]. Furthermore, glass had a much larger zeta potential than that of ITO indicating that a much larger repulsive cell-substrata interaction should be expected with glass.

Thermodynamic model

Table 4.3 summarizes the free energy of adhesion and the associated AB and LW components based on the thermodynamic model. The results indicate that adhesion is expected for *B. sudeticus* interacting with glass or ITO and *C. vulgaris* interacting with ITO. Adhesion is not expected for the *C. vulgaris*-glass system as both surfaces are hydrophilic. The largest magnitude of attractive energy is observed for the *B. sudeticus*-ITO system due to the hydrophobicity of both surfaces resulting in large AB attraction. Attractive LW interaction is expected for all systems, while those associated with *C.*

vulgaris systems were larger in magnitude than those with *B. sudeticus*.

Table 4.3: Interaction energy between the algae species and substrata according to the thermodynamic model.

Interacting pair	Total free energy of adhesion, LW and AB components (mJ m^{-2})		
	ΔG_{LW}	ΔG_{AB}	ΔG_{adh}
C. vulgaris - glass	-6.5	33.9	27.4
C. vulgaris - ITO	-3.5	-6.8	-10.3
B. sudeticus - glass	-5.8	-2.9	-8.7
B. sudeticus - ITO	-1.5	-63.8	-65.3

DLVO model

Figure 4.3 shows the EL, LW and total energy of *C. vulgaris* interacting with glass and ITO. The total interaction energy between the cell and the substratum determines the strength and rate of adhesion. For instance, the type of adhesion that occurs due to presence of an attractive energy minimum at a distance from the substratum surface is called adhesion at secondary minimum. This type adhesion is considered to be weaker and more reversible compared primary adhesion where the cell and the substratum interaction results in adhesion at the substratum surface [91].

Based on the total energy of interaction between *C. vulgaris*-glass system adhesion at secondary minimum is expected and *C. vulgaris*-ITO system results in adhesion at primary minimum. Thus, the strength and the rate of adhesion is expected to be larger with *C. vulgaris*-ITO system compared to those for *C. vulgaris*-glass system. Adhesion at the secondary minimum is predicted for the *C. vulgaris*-glass system since (i) LW attraction has a longer

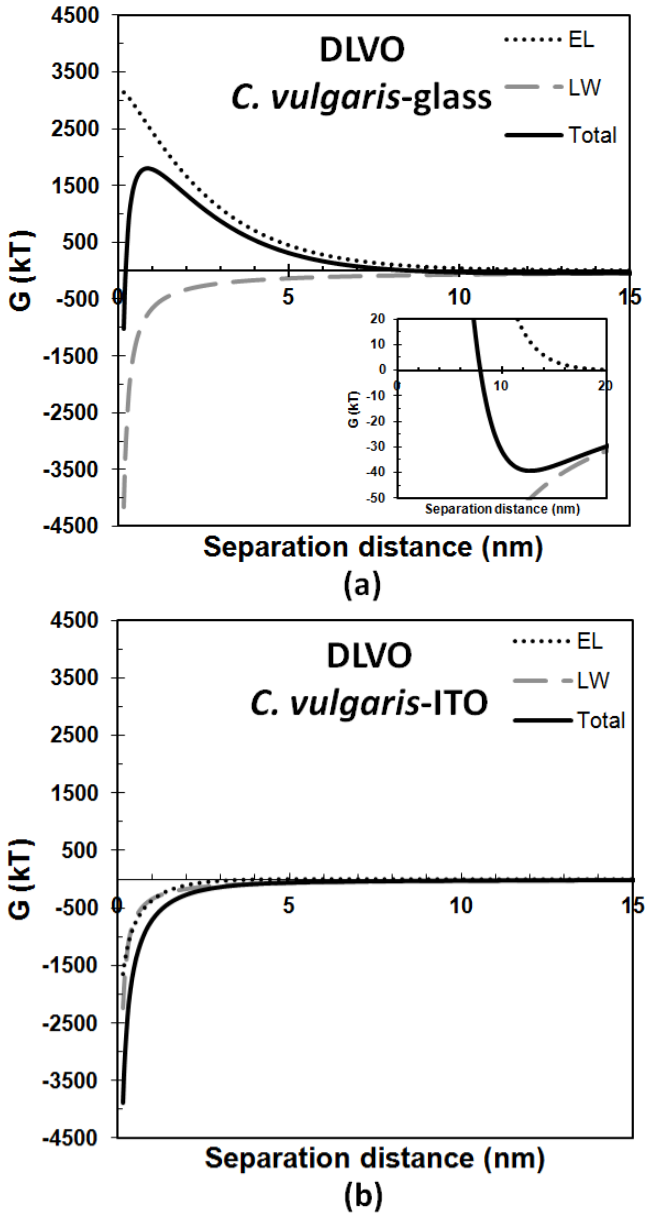

Figure 4.3: Interaction energy of *C. vulgaris* with (a) glass and (b) ITO according to the DLVO model.

range compared to EL repulsion and (ii) the magnitude of LW interaction is smaller compared to EL interaction at small separation distances. Thus, the adhesion at the secondary minimum with a magnitude of -39 kT is predicted at a separation distance of 13 nm for *C. vulgaris*-glass system. The domination of LW interaction over EL interaction is due to the large ionic strength of PBS that compresses the double layer thicknesses lowering the repulsive EL interaction [91]. At higher ionic strengths the double layer thicknesses can be compressed further and instead of at secondary minimum, adhesion at primary minimum is expected. For the *C. vulgaris*-ITO system, adhesion at the primary minimum is expected with a magnitude of -3883 kT as (i) LW interaction is attractive for this system and (ii) EL repulsion is negligible due to the small surface potential of ITO.

Figure 4.4 presents the EL, LW and total energy of interaction for *B. sudeticus*-glass and *B. sudeticus*-ITO systems. Similar to results with *C. vulgaris*, adhesion at secondary and primary minima are expected for the interaction of *B. sudeticus* with glass and ITO, respectively. Based on this approach, adhesion of this species over ITO is preferred over glass. The magnitude of the total interaction energy at the secondary minimum for *B. sudeticus*-glass system is equal to -11.8 kT at a separation distance of 17 nm which is smaller compared to the total interaction energy of *C. vulgaris* with the same surface. This is attributed (i) to the larger surface potential of *B. sudeticus* giving rise to larger EL repulsion and (ii) to the smaller LW component of this species resulting in weaker LW attraction. The lower secondary energy minimum of

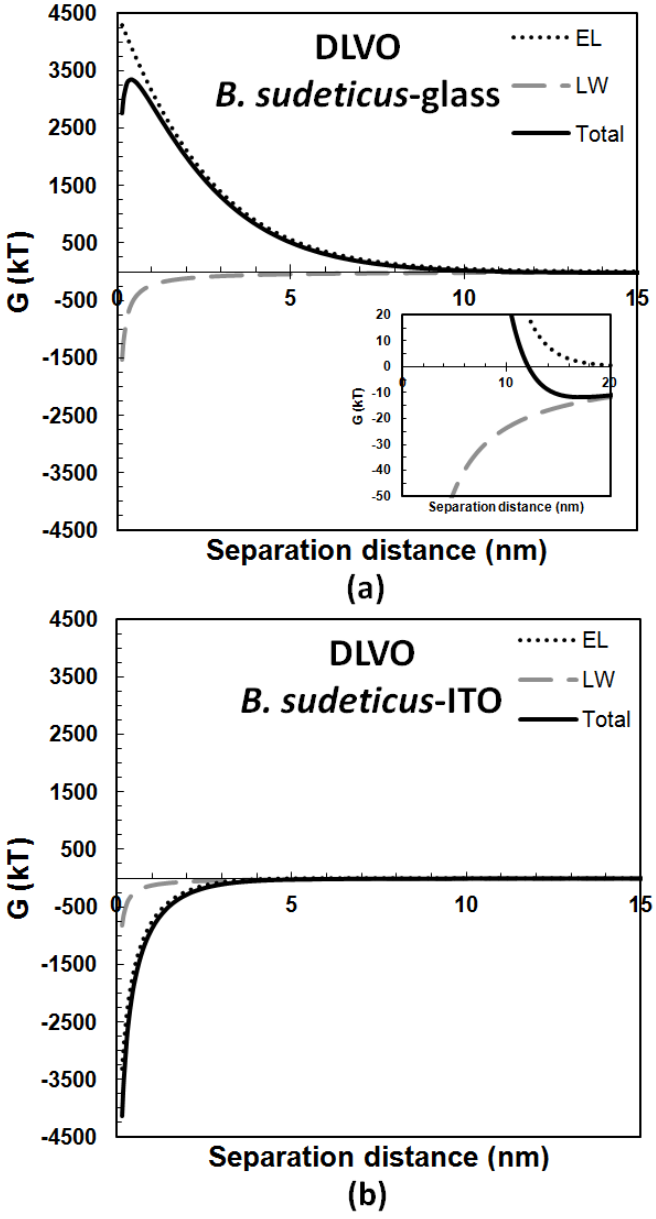

Figure 4.4: Interaction energy of *B. sudeticus* with (a) glass and (b) ITO according to the DLVO model.

the *C. vulgaris*-glass system indicates a larger attractive interaction for this system compared to the *B. sudeticus*-glass system. Finally, the total energy at the primary minimum is equal to -4130 kT for *B. sudeticus*-ITO system indicating strong attractive interaction predicted.

XDLVO approach

Figure 4.5 illustrates the EL, LW, AB, and total interaction energy for *C. vulgaris*-glass and *C. vulgaris*-ITO systems as a function of separation distance. Based on the AB components, hydrophilic repulsion and hydrophobic attraction is predicted for *C. vulgaris*-glass and *C. vulgaris*-ITO, respectively. Compared to the DLVO model, the addition of AB component does not change the mode of adhesion for *C. vulgaris* interacting with either of the surfaces. Adhesion at the secondary and at the primary minimum are expected for glass and ITO, respectively. However, the magnitude of the attractive interaction energy at the primary minimum increases to -45525 kT for *C. vulgaris*-ITO. Due to the increased magnitude of attractive energy, a larger strength and rate of adhesion are expected for the *C. vulgaris*-ITO system with the XDLVO model. The introduction of this attractive energy is due to the hydrophobicity of the ITO. On the other hand, the magnitude of the secondary minimum is unaltered for the *C. vulgaris*-glass system as the AB repulsion decays rapidly and is negligible for separation distances exceeding 6 nm. However, the magnitude of the repulsive energy between the glass and *C. vulgaris*, i.e., the energy barrier between the cell and the substratum, is larger due to the AB repulsion.

Similarly, Figure 4.6 shows the EL, LW, AB, and total interaction en-

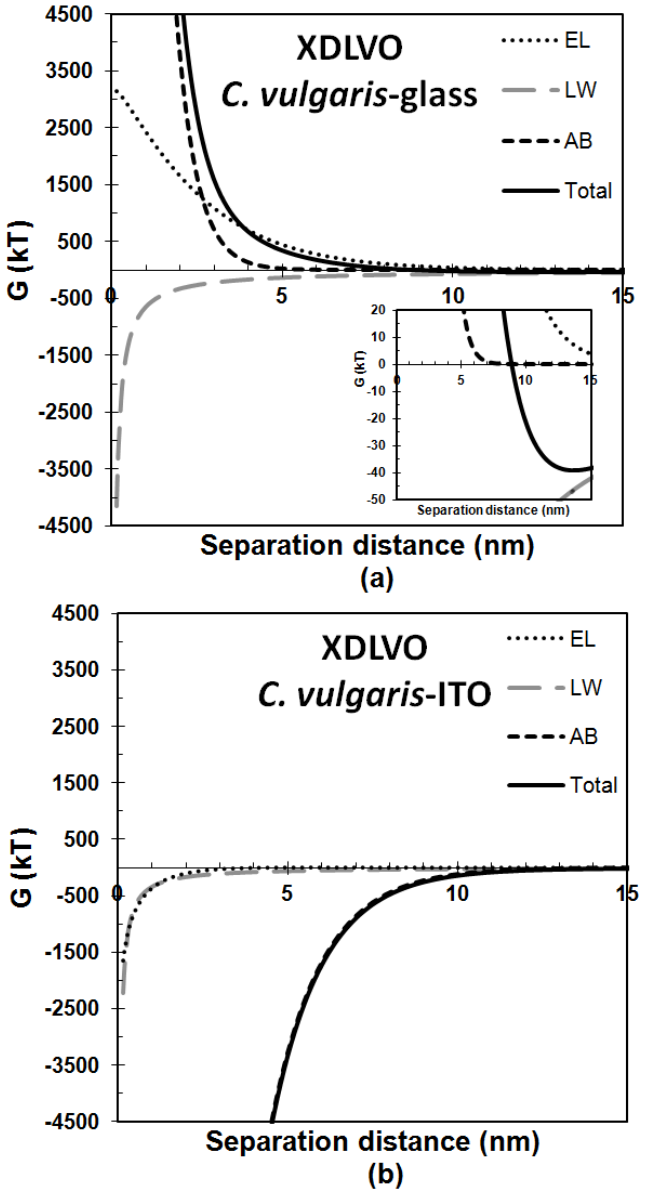

Figure 4.5: Interaction energy of *C. vulgaris* with (a) glass and (b) ITO according to the XDLVO model.

ergy of *B. sudeticus*. Adhesion at the primary minimum is expected for *B. sudeticus* interacting with either of the substrate surfaces. Compared to the DLVO model, the introduction of the AB interaction changes the mode of adhesion for *B. sudeticus*-glass from adhesion at the secondary minimum to the adhesion at the primary minimum. Moreover, compared to the DLVO model, a larger attractive interaction energy is expected at contact for the *B. sudeticus*-ITO system. Thus, based on these results a larger strength and rate of adhesion are expected for both systems with the XDLVO model. Moreover, XDLVO model predicts the strength of adhesion to increase for the systems in the following order from the smallest to the largest: *C. vulgaris*-glass, *B. sudeticus*-glass, *C. vulgaris*-ITO, and *B. sudeticus*-ITO. Finally, the reason for the adhesion at the primary minimum for the *B. sudeticus*-glass system is attributed to the attractive AB interactions due to the hydrophobicity of this species. Thus the repulsive energy between *B. sudeticus* and glass based on DLVO model no longer exist. The total interaction energy for glass and ITO systems are equal to -29693 kT and -334580 kT, respectively.

4.3.2 Parallel plate flow experiments

Figure 4.7 shows the adhesion density, ϱ, in number of cells adhered per mm^2 for *C. vulgaris* as a function of time over the glass surface. The results indicate that the rate of adhesion density of *C. vulgaris* over glass can be approximated into three linear parts: in the first two hours the adhesion density increased with a rate of about 56 cells mm^{-2} hour^{-1}, in the next four

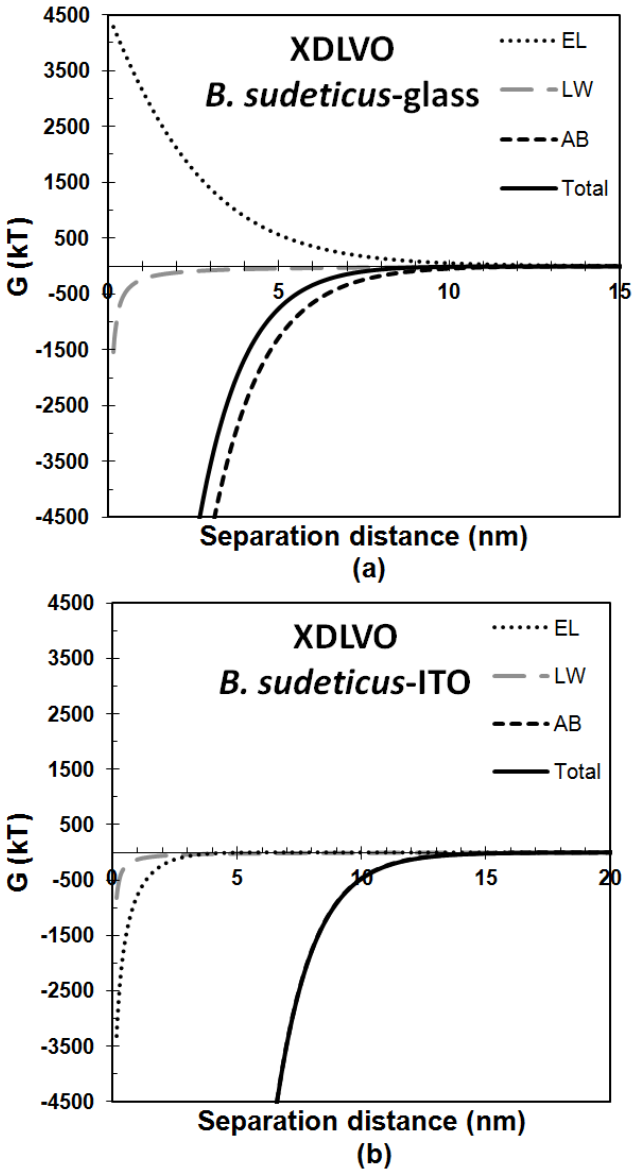

Figure 4.6: Interaction energy of *B. sudeticus* with (a) glass and (b) ITO according to the XDLVO model.

hours the adhesion rate decreased to about 30 cells mm^{-2} $hour^{-1}$, and finally in the last four hours the rate was about 5 cells mm^{-2} $hour^{-1}$ resulting in a final adhesion density of about 250 cells mm^{-2}.

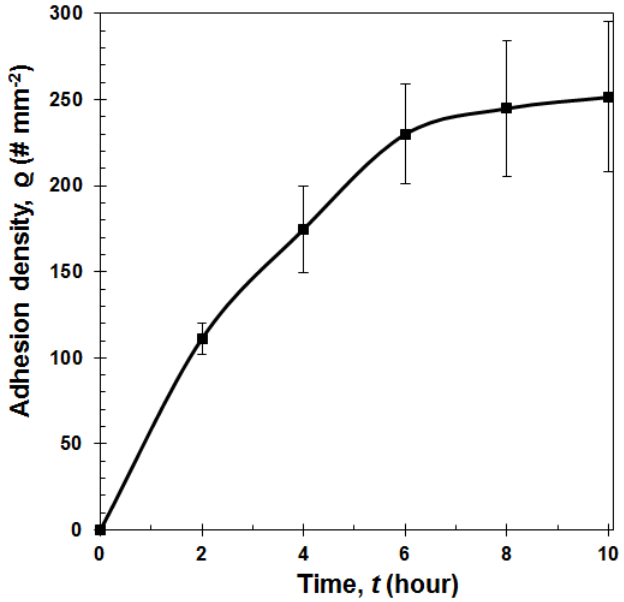

Figure 4.7: Adhesion density of *C. vulgaris* over glass surfaces as a function of time.

The rate of adhesion of *C. vulgaris* over the ITO was quite different from that over glass. At the end of the first two hours without shear, all the cells over the ITO were attached and resulted in an adhesion density of 8504±498 mm^{-2}. Moreover, none of the adhered cells desorbed after the following washout period of 5 minutes with a shear rate of 10 s^{-1}. Similarly, none of *B. sudeticus* adhered over the ITO were removed for the same shear

rate with the same duration and resulted in an adhesion density of 7960±11 mm^{-2} cells. Finally, *B. sudeticus*-glass interaction resulted in an adhesion density of 7189 ±13 mm^{-2} at the end of two hours.

Figure 4.8 presents the percentage of the cells remaining over each substratum after washout with a wall shear rate of 10 s^{-1} for five minutes. The results indicate that 3.37±0.13% of *C. vulgaris* cells that were present over the glass adhered over this substratum. The percentage of the attached cells that remained after washout was equal to 87.85±0.81% for the *B. sudeticus*-glass system. Finally, for either species interaction with ITO resulted in adhesion of all cells present in the suspension. Based on these findings it can be concluded

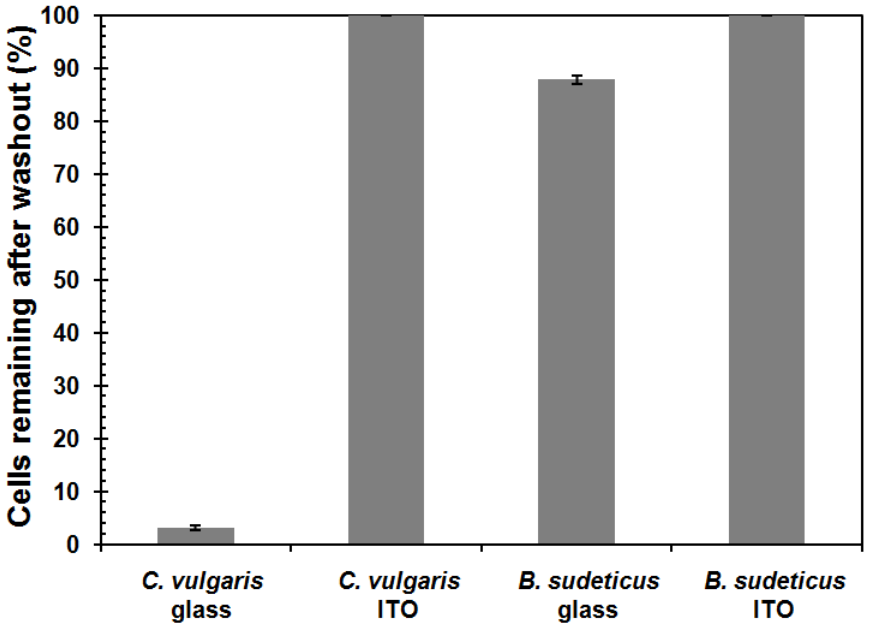

Figure 4.8: Ratio of *C. vulgaris* and *B. sudeticus* remained adhered over glass and ITO after a washout with a shear rate of 10 s^{-1} and duration of 5 minutes.

that for an intermittent shear rate of 10 s^{-1} (i) the rate of adhesion for the *C. vulgaris*-glass system was about 1/26 times and 1/30 times as much as the *B. sudeticus*-glass and *C. vulgaris*-ITO systems, respectively, (ii) the adhesion rates of *B. sudeticus* and *C. vulgaris* interacting with ITO were larger than their adhesion rates over glass glass, and (iii) similar adhesion rates can be expected with each species interacting with the ITO.

At the end of the first two hours of the experiments, the cells covered the entire surface of the substratum for all systems studied except for the *C.vulgaris*-glass. Thus, for these systems adhesion experiments were stopped and desorption experiments were initiated to quantify the adhesion strength of the cells over the respective substrata. During the desorption experiments the flow rate was increased from 4.5 ml min^{-1} to 31.5 ml min^{-1} with 2.25 ml min^{-1} increments resulting in wall shear rates ranging from 100 s^{-1} to 700 s^{-1} with increments of 50 s^{-1}. Each flow rate was for a duration of one minute such that the number of cells remaining on the substrate reached a steady state value. For these flow rates, the cells experienced both lift, in the direction normal to the flow, and drag, in the direction of the flow, that ranged from 8.16×10^{-13} N to 2.9×10^{-11} N and 1.49×10^{-11} N to 1.0×10^{-10} N, respectively. The resultant net force on the cells ranged from 1.49×10^{-11} N to 1.62×10^{-10} N. Thus, drag force is expected to dominate the desorption phenomena for the algal species studied.

Figure 4.9 present the percentage of the initial number of cells that remained attached over glass and ITO as a function of wall shear rate and

net force acting on the cells, respectively, during the desorption experiments. Based on these results the adhesion strength was smallest for *C. vulgaris*-glass and increased in ascending order for *B. sudeticus*-glass, *C. vulgaris*-ITO, and *B. sudeticus*-ITO systems. The results show that all *C. vulgaris* cells that were adhered over the glass were removed after a wall shear rate of 100 s^{-1} corresponding to a net force of 2.28×10^{-11} N acting on the cells. This indicates that the adhesion strength of *C. vulgaris* over glass was smaller than 2.28×10^{-11} N. On the other hand, the results show that desorption characteristics of *C. vulgaris* from ITO followed an S-curve relation. While 99.8% and 87% of the cells remained attached with shear rates of 100 s^{-1} and 200 s^{-1}, respectively, the cells desorbed exponentially with shear rates from 200 s^{-1} to 700 s^{-1}. Only 5% of the cells remained attached after being subjected to a shear rate of about 700 s^{-1}. These results indicate that the adhesion strength of *C.vulgaris* over ITO was less than 1.62×10^{-10} N for 95% of the cells.

The results indicate that *B. sudeticus*-ITO system had the largest adhesion strength. Even at the largest shear rate of 700 s^{-1}, only 8% of the cells were desorbed which indicate that 92% of the cells had an adhesion strength larger than 10.55×10^{-11} N. Moreover, the number of *B. sudeticus* cells remained over the ITO decreased linearly with increasing shear rates and net force. On the other hand, *B. sudeticus* desorbed from glass in an exponential fashion. A shear rate of 100 s^{-1} corresponding to a net force of 1.49×10^{-11} N resulted in desorption of 56% of the cells. At a shear rate of 700 s^{-1} about 9% of the cells remained adhered indicating that 91% of the cells had adhesion

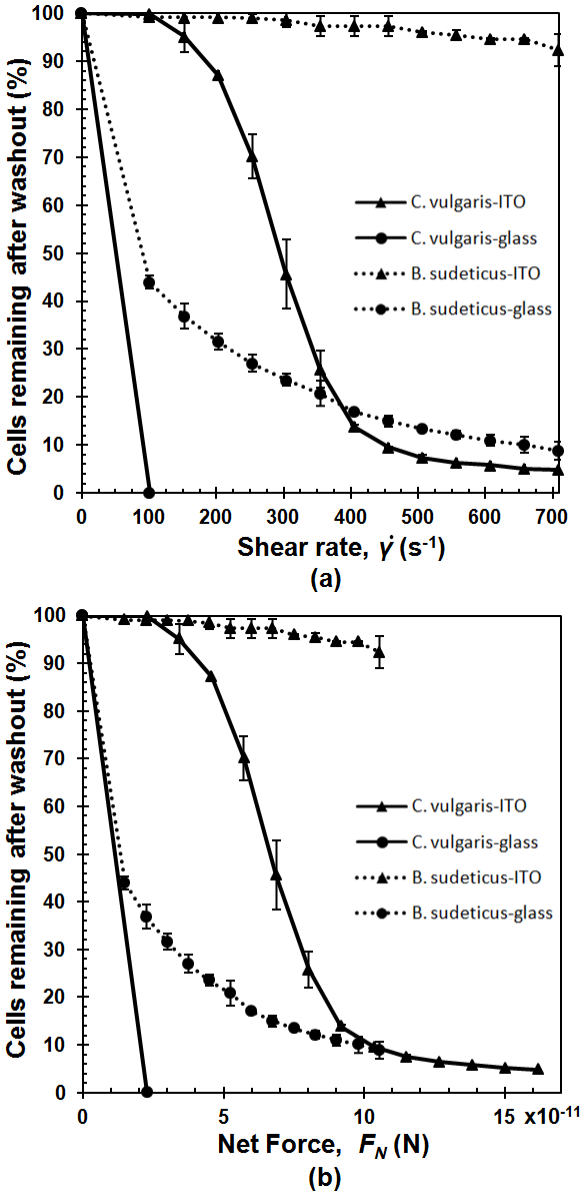

Figure 4.9: Ratio of *C. vulgaris* and *B. sudeticus* remained attached over glass and ITO as a function of (a) wall shear rate and (b) net force during incremental washouts.

strength lower than 10.55×10^{-11}N. The results also show that due to larger size of *C. vulgaris*, the net force acted on this species was larger than that of *B. sudeticus*.

4.3.3 Comparison of the experimental results with the adhesion models

The thermodynamic model was successful in predicting the adhesion with *C. vulgaris*-ITO, *B. sudeticus*-glass, and *B. sudeticus*-ITO systems. This model predicts that *C. vulgaris* should only adhere over the ITO due to hydrophobicity of this surface. However, the experimental results showed that algae adhered to the hydrophilic glass surface as well. Thus, the thermodynamic model was not successful in predicting the adhesion of *C. vulgaris* to the hydrophilic surface.

DLVO theory successfully predicted the adhesion of the algal species over both surfaces. Moreover, the model was successful in predicting that the adhesion strength of *B. sudeticus* and *C. vulgaris* should be larger over ITO compared to that over glass. This prediction was based on the mode of adhesion of these algal species, adhesion at primary and secondary minimum were expected for either algal strains interacting with ITO and glass, respectively. However, this model failed in predicting the stronger interaction with *B. sudeticus*-glass system compared to *C. vulgaris*-glass system considering that a larger magnitude of adhesive interaction was predicted for *C. vulgaris*-glass system.

The adhesion rate as well as the adhesion strength of all the systems were successfully predicted by the XDLVO model. Based on this model weak and reversible adhesion at the secondary minimum was predicted for *C. vulgaris*-glass system. Moreover, adhesion at primary minimum was expected for *C. vulgaris*-ITO, *B. sudeticus*-glass, and *B. sudeticus*-ITO systems with total interaction energy of -86798 kT, -29693 kT, and -334580 kT, respectively, at the primary minimum. The adhesion strengths determined based on the parallel plate flow experiments are in accordance with these interaction energy. The total interaction energy of *B. sudeticus*-ITO system was about 3 times as large as *C. vulgaris*-ITO system, and while only 8% of the cells were desorbed from the *B. sudeticus*-ITO system subject to a net force of 10.55×10^{-11} N, 90% of the cells desorbed for the same net force from the *C. vulgaris*-ITO system. Moreover, while all the cells were desorbed from *C. vulgaris*-glass system subjected to a net force of 2×10^{-11} N, 44% of the cells remained adhered in the *B. sudeticus*-glass system. These results suggest that AB component is critical for cell-substrata interactions considering that the *B. sudeticus*-glass system had (i) larger EL repulsion, (ii) smaller LW attraction, and (iii) 26 times the adhesion density of the *C. vulgaris*-glass system. Thus, the XDLVO approach was successful in predicting the algae substrata interactions.

4.4 Conclusion

A comprehensive study has been conducted to determine the surface interactions of planktonic and benthic algal species with hydrophilic and hy-

drophobic surfaces. Adsorption-desorption experiments were conducted in a parallel flow chamber at varying shear rates. Moreover, the results were compared to the predictions of thermodynamic, DLVO, and XDLVO models using experimentally quantified surface properties. Based on the results obtained the following conclusions can be drawn:

- The planktonic species *C. vulgaris* had hydrophilic while the benthic species *B. sudeticus* has hydrophobic surfaces.
- The acid base interaction between algae and substrate is critical for the rate and strength of adhesion.
- The *B. sudeticus*-ITO system displayed the strongest adhesion.
- Compared to glass, lower electrostatic repulsion and larger acid base attraction of ITO resulted in about 29 times increase in the adhesion density of *C. vulgaris*.
- Compared to *C. vulgaris*, lower surface energy of *B. sudeticus* resulted in 25 times increase in the adhesion rate over glass.
- XDLVO model was the most successful model in predicting the adhesion rate and strength of the algal species over ITO and glass.

Results obtained can be used to select and design surfaces to promote or inhibit the adhesion of algal cells to substrata. This optimization can be

essential for selecting both algal species and surface materials for algal photobioreactors where cells are cultivated in suspension, and for algal biofilm photobioreactors where algae are grown attached in biofilm over substrata. Finally, the results can also be used for designing surfaces and systems to avoid biofouling over ship hulls and planktonic photobioreactor systems.

Chapter 5

Cell to Substrate and Cell to Cell Interactions of Algal Species

5.1 Introduction

Microalgae are a diverse group of photosynthetic microorganisms that have adapted to grow productively in many earth ecosystems including hot springs, snow, and highly saline or caustic environments [133]. Based on their preferred mode of survival, algae can be grouped as planktonic or benthic. Planktonic algae grow suspended in water bodies and benthic algae grow attached over substrata. Planktonic microalgae have been extensively studied for production of many economically valuable products such as lipids and pharmaceuticals as well as removal of nitrogen, phosphorus, and heavy metals from wastewater with various origins [133]. Suspended cultivation of microalgae requires large inputs of energy and water and usually results in low biomass concentrations, in the range from 0.1 to 8 g L^{-1} [11]. A wide variety of processes such as centrifugation, filtration, electrocoagulation, and flocculation have been used to harvest and dewater algal suspensions [12]. The use of these processes is a major bottleneck for production of low value products, such as fuel, as they require large capital and operating costs [12]. Moreover, the large energy requirements for these processes render the algal fuel production

energetically unfeasible. Thus, alternative methods such as bioflocculation is receiving increased attention. In bioflocculation, flocculation of cultivated algae is induced by the addition of other flocculating algal species. This method has advantages over conventional means of algae harvesting as it is energy efficient and it does not require addition of chemicals [33]. On the other hand, significant amount of flocculating algae inputs are required to increase the harvesting efficiency [33].

Microalgal biofilm growth is studied as an alternative to suspended growth of microalgae for metabolite production and wastewater treatment, as large biomass concentrations can be reached with minimal energy and water consumption using these systems [38, 40, 147]. However, benthic microalgae growth is mostly considered as a nuisance for man made structures in aquatic and aerial systems. For instance, in planktonic photobioreactors algal biofouling is undesirable as it lowers the productivity of these systems [2]. Attached algal growth over ship hulls can increase the skin friction of ships by up to 80%, increasing the fuel consumption and maintenance costs [158]. In thermal cooling systems algal biofouling decreases the heat transfer and increase the pumping power requirements [83]. Moreover, microalgal biofilms are also undesirable in potable water storage and water pipes due to dissolved organic carbon they secrete that create undesirable taste and odor [77]. In aerial environment, algal biofilms grow over buildings and monuments where they corrode metals and create an untidy look [77].

The study of cell to cell and cell to substrata interactions of algal species

may offer improvements in design and performance of both planktonic and benthic algal photobioreactors. In planktonic photobioreactors based on cell to cell interactions, target and harvesting species can be selected to improve the performance of bioflocculation based harvesting. In biofilm photobioreactors based on cell to substrata interactions, algal species-substrata couples favoring adhesion and biofilm growth can be identified or designed. Furthermore, unintended biofouling of substrata can be avoided by understanding algae cell-substrata interactions. To the best of our knowledge there is no systematic study on physico-chemical surface properties of planktonic and benthic algal species and the influence of these parameters on cell to cell and cell to substrata interactions. This chapter addresses this gap in the literature (i) by reporting the physico-chemical surface properties of seven green algae and three diatoms, and substrata with varying surface properties and (ii) by modeling cell to cell and cell to substrata interactions between the algal cells, and algal cells and substrata using the thermodynamic and XDLVO models.

5.2 Materials and Methods

5.2.1 Algae culturing and sample preparation

All algal species were obtained from the Culture Collection of Algae at the University of Texas at Austin, UTEX. Freshwater species, *Ankistrodesmus falcatus var. stipitatus* (green alga, UTEX B 242), *Botryococcus braunii* (green alga, UTEX 572), *Botryococcus sudeticus* (green alga, UTEX B 2629), *Chlorella vulgaris* (green alga, UTEX 2714), *Nannochloris oculata* (green alga, UTEX

LB 1998), and *Scenedesmus dimorphus* (green alga, UTEX 1237), were cultivated as batch cultures in BG-11 nutrient medium [148] supplied with 1.5 vol.% CO_2. Cells were irradiated with 125 μE m^{-2} sec^{-1} (26.25 W m^{-2}) photosynthetically active radiation under 12/12 hour light dark cycle. *Amphora coffeaeformis* (diatom, UTEX B 2036), *Cylindrotheca fusiformis* (diatom, UTEX B 2085), *Nannochloris* sp. (green algae, UTEX LB 1999), and *Nitzschia frustulum* (diatom, UTEX B 2042) were cultivated in ASP-M medium prepared that were devoid of S3 vitamins and trace metals II solutions [148] under same conditions as the freshwater species. After equilibration with atmospheric CO_2, BG-11 and ASP-M had pH of 7.42 and 7.53 (Accumet AB15 Plus, Fisher Scientific, USA), and conductivity of 2.09 and 45.93 mS cm^{-1} (Con 2700, Oakton, USA), respectively. Moreover, the ionic strengths of BG-11 and ASP-M medium were 21 mM and 584 mM, respectively.

Algal suspensions in the log phase of growth were used for the experiments. The species cultivated with BG-11 were washed twice and resuspended in deionized water before subsequent filtration step. Algal strains cultivated in ASP-M nutrient medium were washed twice and resuspended in phosphate buffered saline (PBS) containing 1.62 mM K_2HPO_4, 6.49 mM KH_2PO_4, and 581.76 mM NaCl resulting in a pH of 7.02 $\pm$0.01. The contents of the PBS were selected to match the ionic strength of ASP-M medium to avoid cytolysis of the cells. The cells grown in the freshwater medium BG-11 could be washed with deionized water as no cytolysis was observed under these conditions.

For determining the surface properties of the algal species, algae lawns

with thicknesses of approximately 200 μm were prepared on 0.45 μm mixed cellulose acetate filter (Nalge Nunc International, USA) by filtering washed algal suspensions. Before filtration, algal suspensions containing algal flocs were passed through a syringe needle with an opening diameter of 0.34 mm multiple times to ensure the presence of a homogeneous size distribution. Homogeneity of the size distribution is critical to prepare a smooth algal lawn, and smoothness of the algal lawn is important for accurate contact angle measurements [84]. The filters with the algal lawns were placed over agar plates containing 10% (vol/vol) glycerol until the start of contact angle measurements to keep the lawns moist [149].

5.2.2 Surface energy of algal cells and adhesion substrates

Surface energy of algal cells and adhesion substrates were quantified based on contact angle measurements made with the sessile drop technique using water, diiodomethane and formamide as the reference liquids [149]. Contact angles of all the probe liquids were measured using a goniometer (Model 190 CA, Rame-Hart, USA). Successive droplets of deionized water with 5 μL volume were placed over the mats until contact angle measurements were stabilized. After stabilization, contact angles of all the probe liquids were determined. The results presented are the average of at least 10 measurements done with each probe liquid.

5.2.3 Zeta potential measurements of algal cells and substrata

After the algae cells were washed twice and resuspended in their respective nutrient medium, their electrophoretic mobilities were measured using a zeta meter (ZetaCompact, CAD, France). Based on the measured electrophoretic mobilities, zeta potential of the cells were quantified using Smoluchowski's model. This model was selected as it is the most accurate model given the size distribution of the cells and the ionic strengths of the nutrient medium used for the experiments [159].

Microscope glass slides were cleaned in hydrochloric acid for 5 hours. Cleaned slides were rinsed with deionized water and cleaned in ultrasonic bath with 1% Alconox (Alconox Inc., Alconox, NY) solution, ethanol, and acetone for 10 minutes each, and air dried after rinsing. ITO coated glass surfaces were cleaned in the ultrasonic bath with 1% Alconox solution for 10 minutes. After sonication and rinsing, the slides were air dried. Zeta potentials of cleaned glass and ITO slides were quantified when they were in BG-11 nutrient medium. An electrokinetic analyzer (SurPASS, Anton Paar GmbH, Austria) was used to measure the streaming potential and current of glass and ITO, respectively. The Fairbrother-Mastin approach was used to quantify the zeta potentials of the substrata based on the streaming potential and current measured [153, 154].

5.3 Results and Discussions

5.3.1 Morphological properties of algal species and substrata

Table 5.1 summarizes the morphological properties including major, minor, and equivalent spherical diameter, and circularity of the algal species studied. The major and minor diameters of the cells were determined based on images of the cells obtained with an inverted microscope and the spherical diameter and circularity were determined based on the method presented in Section 4.2.2. The results indicate that the algal species had equivalent spherical diameters ranging from 2.50 μm to 13.65 μm. These diameters were used as the size parameters for the subsequent modeling studies. Moreover, based on their morphological properties algal species can be divided into three groups, namely those having spherical, ellipsoidal, and needle shapes. *C. vulgaris*, *N. oculata*, and *B. sudeticus* were the spherical algal species with circularity close to one. *Nannochloris* sp., *A. coffeaeformis*, *B. braunii*, and *N. frustulum* had ellipsoidal shapes with circularity ranging from 0.73 to 0.82. Finally, *A. falcatus*, *S. dimorphus*, and *C. fusiformis* were the needle shaped algal species with circularity smaller than 0.3.

Table 5.2 summarizes (i) the contact angles measured with the probe liquids, (ii) the surface free energy components, (iii) the free energy of cohesion, and (iv) the zeta and surface potentials of algal species and adhesion substrata studied. The data from the contact angle measurements indicate two trends (i) in average hydrophobic species had larger contact angles with all the probe liquids and (ii) the saltwater species, especially the diatoms, had

Table 5.1: Morphological properties of algal species.

	Major Diameter	Minor Diameter	Equivalent Spherical Dia.	Circularity
Green Algae				
A. falcatus	25.60±7.80	4.23±1.42	10.41±2.36	0.23±0.08
B. braunii	11.38 ±1.77	9.01±1.64	10.13±1.21	0.78±0.11
B. sudeticus	4.48±1.43	4.17±1.46	4.32±1.02	0.94±0.02
C. vulgaris	5.62±1.15	5.08±0.70	5.34±0.66	0.93±0.70
N. oculata	2.70±0.36	2.31±0.33	2.50±0.25	0.91±0.03
Nannochloris sp.	3.98±1.13	2.02±0.33	2.84±0.47	0.73±0.11
S. dimorphus	16.86±4.48	11.77±2.26	14.09±2.31	0.30±0.13
Diatoms				
A. coffeaeformis	13.41±1.70	9.65±1.17	11.37±1.00	0.82±0.08
C. fusiformis	30.88 ±5.86	6.04±1.24	13.65±1.91	0.28±0.06
N. frustulum	8.78±1.41	4.86±0.93	6.53±0.81	0.77±0.09

larger contact angles with diiodomethane. The reason for the variation of the contact angles between species was the difference in their surface groups. For instance, while the presence of surface groups such as ethenyl groups increases the water contact angle and decreases the electron donor parameter (γ^-), the presence of carbonyl, carboxylic, and hydroxyl groups decrease the contact angle and increases the electron donor parameter making the surface more hydrophilic [160].

The difference between the cell wall structures, particularly surface groups, of green algae and diatoms can explain differences observed with green algae and diatom contact angles. Diatom cell walls consist of silica shells that are covered with organic coating, mainly proteins and polysaccharides, and possibly with metal ions [142, 161, 162]. In contrast, cell walls of green algae in general consist of cellulose fibrils and polysaccharide composites [162].

Table 5.2: The measured contact angle and physico-chemical surface properties of algal species and substrata.

Species	Contact angle (degrees)			Free energy compon., free energy of cohesion (mJ m^{-2}), and zeta and surface poten. (mV)					
	W.	F.	D.	${\gamma_s}^{LW}$	${\gamma_s}^-$	${\gamma_s}^+$	ΔG_{sls}	ζ	ψ
Planktonic									
A. falcatus	85.6	62.2	45.3	36.8	3.4	0.1	-64.6	-20.1	-25.6
C. vulgaris	42.7	41.8	43.5	37.8	41.2	0.2	20.8	-23.3	-29.7
N. oculata	39.5	46.3	49.5	34.5	49.9	0.1	35.2	-35.9	-45.6
Nanno. sp.	31.2	80.1	74.0	20.7	118.7	0.0	118.0	-18.4	-64.5
S. dimorphus	58.4	59.1	44.1	37.5	33.9	0.0	11.4	-18.4	-23.3
Benthic									
A. coffeae.	73.9	71.0	97.1	9.7	19.0	3.8	-13.4	-21.1	-74.0
B. braunii	112.3	88.8	57.9	29.8	0.0	0.0	-103.3	-27.5	-34.9
B. sudeticus	94.3	75.7	60.4	28.3	2.8	0.0	-69.1	-23.1	-29.4
C. fusiformis	91.5	65.6	83.4	15.8	1.0	5.4	-44.6	-26.2	-92.0
N. frustulum	55.8	49.9	89.4	13.0	26.6	7.7	-1.28	-19.1	-67.1
Substrata									
Glass	7.9	5.9	22.3	47.1	54.7	0.4	32.0	-36.2	-46.0
ITO	88.0	68.2	50.1	34.2	4.1	0.0	-63.9	-1.1	-1.4
S. steel (316L)	-	-	-	37.0[a]	17.0[a]	0.2[a]	-21.1[a]	-29.1[b]	-37.0
Polycarbonate	-	-	-	33.2[a]	0.5[a]	1.4[a]	-69.1[a]	-54.0[c]	-68.7
Polyethylene	98.5	78.5	49.5	34.6	1.8	0.4	-68.5	-49.2[d]	-62.6
Polystyrene	90.0[e]	70.6[e]	28.1[e]	45.0[e]	4.0[e]	0.0[e]	-69.9[e]	-30.1 [c]	-38.3

[a] based on surface free energy data reported by Keijbets *et al.* [163].
[b] based on data reported by Boulange *et al.* [164].
[c] based on data reported by Kirby *et al.* [154].
[d] based on data reported by Benes *et al.* [165].
[e] based on contact angle data reported by Shimizu *et al.* [166].

Based on the contact angles measured the surface free energy and the free energy of cohesion of the algal species and substrata were quantified. The results show that the free energy of cohesion for all the benthic species were negative indicating that these surfaces were hydrophobic while all the planktonic species, excluding *A. falcatus*, had hydrophilic surface properties. As opposed to the planktonic species that grow in suspension, benthic species

adhere over substrata and grow in biofilms. Thus, the results indicate that the surface hydrophobicity, or the AB attraction, might be one of the main mechanisms that promotes the adhesion of benthic algae to surfaces. Data in the literature support this concept. For instance, van Loosdrecht *et al.* studied the adhesion of 16 bacterial strains and reported that (i) hydrophobicity increased the adhesion of cells to sulfated polystyrene and (ii) adhesion density of the cells increased linearly with increasing water contact angle of the bacteria [167]. In a similar study the effects of surface free energy and surface charge on bacteria adhesion were studied by van Loosdrecht *et al.* [168]. They reported that (i) increased hydrophobicity of the bacterial cells increased the adhesion density over substrata and (ii) an inverse relationship between the surface hydrophobicity of the bacterial strains and the effects of electrostatic repulsion existed. Another difference between the hydrophilic and hydrophobic algae was the LW components that they had. On average the hydrophobic species had smaller LW components of free energy. Thus, compared to the hydrophilic species a smaller LW attraction is expected with the hydrophobic algae.

Zeta potential of the algal species ranged from -18.4 to -35.9 mV. Similar range of zeta potentials have also been reported for other green algae and diatoms [169]. In average saltwater species had 15% smaller zeta potential compared to the freshwater species. The reason for this difference was the larger ionic strength of the saltwater medium that compressed the electric double layers around the cells and reduced the zeta potentials [3]. Surface

potentials of the cells were calculated based on the zeta potentials quantified, ionic strength of the medium, and the hydration layer thicknesses associated with the cells using Equation (2.16) [84]. As opposed to the zeta potentials, surface potentials of the saltwater species were larger than that of the freshwater species. The reason for the larger surface potentials in saltwater media was the presence of thinner hydration layers around the cells that were more concentrated with cations [93].

The zeta potentials of glass and ITO were quantified when these substrata were in BG-11 nutrient medium. The zeta potentials of polyethylene, polystyrene, polycarbonate, and stainless steel (316L) were based on the data reported in the literature for aquatic systems with ionic strengths and pH close to those of BG-11. Polyethylene, polystyrene, and stainless steel were selected for this study as successful formation and growth of algal biofilms were achieved using these substrata [38, 39, 144]. Moreover, polycarbonate was one of the substrata analyzed for algal adhesion as this substrata is transparent which might be an advantage for growth and analysis of photosynthetic biofilms [170]. The surface potentials of all the substrata were also calculated using Equation (2.16). In the limit as the diameter approaches infinity the surface potential approaches $\zeta\ e^{\kappa v}$. Furthermore, the surface potentials of the substrata were assumed to be equal for BG-11 and ASP-M nutrient medium as no data is available in the literature for the zeta potentials of these substrata in the ionic strength range of ASP-M medium. The effects of this assumption on the subsequent modeling studies were negligible since electrostatic repulsion

was negligible at these large ionic strengths.

5.3.2 Cell to surface interactions

In this section algal species studied were grouped into three, namely hydrophobic green algae and diatoms, and hydrophilic algae. This grouping made the discussion of the results easier as the species within each group have similar results from the models.

Thermodynamic approach

The advantage of using the thermodynamic over the XDLVO model is its cell size or shape independence for prediction of the cell to substrata and cell to cell interactions. This independence may be especially advantageous for the current study as the interactions of algal species with circularity ranging from 0.28 to 0.94 were studied. Table 5.3 summarizes the results from the hydrophobic algal species. The thermodynamic model predicts the adhesion of all the hydrophobic green algae, including *A. falcatus*, *B. braunii*, and *B. sudeticus*, over all the adhesion substrata studied. Moreover, except *A. coffeaeformis*-glass and *N. frustulum*-glass systems adhesion is also predicted for all the hydrophobic diatoms interacting with either of the substrata. There are numerous studies in the literature that support these predictions. For instance, *B. braunii* and *A. coffeaeformis* are known to be capable of attaching to substrata and forming biofilms [147, 171]. Moreover, members of the *Navicula* and *Cylindrotheca* genera and *A. coffeaeformis* can colonize substrata such as plastics, steel, perspex, and cooper immersed in seawater [77].

Table 5.3: Interaction energy between the hydrophobic algae species and substrata according to the thermodynamic model (in mJ m^{-2}).

Species	LW, AB comp. and free energy of adhesion						
		Glass	ITO	PE	PS	PC	SS
A. falcatus	ΔG_{LW}	-6.13	-3.29	-3.39	-5.70	-3.05	-3.95
	ΔG_{AB}	-6.29	-60.78	-63.43	-61.25	-65.73	-38.26
	ΔG_{adh}	-12.42	-64.08	-66.82	-66.95	-68.78	-42.21
A. coffeaeformis	ΔG_{LW}	6.82	3.67	3.77	6.34	3.39	4.40
	ΔG_{AB}	8.39	-25.58	-29.10	-25.89	-32.20	-12.12
	ΔG_{adh}	15.22	-21.92	-25.32	-19.55	-28.81	-7.72
B. braunii	ΔG_{LW}	-3.47	-1.86	-1.92	-3.22	-1.72	-2.23
	ΔG_{AB}	-21.19	-81.30	-82.06	-81.80	-82.67	-55.78
	ΔG_{adh}	-24.65	-83.16	-83.98	-85.02	-84.39	-58.01
B. sudeticus	ΔG_{LW}	-2.86	-1.53	-1.58	-2.65	-1.42	-1.84
	ΔG_{AB}	-6.32	-64.40	-67.28	-64.90	-69.78	-40.41
	ΔG_{adh}	-9.18	-65.94	-68.86	-67.56	-71.20	-42.25
C. fusiformis	ΔG_{LW}	3.05	1.64	1.68	2.83	1.51	1.96
	ΔG_{AB}	-23.20	-57.26	-55.99	-57.53	-54.82	-42.27
	ΔG_{adh}	-20.15	-55.62	-54.31	-54.70	-53.30	-40.30
N. frustulum	ΔG_{LW}	4.67	2.51	2.58	4.34	2.32	3.01
	ΔG_{AB}	11.62	-12.56	-15.92	-12.79	-18.90	-3.25
	ΔG_{adh}	16.29	-10.05	-13.34	-8.45	-16.58	-0.24

One important difference between the hydrophobic diatom-substrata and hydrophobic green algae-substrata interactions is the LW component of the free energy. While all the LW interactions between green algae and substrata are attractive, repulsive interactions are predicted for the diatom-substrata interactions. As discussed earlier this might be due to the differences in cell wall structures of the diatoms and the green algae.

Table 5.4 presents the results of the thermodynamic model for the hydrophilic algal species interacting with the adhesion substrata. The interactions of all the species, except *Nannochloris* sp., with ITO, polyethylene,

polystyrene, and polycarbonate are predicted to result in adhesion due to LW and AB attraction. None of the *Nannochloris* sp.-substrata interactions are expected to result in adhesion due to (i) repulsive LW interaction and (ii) large electron donor parameter this species has that results in AB repulsion. Moreover, adhesion is not predicted for the interaction of the hydrophilic green algae with the hydrophilic substrata such as glass due to the hydrophilic surface properties both have that creates AB repulsion. Finally, the interaction of *C. vulgaris* and *S. dimorphus* with stainless steel results in adhesion. Indeed, Sekar *et al.* reported the adhesion of *C. vulgaris* over stainless steel [83] and

Table 5.4: Interaction energy between the hydrophilic algae species and substrata according to the thermodynamic model (in mJ m^{-2}).

Species	LW, AB comp. and free energy of adhesion						
		Glass	ITO	PE	PS	PC	SS
C. vulgaris	ΔG_{LW}	-6.49	-3.49	-3.59	-6.03	-3.23	-4.18
	ΔG_{AB}	33.73	-13.79	-22.04	-14.25	-29.73	4.00
	ΔG_{adh}	27.24	-17.28	-25.63	-20.28	-32.59	-0.19
N. oculata	ΔG_{LW}	-5.29	-2.84	-2.92	-4.91	-2.63	-3.41
	ΔG_{AB}	40.08	-8.06	-17.31	-8.53	-25.54	9.68
	ΔG_{adh}	34.79	-10.90	-20.23	-13.44	-28.16	6.27
Nannochloris sp.	ΔG_{LW}	0.52	0.28	0.29	0.49	0.26	0.34
	ΔG_{AB}	75.59	28.73	14.19	28.23	1.22	44.27
	ΔG_{adh}	76.11	29.01	14.48	28.72	1.48	44.61
S. dimorphus	ΔG_{LW}	-6.38	-3.43	-3.53	-5.93	-3.17	-4.11
	ΔG_{AB}	30.53	-22.50	-30.62	-23.00	-37.84	-2.31
	ΔG_{adh}	24.15	-25.93	-34.15	-28.93	-41.01	-6.43

Cao *et al.* reported that *S. dimorphus*-stainless steel interaction resulted in adhesion for the mechanical-biological energy manufacturing system that they developed [39].

When the results from both hydrophilic and hydrophobic species are combined, the following conclusions can be drawn with the thermodynamic model. Larger magnitude of attractive total free energy is predicted for ITO, polyethylene, polystyrene, and polycarbonate compared to stainless steel and glass and with these substrata larger attractive total free energy is predicted for the hydrophobic species compared to the hydrophilic species. Thus, the results show that hydrophobic species and substrata should be selected to promote biofilm formation and hydrophilic species and substrata should be selected for demoting the adhesion of cells to surfaces. Johnson and Wen's findings support these conclusions [38]. In their search for adhesion substrata for their attached microalgal growth system they were able to cultivate *Chlorella* sp. in biofilm over the hydrophobic substrata polystyrene foam and polyethylene fabric [38]. Furthermore, polyethylene is also used as the substrata for algal turf scrubbers that were used for formation and growth of algal biofilms for wastewater treatment [144]. The thermodynamic model also predicts the adhesion of all the algal species studied over polystyrene and polyethylene except for *Nannochloris* sp.

XDLVO approach

The interaction of the hydrophobic green algae, including *A. falcatus*, *B. braunii*, and *B. sudeticus*, with either of the substrata result in adhesion at the primary minimum, or in other words, adhesion at the minimum separation distance. Primary energy minima are also predicted for the interaction of the hydrophobic diatoms, including *A. coffeaeformis*, *N. frustulum*, and *C.*

fusiformis. However, for these interactions, energy barriers are present at large separation distances due to repulsive LW interactions between the cells and the substrata. Thus, while hydrophobic green algae are predicted to adhere over either of the substrata spontaneously, the hydrophobic diatoms have to possess the energy required, i.e., kinetic energy, to overcome the repulsive energy barrier due to the dominance of repulsive LW interactions at large separation distances.

The LW, AB, EL, and total interaction energy plots of all the hydrophobic green algae interacting with either of the substrata have the same trends. Thus, *A. falcatus*-polystyrene system is selected as the exemplary system to discuss the trends of these interaction energy between the hydrophobic cells and either of the substrata. Figure 5.1 presents these interaction energies as functions of separation distance for this system. Appendix B.1 includes the interaction energy between other hydrophobic green algae and substrata. Similar to *A. falcatus* interacting with polystyrene, for all the other hydrophobic green algae systems, LW and AB interactions are attractive and EL interactions are repulsive. The results show that the repulsive EL interactions are dominated by attractive LW and AB interactions at large, i.e., larger than 10 nm, and small separation distances, respectively. EL interactions are repulsive for algal species interacting with either of the substrata as all the surfaces experimented have negative surface potentials. Thus, combined effects of attractive LW and AB interactions are critical for the attainment of attractive interaction energy at all separation distances. For these systems the reason for

the domination of LW over EL interaction is the large ionic strength of BG-11 nutrient medium that compresses the electric double layers present around the cells and the substrata [91].

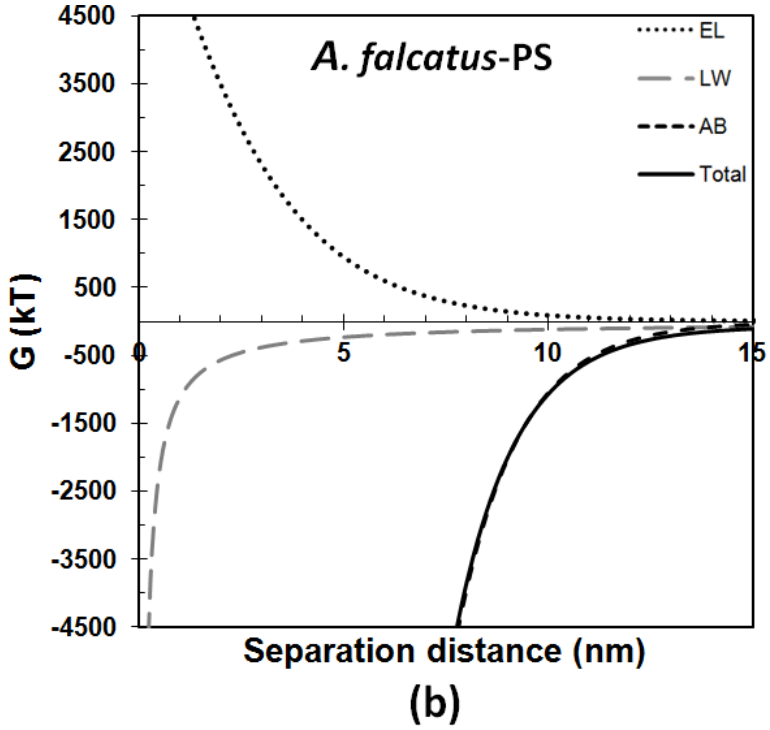

Figure 5.1: Energy of interaction between *A. falcatus* and polystyrene according to the XDLVO model. Interaction energy scale of kT is used for comparison with the energy of thermal (Brownian) motion associated with the microorganisms [3].

Table 5.5 presents the LW, AB, EL, and total interaction energy at the primary minimum for the hydrophobic green algae interacting with the substrata. These results can be used for the estimation of the relative adhesion

Table 5.5: Energy of interaction (in kT) between hydrophobic green algae and substrata at minimum separation distance.

Species		EL, LW, AB, and total interaction energy					
		Glass	ITO	PE	PS	PC	SS
A. falcatus	G_{Total}	-77703	-744200	-769215	-743627	-798245	-462677
	G_{EL}	6367	-2965	4218	6328	2662	6257
	G_{LW}	-7779	-4180	-4301	-7230	-3866	-5013
	G_{AB}	-76291	-737055	-769131	-742725	-797041	-599524
B. braunii	G_{Total}	-243424	-967356	-959118	-959685	-966507	-651699
	G_{EL}	10882	-5687	11590	9548	11107	9260
	G_{LW}	-4279	-2300	-2366	-3977	-2127	-2757
	G_{AB}	-250027	-959369	-968342	-965255	-975487	-658201
B. sudeticus	G_{Total}	-29825	-326564	-336297	-324729	-349286	-201141
	G_{EL}	3505	-1670	3098	3264	2630	3196
	G_{LW}	-1503	-808	-831	-1397	-747	-968
	G_{AB}	-31827	-324086	-338564	-326596	-351169	-203369

strength between the algae and the substrata [172]. Based on these results it can be concluded that (i) AB interactions dominate the total interaction energy at the minimum separation distance, (ii) for any of the species interaction with ITO, polyethylene, polystyrene, and polycarbonate result in similar and largest magnitudes of attractive energy, and (iii) for any substrata interaction with *B. braunii* creates the largest strength of adhesion. Thus, based on the species and substrata studied to promote the formation of algal biofilms ITO, polyethylene, polystyrene, or polycarbonate should be selected as the substrata and *B. braunii* should be selected as the algal species. As presented in Sections 2.5.3 and 2.5.4, the magnitudes of EL, LW, and AB interactions increase with increasing cell size. Thus, for two identical cell to substrata systems other than the difference in the cell size, increase in this parameter

increases the magnitude of attractive or repulsive total interaction energy. For instance, keeping all parameters constant and decreasing the diameter of *A. falcatus* from 10.41 to 4.32 μm, which is equal to the diameter of *B. sudeticus*, decreases the total interaction energy at the primary minimum from -743627 to -308593 kT for interaction with polystyrene. However, it should also be kept in mind that as presented in Section 4.2.7, the lift and drag forces acting on cells also increases with increasing cell size. For instance, using the parallel plate flow chamber presented in Section 4.2.6 for a flow rate of 1 ml min^{-1}, the net force acting on a cell adhered over substrata decreases from 1.92×10^{-11} to 3.32×10^{-12} N with the same decrease in cell size. Thus, to select algae species-substrata couples either to promote or inhibit the adhesion of algae cells both the interaction energy and the hydrodynamic effects of cell size should be taken into account.

All the hydrophobic diatom substrata interactions resulted in similar LW, EL, AB, and total interaction energy as functions of separation distance, except *A. coffeaeformis* and *N. frustulum* interacting with glass. Thus, instead of presenting all the diatom substrata interaction energy plots, *C. fusiformis* polyethylene interaction presented in Figure 5.2 is selected as the exemplary system. The interaction energy plots of all the hydrophobic diatom substrata systems are presented in Appendix B.2. As can be seen from Figure 5.2, XDLVO approach predicts the presence of primary energy minimum for all hydrophobic diatoms interacting with either of the substrata. However, as opposed to hydrophobic green algae-substrata systems, the interaction between

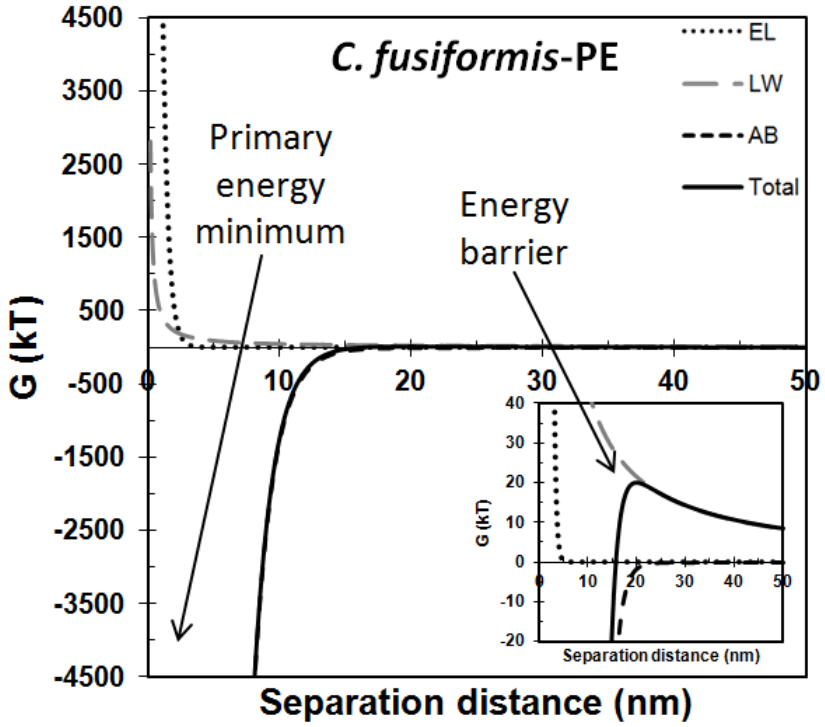

Figure 5.2: Energy of interaction between *C. fusiformis* and polyethylene according to the XDLVO model.

the diatoms and the substrata result in repulsive interaction energy at separation distances larger than about 13 nm. The reason for the prediction of primary minimum and the repulsive energy barrier is the short range attractive AB and long range repulsive LW interactions, respectively. Moreover, for these systems the range of EL interaction is shorter compared to the hydrophobic green algae due to higher ionic strength of the ASP-M medium used to cultivate these species. Finally, *A. coffeaeformis*-glass and *N. frustulum*-glass systems result in repulsion at all separation distances as the AB, EL, and LW

interactions are repulsive for these systems.

For any adhesion to occur with the hydrophobic diatoms in the primary minimum, the cells have to possess sufficient kinetic energy to overcome the energy barriers that are present due to LW repulsion. Table 5.6 presents the magnitude and separation distance of energy barriers that are present between the diatoms and the substrata. Based on the results energy barriers ranging from 16.7 to 75.9 kT are predicted for separation distances ranging from 15.5 nm to 20.1 nm. Assuming that the hydrophobic diatoms have a cellular density of 1.1 g mL^{-1} [173], minimum velocity ranges of 0.60 mm s^{-1} to 0.85 mm s^{-1}, 0.32 mm s^{-1} to 0.48 mm s^{-1}, and 0.86 mm s^{-1} to 1.24 mm s^{-1} are required to attain the kinetic energy required to overcome these energy barriers for *A. coffeaeformis*, *C. fusiformis*, and *N. frustulum*, respectively. In biofilm photobioreactor systems these energy can be given to the algae cells through pumping to ensure algal adhesion. A similar repulsion may be the reason why Johnson and Wen could initiate the formation of *Chlorella* sp. biofilms only under constant agitation of the cells with a rocking shaker [38].

Table 5.7 summarizes the interaction energy between the hydrophobic diatoms and the adhesion substrata at the primary energy minimum. The results show that the total interaction energy are dominated by the attractive AB interactions at the primary minimum similar to hydrophobic green algae. For desorption of the diatoms from the substrata, the cells must possess an energy that is at least equal to the sum of the total interaction energy at the primary minimum and the energy barrier that exist due to LW repul-

Table 5.6: The magnitude (in kT) and the separation distance (in nm) of the energy barrier to be overcome for the cell adhesion in the primary minimum for the hydrophobic diatom-substrata interactions.

Species	The magnitude and the separation distance of the energy barrier						
		Glass	ITO	PE	PS	PC	SS
A. coffeaeformis	Energy bar.	-	41.6	42.4	75.9	37.4	54.9
	Sep. dist.	-	17.2	17.3	16.2	17.7	15.5
C. fusiformis	Energy bar.	41.3	19.4	20.0	35.1	17.9	24.2
	Sep. dist.	17.3	20.0	20.0	19.1	20.1	19.2
N. frustulum	Energy bar.	-	16.7	16.8	30.5	14.7	23.8
	Sep. dist.	-	16.6	16.9	15.6	17.4	13.7

sion [172]. When the sum of these two interaction energies is considered for each hydrophobic diatom-substratum system, to promote cell adhesion ITO, polyethylene, polystyrene, and polycarbonate should be selected as the substrata and *C. fusiformis* should be selected as the algal species.

The interaction of the hydrophilic green algae, including *C. vulgaris*, *N. oculata*, and *S. dimorphus*, with ITO, polyethylene, polystyrene, and polycarbonate are expected to result in adhesion at the primary minimum. The reason for these predictions is the attractive LW and AB interactions between these species and the substrata. Adhesion is not predicted for the interaction of *Nannochloris* sp. with either of the substrata as (i) LW interaction is repulsive for this specie and (ii) this species has a large electron donor parameter that results in AB repulsion at interaction with either of the substrata. The interaction energy between these hydrophilic green algae and the substrata are presented in Appendix B.3.

Table 5.7: Energy of interaction (in kT) between diatoms and substrata at minimum separation distance.

Species	EL, LW, AB, and total interaction energy with the substrata						
		Glass	ITO	PE	PS	PC	SS
A. cofeaeformis	G_{Total}	74021	-342891	-351054	-342875	-389684	-139644
	G_{EL}	20095	-9152	29089	15575	32136	14790
	G_{LW}	9453	5080	5227	8786	4698	6091
	G_{AB}	44473	-338819	-385369	-342875	-426517	-160525
C. fusiformis	G_{Total}	-336336	-925055	-845685	-889655	-822292	-651104
	G_{EL}	27441	-17352	41842	20343	46824	19118
	G_{LW}	5067	2723	2802	4710	2518	3265
	G_{AB}	-368844	-910426	-890329	-914708	-871634	-672065
N. frustulum	G_{Total}	49813	-97830	-103786	-85357	-125134	-14258
	G_{EL}	10746	-4269	15248	8458	16755	8059
	G_{LW}	3713	1996	2053	3451	1845	2393
	G_{AB}	35354	-95557	-121087	-97266	-143734	-24710

Similar to the interaction energy presented in Figure 5.1 for *A. falcatus*-polystyrene system, the repulsive EL interaction is overcome by attractive LW or AB interactions at large and small separation distances, respectively, for *C. vulgaris*, *N. oculata*, and *S. dimorphus* interacting with ITO, polyethylene, polystyrene, and polycarbonate. The result is attractive total interaction energy at all separation distances for these systems. Finally, attractive AB interactions are attributed to the small electron donor and acceptor parameters these substrata have.

Table 5.8 summarizes the interaction energy between the hydrophilic cells with ITO, polyethylene, polystyrene, and polycarbonate. Similar to the interaction of hydrophobic algae with these substrata, attractive AB interactions dominate the total interaction energy at minimum separation distance.

However, the magnitude of the attractive AB interactions is smaller due to hydrophilicity of these algal species. Thus, smaller magnitude of attractive total interaction energy are predicted for these species indicating weaker adhesion strength compared to algae with hydrophobic surface properties.

Table 5.8: Energy of interaction (in kT) between hydrophilic algae and substrata at minimum separation distance.

Species	EL, LW, AB, and total interaction energy				
		ITO	PE	PS	PC
C. vulgaris	G_{Total}	-90173	-135479	-88460	-181400
	G_{EL}	-2108	3948	4089	3386
	G_{LW}	-2269	-2335	-3925	-2099
	G_{AB}	-85795	-137091	-88623	-182687
N. oculata	G_{Total}	-26823	-46624	-23309	-70324
	G_{EL}	-2481	4675	3025	4842
	G_{LW}	-865	-890	-1496	-800
	G_{AB}	-23477	-50409	-24839	-74367
S. dimorphus	G_{Total}	-378443	-505650	-380400	-625891
	G_{EL}	-3276	3045	7252	600
	G_{LW}	-5891	-6062	-10189	-5448
	G_{AB}	-369276	-502634	-377463	-621043

The interactions of the hydrophilic green algae species, including *C. vulgaris*, *N. oculata*, and *S. dimorphus*, with glass and stainless steel result in adhesion at the secondary minimum except *S. dimorphus*-stainless steel system that results in adhesion at the primary minimum. Moreover, adhesion is not predicted for the interaction of the hydrophilic algae *Nannochloris* sp. with either of the substrata. The reason for the prediction of adhesion at the secondary minimum for *C. vulgaris*, *N. oculata*, and *S. dimorphus* interacting with these substrata is the attractive LW interaction that dominates the

repulsive EL and AB interactions at large separation distance. For instance, as presented in Figure 5.3 for *C. vulgaris*-stainless steel system a secondary energy minimum of -23.0 kT is predicted at a separation distance of 15.5 nm. The cells can adhere over the substrata in this secondary minimum. However, these interactions are considered to be weaker and more reversible compared to adhesion at the primary minimum as the magnitude of interaction is small and the cells are kept at a distance from the surface [91, 172]. For instance, at a velocity of 1.5 mm s^{-1}, *C. vulgaris* has the kinetic energy equivalent to this

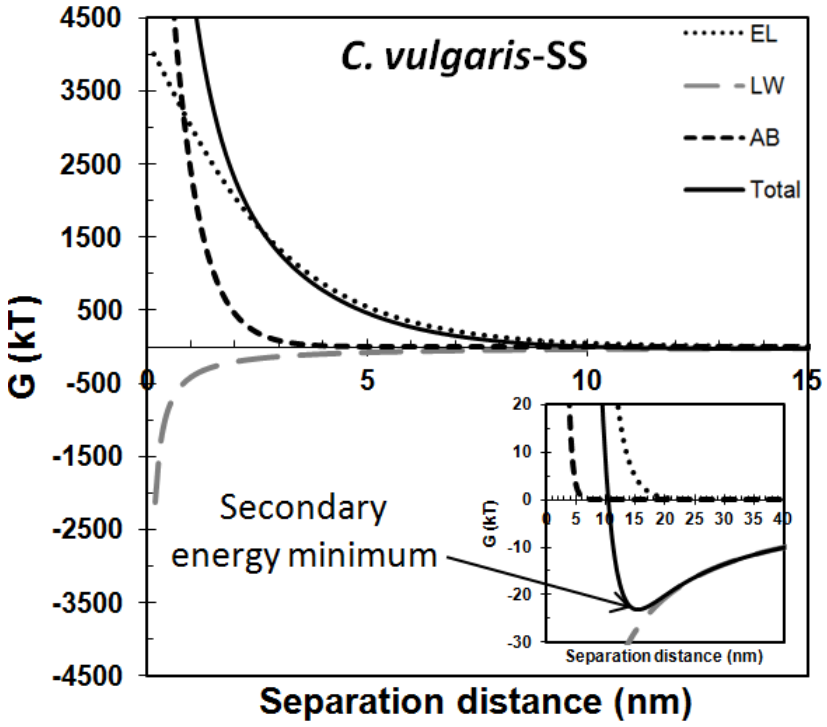

Figure 5.3: Energy of interaction between *C. vulgaris* and stainless steel according to the XDLVO model.

attractive energy. The interaction energy plots of these hydrophilic algae interacting with glass and stainless steel are presented in Appendix B.3. Table 5.9 summarizes the magnitude of the secondary minimum for all the hydrophilic algal species. The results show that interaction energy ranging from -12 kT to -102 kT is predicted at separation distances ranging from 14.2 to 17.3 nm. Thus the results indicate that for any aquatic system to avoid algal biofouling hydrophilic substrata such as glass should be utilized. This can also be achieved through application of hydrophilic coatings on other more economical substrata.

Table 5.9: Total interaction energy (in kT) and separation distance (in nm) at the secondary minimum for hydrophilic green algae interacting with glass and stainless steel

Substrata	Inter. energy and sep. dist. for the secondary energy min.			
		C. vulgaris	*N. oculata*	*S. dimorphus*
Glass	Inter. energy	-37.0	-12.4	-101.7
	Sep. dist.	14.9	16.7	14.2
Stainless steel	Inter. energy	-23.0	-7.7	-
	Sep. dist.	15.5	17.3	-

5.3.3 Cell to cell interactions

The results of only the interaction of the hydrophilic-hydrophobic species are included in this chapter since (i) the interaction of the hydrophobic algal cells of the same species result in co-aggregation thus do not necessitate bioflocculation and (ii) hydrophilic-hydrophilic cell interactions do not result in co-aggregation. Appendix B.4-B.5 and Appendix C.1-C.2 include the interaction

energy between all the algal species based on XDLVO and thermodynamic models, respectively. Moreover, the interactions of the freshwater species and saltwater species are discussed separately since (i) the addition of saltwater algae to freshwater as a bioflocculant result in cytolysis of the saltwater species and (ii) mixing of two medium with large difference in water chemistry makes the recycle of the final medium impractical.

Thermodynamic approach

Table 5.10 presents the free energy of interaction between the hydrophilic, *C. vulgaris*, *N. oculata*, and *S. dimorphus*, and the hydrophobic algal species, *A. falcatus*, *B. braunii*, and *B. sudeticus*. The results show that the interaction of either of the hydrophilic algae with either of the hydrophobic algae result in coaggregation since both of the LW and AB interactions are attractive for all these systems. Indeed Salim *et al.* reported an increase in gravitational *C. vulgaris* recovery from 20% to 45% with addition of *A. falcatus* as a bioflocculant [33]. Moreover, the interaction of the hydrophilic species with *B. braunii* result in the largest magnitude of attractive free energy of coaggregation indicating that the coaggregation strength should be the largest with this species.

The free energy of co-aggregation between the the hydrophilic, *Nannochloris* sp. and hydrophobic diatoms, *A. coffeaeformis*, *C. fusiformis*, and *N. frustulum*, are summarized in Table 5.11. The results show that only the interaction of *C. fusiformis* with *Nannochloris* sp. result in adhesion as both AB and LW interactions are attractive for this system. Adhesion is not predicted for the interactions of *Nannochloris* sp. with *A. coffeaeformis* and *N. frus-*

Table 5.10: Interaction energy between the freshwater species according to the thermodynamic model (in mJ m^{-2}).

Species to be flocculated-LW, AB components and total free energy of co-aggregation		Species added for flocculation		
		A. falcatus	*B. braunii*	*B. sudeticus*
C. vulgaris	ΔG_{LW}	-4.13	-2.34	-1.93
	ΔG_{AB}	-16.55	-32.66	-17.25
	ΔG_{co-agg}	-20.68	-34.99	-19.18
N. oculata	ΔG_{LW}	-3.37	-2.34	-1.93
	ΔG_{AB}	-11.28	-27.46	-11.62
	ΔG_{co-agg}	-14.65	-29.80	-13.55
S. dimorphus	ΔG_{LW}	-4.07	-2.30	-1.89
	ΔG_{AB}	-25.06	-43.20	-26.30
	ΔG_{co-agg}	-29.13	-45.50	-28.19

tulum due to AB repulsions. The reason for these AB repulsions is the large electron donor and acceptor parameters of these species. Thus, the results indicate that *C. fusiformis* should be used as the species for the bioflocculation in saltwater medium.

Table 5.11: Interaction energy between the saltwater algae species according to the thermodynamic model (in mJ m^{-2}).

Species to be flocculated-LW, AB components and total free energy of adhesion		Species added for flocculation		
		A. coff.	*C. fusi.*	*N. frus.*
Nannochloris sp.	ΔG_{LW}	-0.37	-0.17	-0.25
	ΔG_{AB}	29.27	-9.03	27.68
	ΔG_{co-agg}	28.90	-9.20	27.43

XDLVO approach

XDLVO approach predicts adhesion at the primary minimum for the interaction of the hydrophilic species *C. vulgaris*, *N. oculata*, and *S. dimorphus* with either of the hydrophobic species. Figure 5.4 presents the exemplary interac-

tion between *N. oculata* and *B. braunii*. As can be concluded from the figure, the EL repulsion between *C. vulgaris* and *B. braunii* is overcome by the AB and LW forces at small and large separation distances resulting in prediction of attractive interaction at all separation distances. Table 5.12 presents the interaction energy between the hydrophilic and hydrophobic cells at the primary minimum. Results indicate that from the interaction of the hydrophilic and hydrophobic green algae the largest magnitude of attractive energy were obtained with *B. braunii*. Thus, based on the XDLVO model *B. braunii* is the algal species that should be used for bioflocculation of freshwater algae.

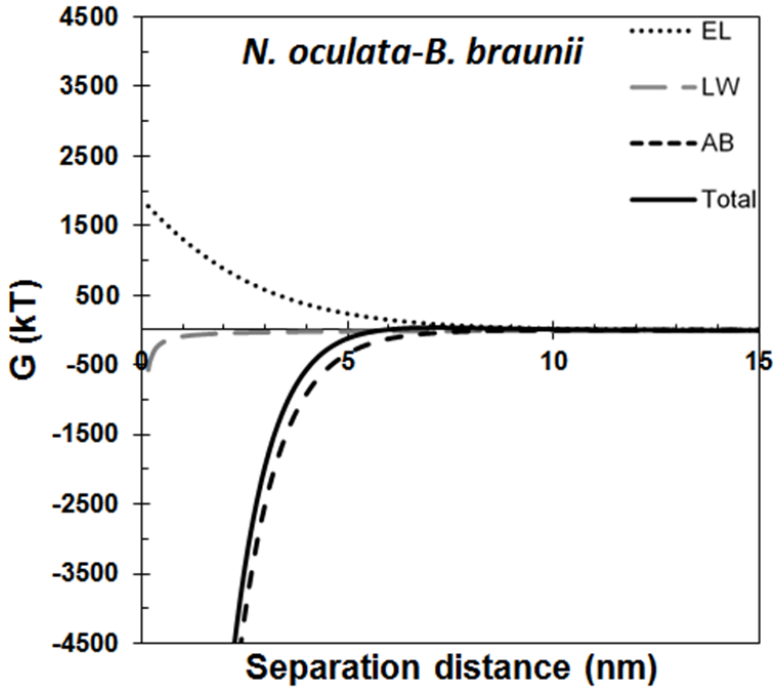

Figure 5.4: Energy of interaction between *B. braunii* and *N. oculata* according to the XDLVO model.

Table 5.12: Energy of interaction (in kT) between hydrophilic and hydrophobic green algae at minimum separation distance.

Species to be flocculated-EL, LW, AB components, and total interaction energy		Species added for flocculation		
		A. falcatus	*B. braunii*	*B. sudeticus*
C. vulgaris	G_{Total}	-67955	-131496	-31403
	G_{EL}	1867	2520	1476
	G_{LW}	-1779	-996	-560
	G_{AB}	-68043	-133020	-32319
N. oculata	G_{Total}	-25938	-62938	-20663
	G_{EL}	1196	1780	1147
	G_{LW}	-644	-571	-372
	G_{AB}	-26490	-64147	-21439
S. dimorphus	G_{Total}	-175236	-295200	-100501
	G_{EL}	2515	2985	1543
	G_{LW}	-2967	-1651	-763
	G_{AB}	-174785	-296533	-101280

Similar to the interaction between hydrophobic and hydrophilic green algae, as presented in Figure 5.4, adhesion at the primary minimum is predicted for the interaction of the hydrophobic diatom *C. fusiformis* with *Nannochloris* sp., and *N. frustulum*. As adhesion at the secondary minimum is predicted for the interaction of two *N. frustulum* cells, this species is also considered as one of the species that require flocculation. Table 5.13, presents the interaction energy at the minimum separation distance for the interaction of the saltwater species. The results show that XDLVO theory predicts flocculation of *N. frustulum* interacting with either *A. coffeaeformis* or *C. fusiformis*. However, for *Nannochloris* sp. bioflocculation is only predicted for the interaction with *C. fusiformis* due to more hydrophobic surface properties of the later species.

Table 5.13: Energy of interaction (in kT) between the hydrophilic and hydrophobic saltwater species at minimum separation distance.

Species to be flocculated-EL, LW, AB components and total free energy of adhesion		Species added for flocculation	
		A. coffeaeformis	*C. fusiformis*
N. frustulum	G_{Total}	-980	-77694
	G_{EL}	12174	14879
	G_{LW}	-1196	-795
	G_{AB}	-11958	-91778
Nannochloris sp.	G_{Total}	36945	-17615
	G_{EL}	6209	7511
	G_{LW}	-103	-47
	G_{AB}	30838	-25079

In addition to bioflocculation, cell to cell interactions can also be essential for algal biofilms considering that after the algae cells adhere over a substrata, cell to cell interactions are the systems that control the growth of the biofilm. Although the interaction of hydrophilic strains, such as *C. vulgaris*, *S. dimorphus*, and *N. oculata*, and hydrophobic substrata is predicted to result in adhesion, when the interaction between the cells of same species are considered the following cell to cell interactions are repulsive which might inhibit the growth of the biofilm. The hydrophobic strains such as, *A. falcatus*, *B. braunii*, *B. sudeticus*, and *C. fusiformis* not only have larger adhesion strength over the same substrata but also cell to cell interactions of these strains are attractive. Thus, to promote the formation of algal biofilms these hydrophobic strains should be selected.

5.3.4 Effects of aquatic properties on cell to substrata and cell to cell interactions

Effects of pH

The algae cells and substrata contain ionizable functional groups such as hydroxyl (-OH), carboxyl (-COOH), and amine (-NH_2) groups [174, 175]. These groups can get deprotonated or protonated based on the system pH and can create surface charge. For instance when an algae surface containing amine and carboxyl groups are considered; (i) at low pH both of these groups are protonated, i.e., -COOH and -NH_3^+ are present over the algae cell, creating a positive surface charge, (ii) at high pH these surface groups are deprotonated, i.e., surface groups such as -COO^- and -NH_2 are introduced, and (iii) in the intermediate pH, while carboxyl groups are deprotonated the amino groups are protonated (-COO^- and -NH_3^+) resulting in a net surface charge of zero and this point is called the point of zero charge (PZC) [174]. This variation in surface charge can be used to induce electrostatic repulsion or attraction for cell to cell and cell to substrata systems.

To put the effects of solution pH on electrostatic interaction into perspective let us consider the interaction of *C. vulgaris* with glass at four different pH values. Figure 5.5 presents the zeta potential of *C. vulgaris* as a function of pH [154]. Based on the figure *C. vulgaris* has a PZC of about 2.9 and the cells have a surface potential of about 16.1, -9.3, -16.9, and -22.1 mV at pH of 2, 4, 6, and 8, respectively [4]. Moreover, for the same ionic strength glass has a surface charge of 11.1, -11.6, -69.7, and -128.4 mV at pH of 2, 4, 6, and 8,

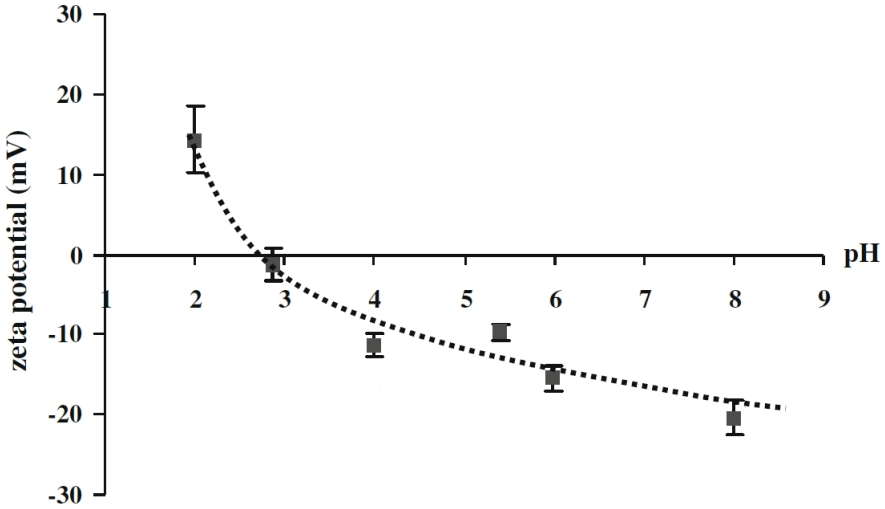

Figure 5.5: Zeta potential of *C. vulgaris* as a function of pH in a 10 mM $NaNO_3$ solution [4].

respectively [154]. Figure 5.6 presents the electrostatic interaction energy between *C. vulgaris* cells and glass at these pH according to the XDLVO model. The results show that by decreasing the system pH from 8 to 4, the electrostatic energy barrier between cell and substrata can be decreased from 2779 to 399 kT. However, when the pH of the system is decreased from 4 to 2, the magnitude of the energy barrier increases from 399 to 604 kT due to charge reversal and increase in the magnitude of the surface charges. Thus, to promote *C. vulgaris* adhesion on glass pH of the system should be kept close to the PZC and to inhibit cell adhesion the system should be run at high pH. Therefore, to optimize the electrostatic interaction for other cell-substrata and cell-cell systems their surface potential should be studied as a function of pH and taking the health of the algal culture also into account system pH should

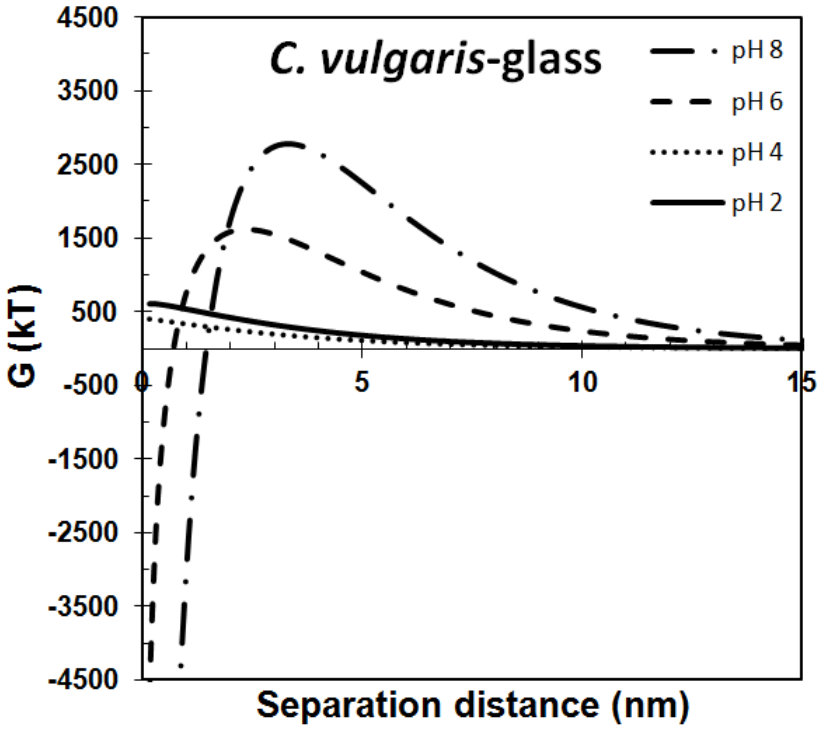

Figure 5.6: Electrostatic interaction energy between *C. vulgaris* and glass according to the XDLVO model at pH of 2, 4, 6, and 8.

be adjusted.

Effects of ionic strength

In general the XDLVO model predicts the domination of LW and AB interactions at small and domination of EL interactions in larger separation distances, respectively [93, 176]. As presented by Equations (2.15) and (2.15), the magnitude of EL interaction is a function of the concentration of ions present in the system, i.e., ionic strength. As the ionic strength increases the availability of the counter ions increase and the length of the electric double layer

decreases [176]. It should also be noted that for the same ion concentration, an increase in ion charge number increases the double layer compression as presented by Equation (2.15). Decreasing length of the electric double layers decreases the range and magnitude of electrostatic interactions considering that the presence of this repulsion is due to the overlapping of the cell and substrata electric double layers [85]. Figure 5.7 presents the EL interaction between *B. braunii* and glass as a function of ionic strength. As can be seen from the figure, the range and the magnitude of EL repulsion decreases with increasing ionic strength. Considering that AB and LW interactions are dominant at small separation distances, the increasing ionic strength decreases the influence of usually repulsive electrostatic interactions for cell to cell and cell to substrata systems. Thus, the use of saltwater algae species may have an advantage over the freshwater species for algae biofilm PBR systems and bioflocculation.

In addition to their effects on electrostatic interaction, the presence of multivalent ions can also influence the acid base interaction of cell to cell and cell to substrata systems [84]. For instance, multivalent cations such as Ca^{2+} and Mg^{2+} can partly neutralize the surface groups that are electron acceptors and decrease the magnitude of the electron acceptor parameter [84]. By doing so the surfaces can attain more hydrophobic surface characteristics which can increase the acid base attraction of cell to cell and cell to substrata systems [84]. Thus, similar to the conclusions drawn for EL interaction, the use of saltwater species may be more advantageous for promoting the attractive AB

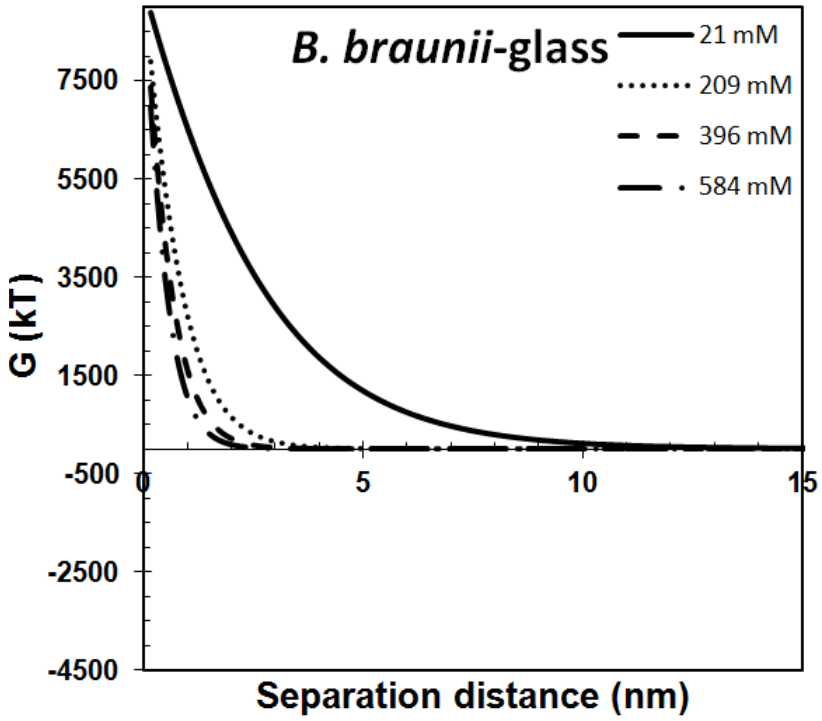

Figure 5.7: Electrostatic interaction energy between *B. braunii* and glass according to the XDLVO model at ionic strengths of 21, 209, 396, and 584 mM.

interactions for cell to cell and cell to substrata systems [84].

5.4 Conclusion

A comprehensive study has been conducted to (i) quantify the physicochemical surface properties of algal cells and (ii) to determine the effects of these parameters on cell to substrata and cell to cell interactions using theoretical models. For this purpose, the surface properties of five planktonic and five benthic algal species, and adhesion substrata were quantified with

electrophoretic mobility, contact angle, and streaming potential and current measurements. Moreover, thermodynamic and XDLVO models were used to estimate the interaction energy between the surfaces studied. Based on the results obtained the following conclusions can be drawn:

- All the benthic species had hydrophobic surfaces while all the planktonic species, except for *A. falcatus*, had hydrophilic surfaces.
- The thermodynamic and the XDLVO models predict adhesion for the interaction of the hydrophobic green algae with either of the hydrophobic or hydrophilic substrata.
- Based on the thermodynamic model, hydrophobic diatom-substrata systems result in adhesion due to domination of the attractive AB interactions over repulsive LW interactions and for the same systems XDLVO theory predicts primary energy minimum at contact due to AB attraction and an energy barrier at large separation distance, i.e., larger than 14 nm, due to long range LW repulsion.
- For the hydrophilic algae-substrata interactions, both models predict adhesion for the interactions with the hydrophobic substrata.
- For all freshwater green algae interacting with hydrophobic species, both models indicate bioflocculation.
- For saltwater species, both models predict bioflocculation for the interaction of the hydrophilic algae, *Nannochloris* sp., with the hydrophobic

diatom *C. fusiformis*.

- The hydrophobic species *A. falcatus*, *B. braunii*, *B. sudeticus*, and *C. fusiformis* are excellent candidates for forming biofilms as (i) the interaction of these species with substrata result in large attractive interaction energy and (ii) cell to cell interactions within each species result in adhesion.

- Moreover, *B. braunii* and *C. fusiformis* have the most favorable surface properties for biofloccuation in freshwater and saltwater aquatic systems, respectively.

- To avoid biofouling in aquatic systems such as photobioreactors, hydrophilic species and substrata with hydrophilic surface properties should be used.

These results can be used for promoting or inhibiting cell to substrata and cell to cell interactions of algal species in freshwater and saltwater aquatic systems. Thus, this study might have implications in selection and design of algal cells and substrata to (i) avoid biofouling in planktonic photobioreactors and ship hulls, (ii) to promote adhesion of cells in biofilm photobioreactor systems, and (iii) increase efficiency in bioflocculation based harvesting of algal cells.

Chapter 6

Conclusions and Recommendations

6.1 Summary

This section summarizes the conclusions of the current study.

Reduction of Water and Energy Requirement of Algae Cultivation Using an Algae Biofilm Photobioreactor

A novel algae biofilm photobioreactor was constructed, operated, and analyzed. The results indicate that the current system is capable of producing highly dense algal outputs with reduced water and energy inputs in comparison to existing systems. Moreover, the biomass and lipid productivities of the system were low due to slow growing nature of *Botryococcus braunii*. Thus, the results show that species capable of biofilm growth with larger biomass and lipid productivities should be identified and incorporated to reach the productivity levels reported in the literature.

Adhesion of Algae Cells to Surfaces

Cell to substrata interactions of benthic and planktonic algal species were studied with hydrophilic and hydrophobic surfaces with theoretical models and parallel plate flow experiments to determine critical parameters controlling the adhesion of algae cells. The results show that the benthic and plank-

tonic species had hydrophobic and hydrophilic surface properties, respectively. Moreover, the interaction of the hydrophobic species with substrata resulted in larger strength and rate of adhesion due to acid base attraction. Thus, the results indicate that AB interactions are critical for the interaction of cells with substrata and hydrophobic species and substrata should be incorporated in design of algal biofilm photobioreactors. Finally, the XDLVO was the most accurate model for predicting algal adhesion.

Cell to cell and cell to substrata interactions of algae species

Surface properties of ten algal species were quantified and their cell to substrata interactions were modeled using XDLVO approach to determine species and substrata suitable for biofilm cultivation. All the benthic species had hydrophobic surface properties whereas all planktonic species (except one) had hydrophilic surface properties. Moreover, the results also show that hydrophobic species and substrata were suitable for biofilm cultivation and associated substrata for growing biofilms on. Thus, based on the results to promote the formation of algal biofilms *Ankistrodesmus falcatus*, *Botryococcus sudeticus*, *Botryococcus braunii*, and *Cylindrotheca fusiformis* should be interacted with hydrophobic substrata such as ITO, polyethylene, polystyrene, and polycarbonate. These interactions not only result in attractive cell to substrata interactions that are required for initiation of biofilm growth but also result in attractive cell to cell interactions which may be essential for the growth of the biofilm.

6.2 Recommendations for Future Research

The future work summarized below is recommended to further develop the current photobioreactor.

- To increase the biomass and lipid productivity of the system, benthic species with larger productivities should be incorporated instead of slow growing algae *Botryococcus braunii*. Based on the current research, fresh-water species *Botryococcus sudeticus*, *Ankistrodesmus falcatus*, and salt-water species *Cylindrotheca fusiformis* are the promising species for the future studies. Moreover, to further increase the areal productivity of the system, photobioreactors with corrugated surfaces should be constructed and operated.

- The diffusional characteristics and photosynthetically active radiation (PAR) profile of algal biofilms should be studied with microsensors to fully understand the mass and light transport of the system. Moreover, photosynthesis versus irradiation intensity (PI) curves should be obtained for the benthic algal species. Based on the light attenuation characteristics of the biofilm , the PI curves, and the solar irradiance, the corrugation angle of the photobioreactor should be determined and algal biofilm photobioreactors should be operated at outdoor conditions. Optimization of the corrugation angle is critical for maximizing the biomass productivity of the system as (i) photoinhibition of the cells can be avoided by working with reflected light over larger surface area rather

than direct irradiation and (ii) by doing so the biofilm growth area per reactor footprint can be increased.

- One of the major barriers for the commercial production of algal biodiesel is the extraction processes of algal lipids. These processes not only require production of algae cakes with high solid contents thereby increasing the energy intensity of the process but also do not let the reuse of the biomass for lipid production as these processes kill the algae. One potential way of avoiding the latter shortcoming is to milk the algal lipids using biocompatible solvents that allow re-cultivation of the biomass for lipid production [126, 177]. Algal biofilm photobioreactors may be the ideal systems for milking of algal lipids as with these systems (i) the nutrient medium is decoupled from the biomass and (ii) large direct algal harvest concentrations are possible. Thus, biocompatible solvents and processes suitable should be determined for lipid milking from the current reactor and the lipid extraction efficiency of the process and its influence on the algal viability should be studied.

- Based on the results from the mass and light transfer studies, a pilot scale corrugated photobioreactor should be constructed and operated at outdoor conditions. Moreover, the life cycle analysis of the system should be conducted to determine energy, economic, and environmental impacts.

- Considering the energy intensive processes for production of nitrogen

and limited sources of phosphorus, the algal biofilm growth using waste resources such as municipal wastewater or anaerobic digestion effluents should be investigated [178, 179]. Moreover, the nutrient removal, biomass and lipid production rates of the system should be determined.

- Algae is known for its capacity to remove heavy metals from water streams through adsorption of metals to the functional groups present over the cell surface [71]. Thus algae have been studied as an alternative to the current heavy metal removal processes as these systems are energy intensive and cost prohibitive [71–73]. The primary draw back of the use of algae is the challenge of the removal of the heavy metal loaded cells from the treated water. Thus, the use of the current photobioreactor can be more advantageous for this process as (i) after removal of heavy metals water streams free of algae cells can be provided and (ii) additional heavy metal removal can be achieved with algal biofilms as heavy metals can also precipitate due to increased pH present around the algal biofilm [74]. Thus, the current reactor's heavy metal removal potential and its kinetics should be studied to determine the feasibility for such use.

Appendices

Appendix A

Nomenclature

Nomenclature

A	Hamaker constant
a	radius of algae cell, m
b	depth of the parallel plate flow chamber, m
c	distance from the surface of the substrata, m
d	separation distance of algae cell and substrate, m
d_0	minimum separation distance between two surfaces, m
e	electron charge, 1.6022×10^{-10} C
k	Boltzmann constant, 1.3807×10^{-23} J K^{-1}
n	concentration of ions, # m^{-3}
N	cell number concentration, # m^{-3}
OD	optical density
Q	volumetric flow rate, m^3 s^{-1}
Re	Reynolds number
T	temperature, K
v	hydration layer associated with algal cells, m
w	width of the parallel plate flow chamber, m
z	charge number of ions

Greek symbols

γ	surface energy, J m^{-2}
ζ	zeta potential, V
ψ	surface potential, V
ε	permitivity of the medium, F m^{-1}
ε_r	relative permitivity
ε_0	permitivity of the vacuum, 8.85×10^{-12} F m^{-1}
θ	contact angle, degrees
η	dynamic viscosity of water at 20^oC , 8.9×10^{-4} Pa s
ρ	density of water at 20 ^{o}C, 997 kg m^{-3}
$\dot{\gamma}$	wall shear rate, s^{-1}
κ^{-1}	double layer thickness, m
λ	correlation length of the molecules of the liquid medium, m

Superscripts

AB	refers to acid-base, i.e., polar component
LW	refers to Lifshitz-van der Waals, i.e., dispersive component
$+$	refers to electron acceptor parameter
$-$	refers to electron donor parameter

Subscripts

s	refers to substrate
sr	refers to surface
l	refers to liquid medium
m	refers to algae

$srlsr$	refers to two identical surfaces in a liquid medium
0	refers to vacuum

Appendix B

Results from the XDLVO Model

This appendix contains the interaction energy plots of the XDLVO model for cell substrata systems.

B.1 Hydrophobic green algae substrata interactions

In this section electrostatic (EL), van der Waals (LW), acid base (AB), and total interaction energy plots of the hydrophobic green algae-substrata systems are presented.

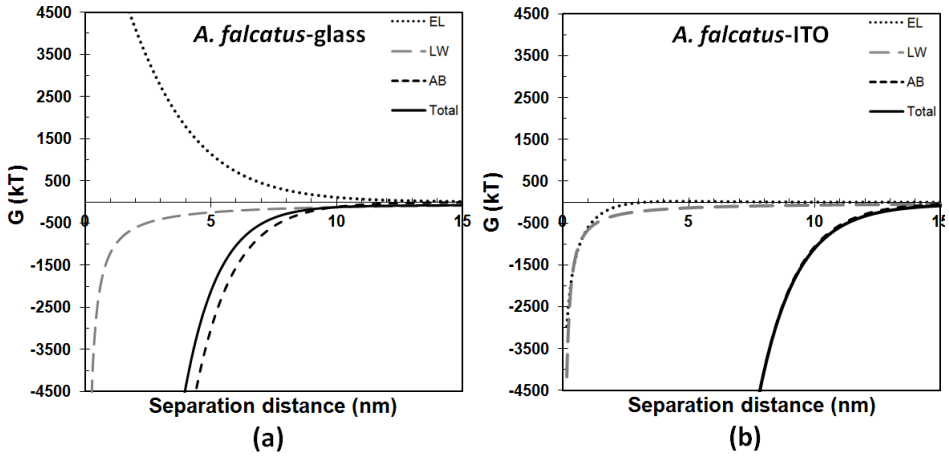

Figure B.1: Energy of interaction between *A. falcatus* and (a) glass and (b) ITO according to the XDLVO model.

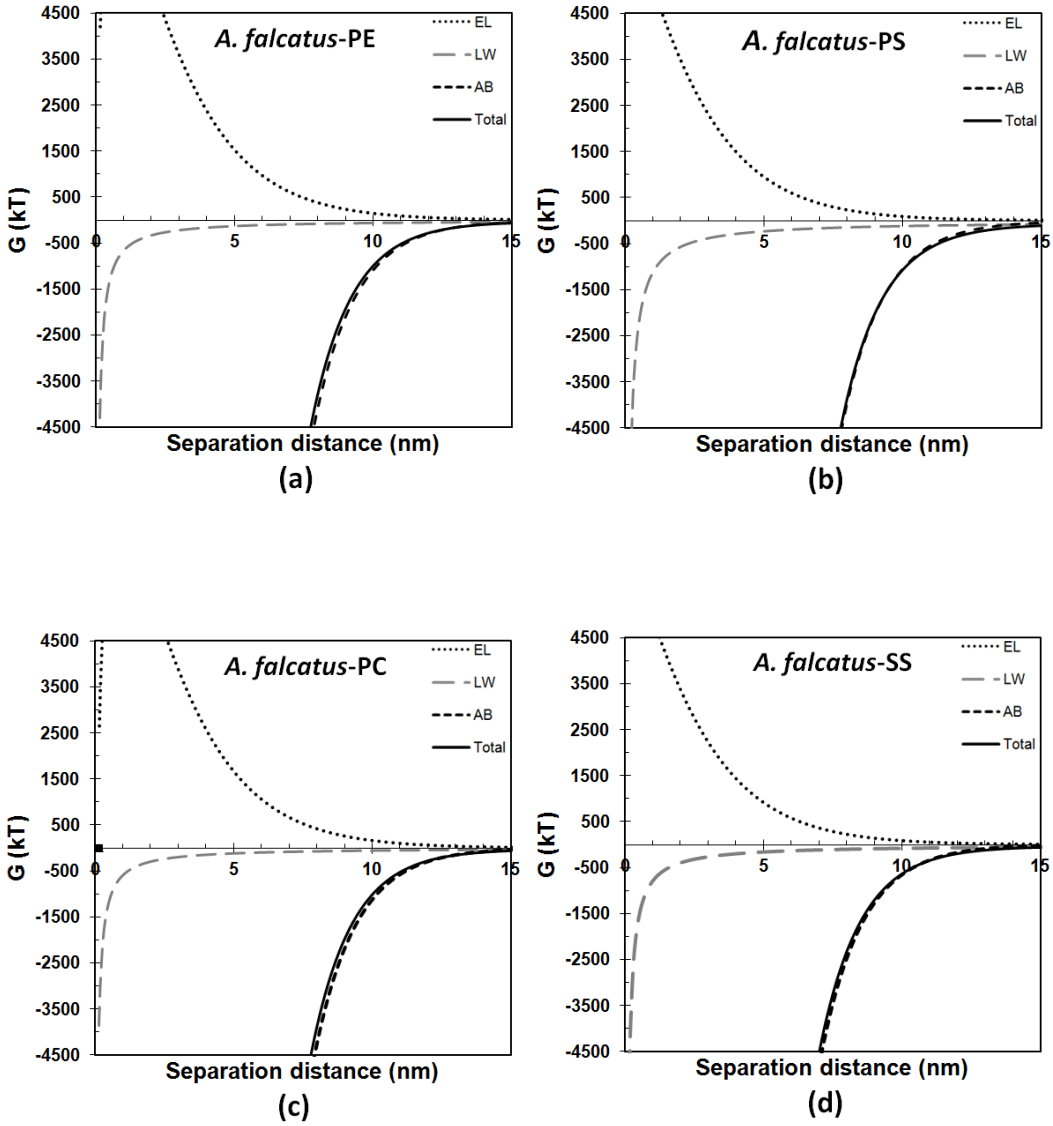

Figure B.2: Energy of interaction between *A. falcatus* and (a) polyethylene, (b) polystyrene, (c) polycarbonate, and (d) stainless steel according to the XDLVO model.

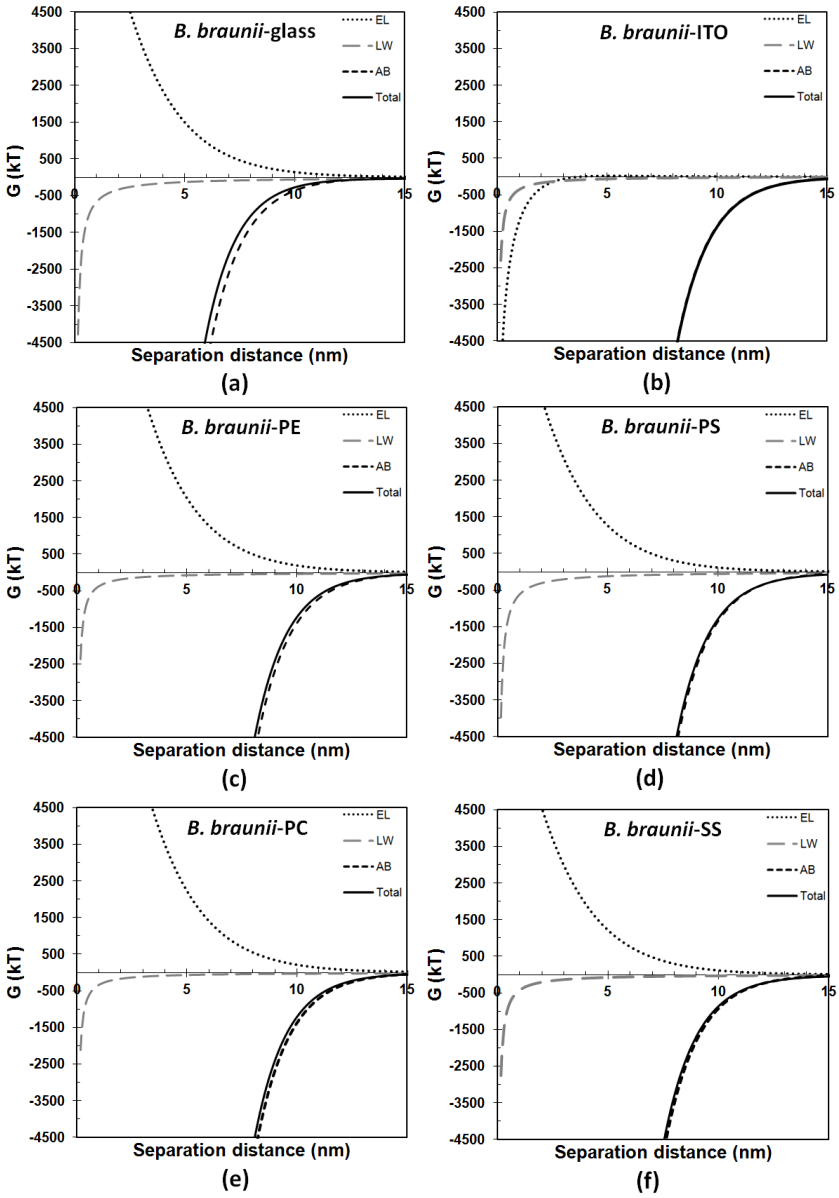

Figure B.3: Energy of interaction between *B. braunii* and (a) glass, (b) ITO, (c) polyethylene, (d) polystyrene, (e) polycarbonate, and (f) stainless steel according to the XDLVO model.

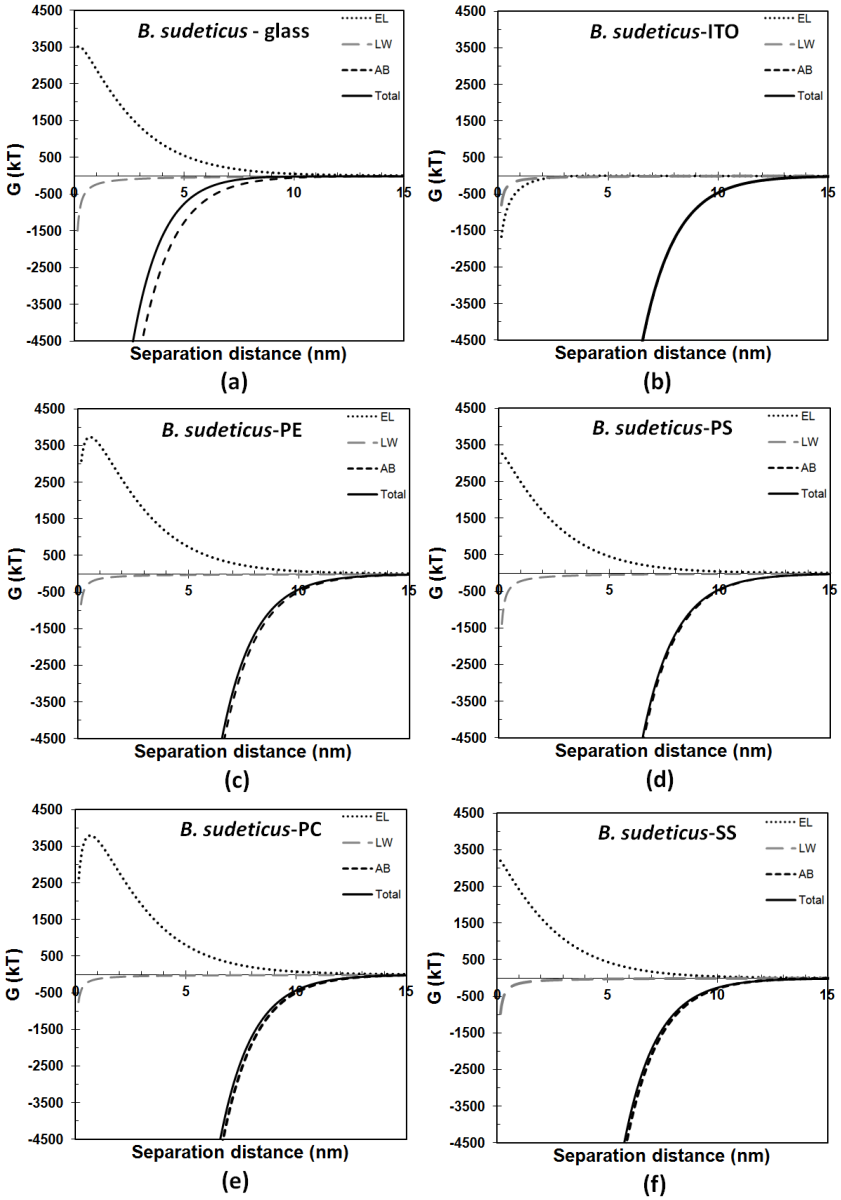

Figure B.4: Energy of interaction between *B. sudeticus* and (a) glass, (b) ITO, (c) polyethylene, (d) polystyrene, (e) polycarbonate, and (f) stainless steel according to the XDLVO model.

B.2 Hydrophobic diatom substrata interactions

In this section electrostatic (EL), van der Waals (LW), acid base (AB), and total interaction energy plots of the hydrophobic diatom-substrata systems are presented.

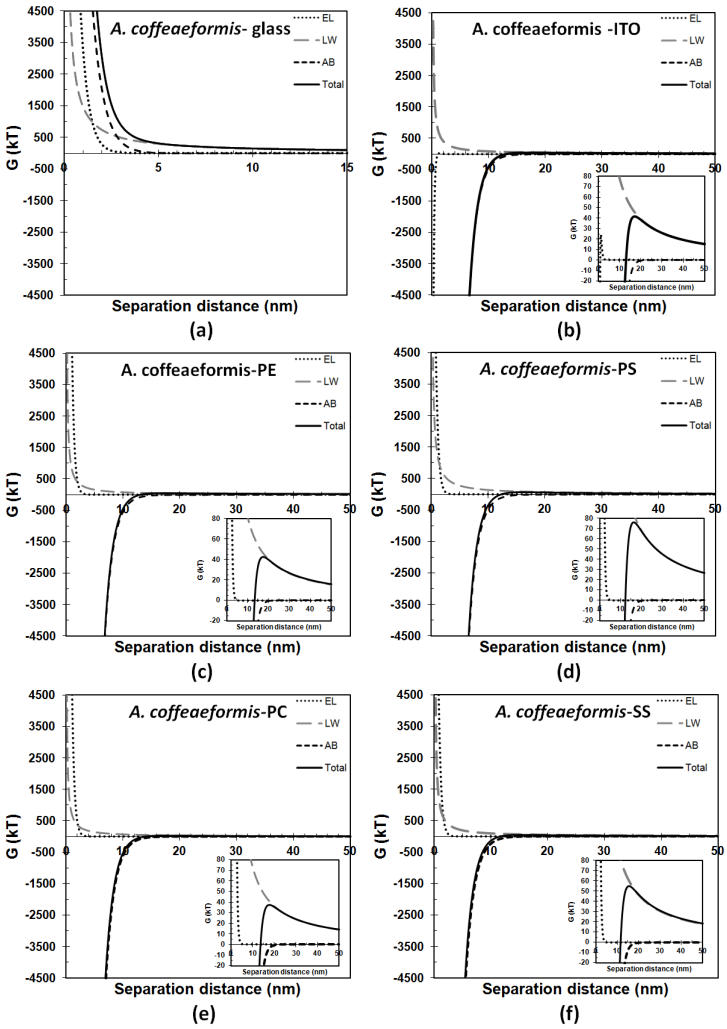

Figure B.5: Energy of interaction between *A. coffeaeformis* and (a) glass, (b) ITO, (c) polyethylene, (d) polystyrene, (e) polycarbonate, and (f) stainless steel according to the XDLVO model.

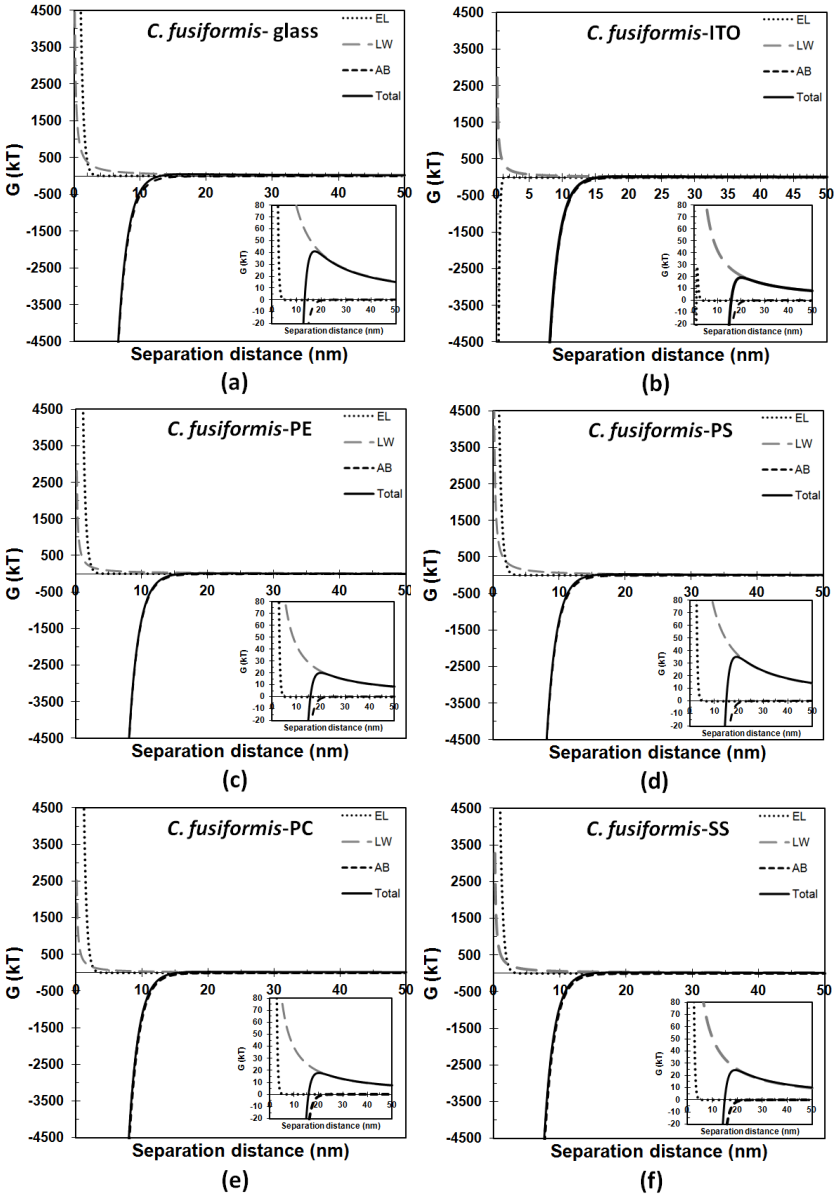

Figure B.6: Energy of interaction between *C. fusiformis* and (a) glass, (b) ITO, (c) polyethylene, (d) polystyrene, (e) polycarbonate, and (f) stainless steel according to the XDLVO model.

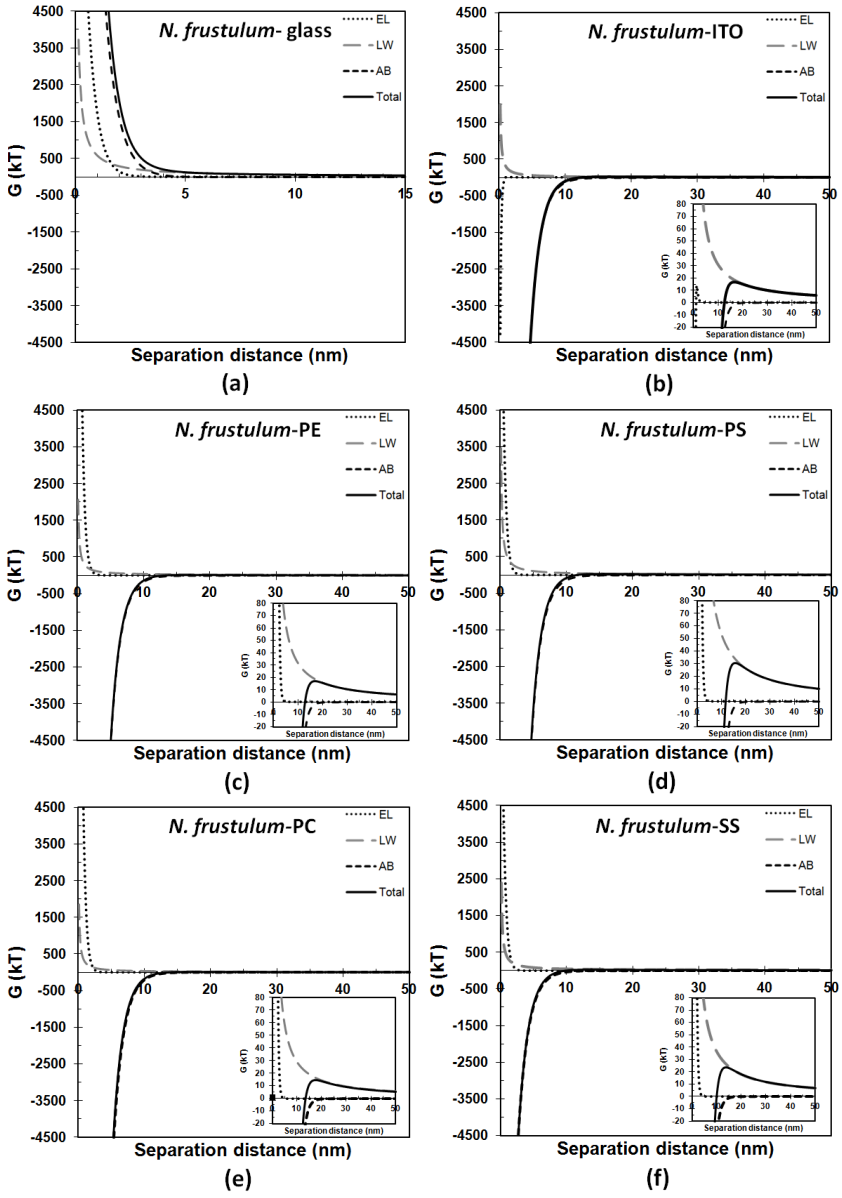

Figure B.7: Energy of interaction between *N. frustulum* and (a) glass, (b) ITO, (c) polyethylene, (d) polystyrene, (e) polycarbonate, and (f) stainless steel according to the XDLVO model.

B.3 Hydrophilic green algae substrata interactions

In this section electrostatic (EL), van der Waals (LW), acid base (AB), and total interaction energy plots of the hydrophilic green algae-substrata systems are presented.

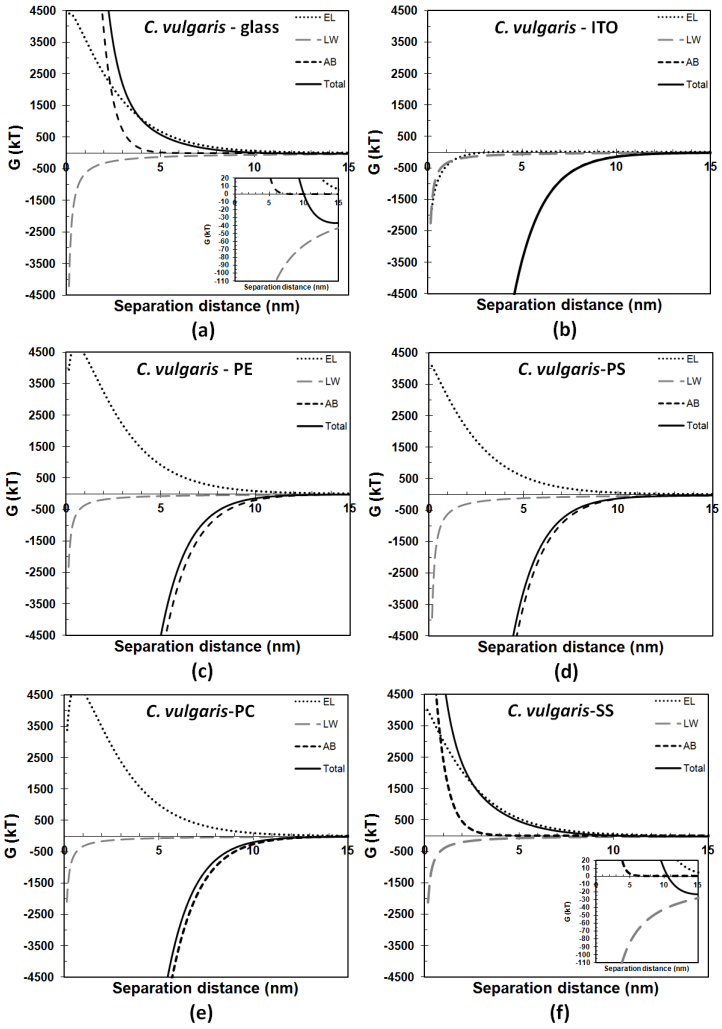

Figure B.8: Energy of interaction between *C. vulgaris* and (a) glass, (b) ITO, (c) polyethylene, (d) polystyrene, (e) polycarbonate, and (f) stainless steel according to the XDLVO model.

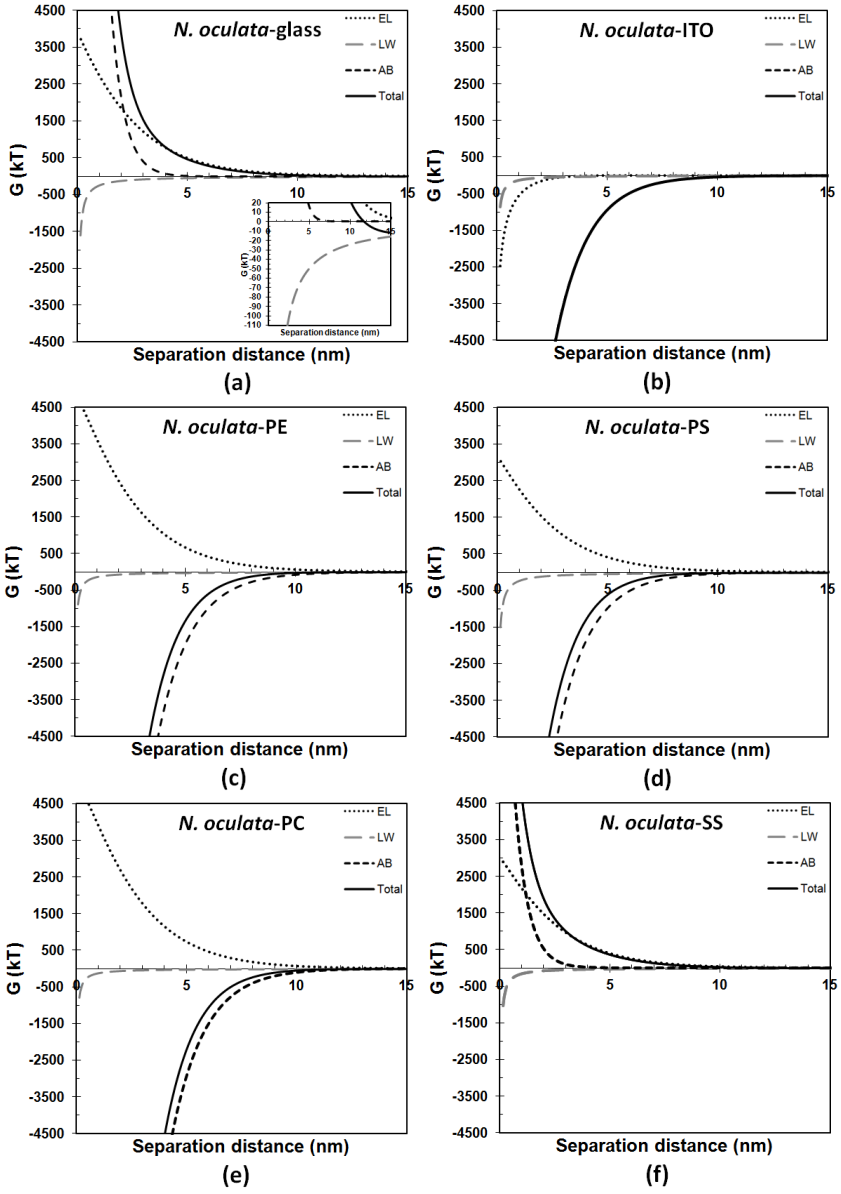

Figure B.9: Energy of interaction between *N. oculata* and (a) glass, (b) ITO, (c) polyethylene, (d) polystyrene, (e) polycarbonate, and (f) stainless steel according to the XDLVO model.

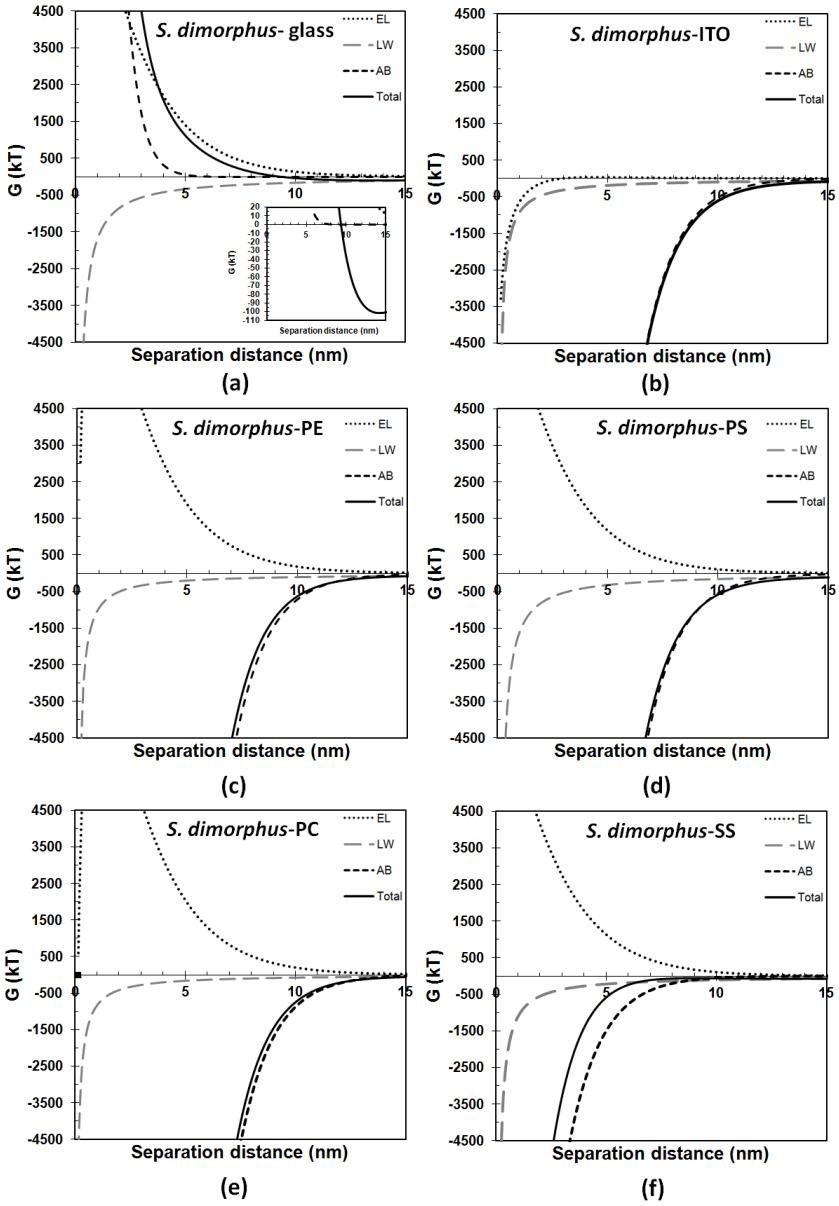

Figure B.10: Energy of interaction between *S. dimorphus* and (a) glass, (b) ITO, (c) polyethylene, (d) polystyrene, (e) polycarbonate, and (f) stainless steel according to the XDLVO model.

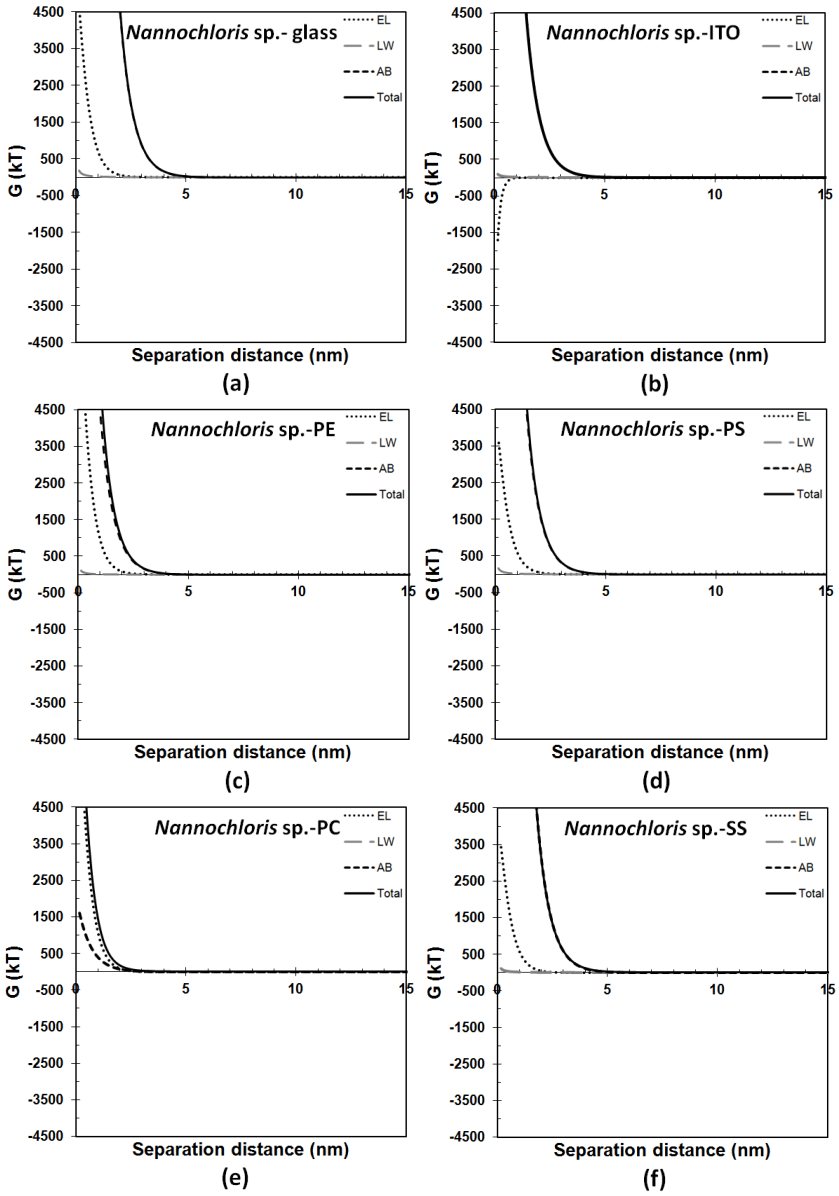

Figure B.11: Energy of interaction between *Nannochloris* sp. and (a) glass, (b) ITO, (c) polyethylene, (d) polystyrene, (e) polycarbonate, and (f) stainless steel according to the XDLVO model.

B.4 Freshwater species-freshwater species interactions

In this section electrostatic (EL), van der Waals (LW), acid base (AB), and total interaction energy of freshwater species-freshwater species systems are presented.

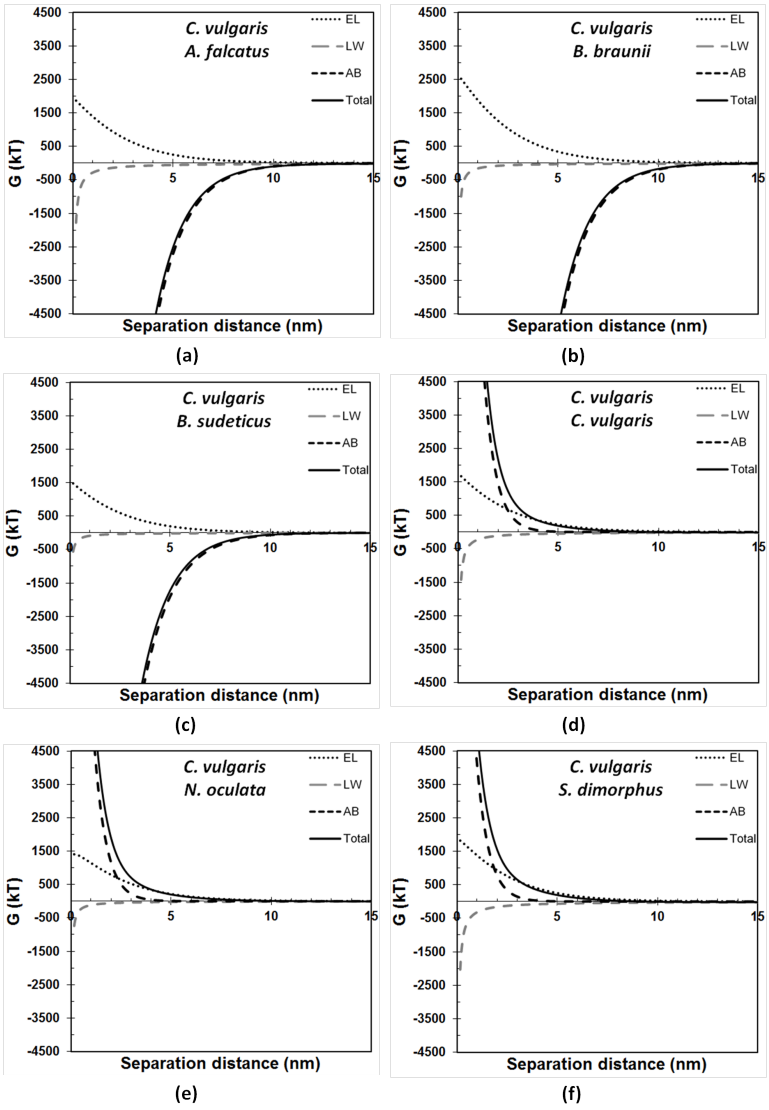

Figure B.12: Energy of interaction for (a) *C. vulgaris-A. falcatus*, (b) *C. vulgaris-B. braunii*, (c) *C. vulgaris-B. sudeticus*, (d) *C. vulgaris-C. vulgaris*, (e) *C. vulgaris-N. oculata*, and (f) *C. vulgaris-S. dimorphus* systems according to the XDLVO model.

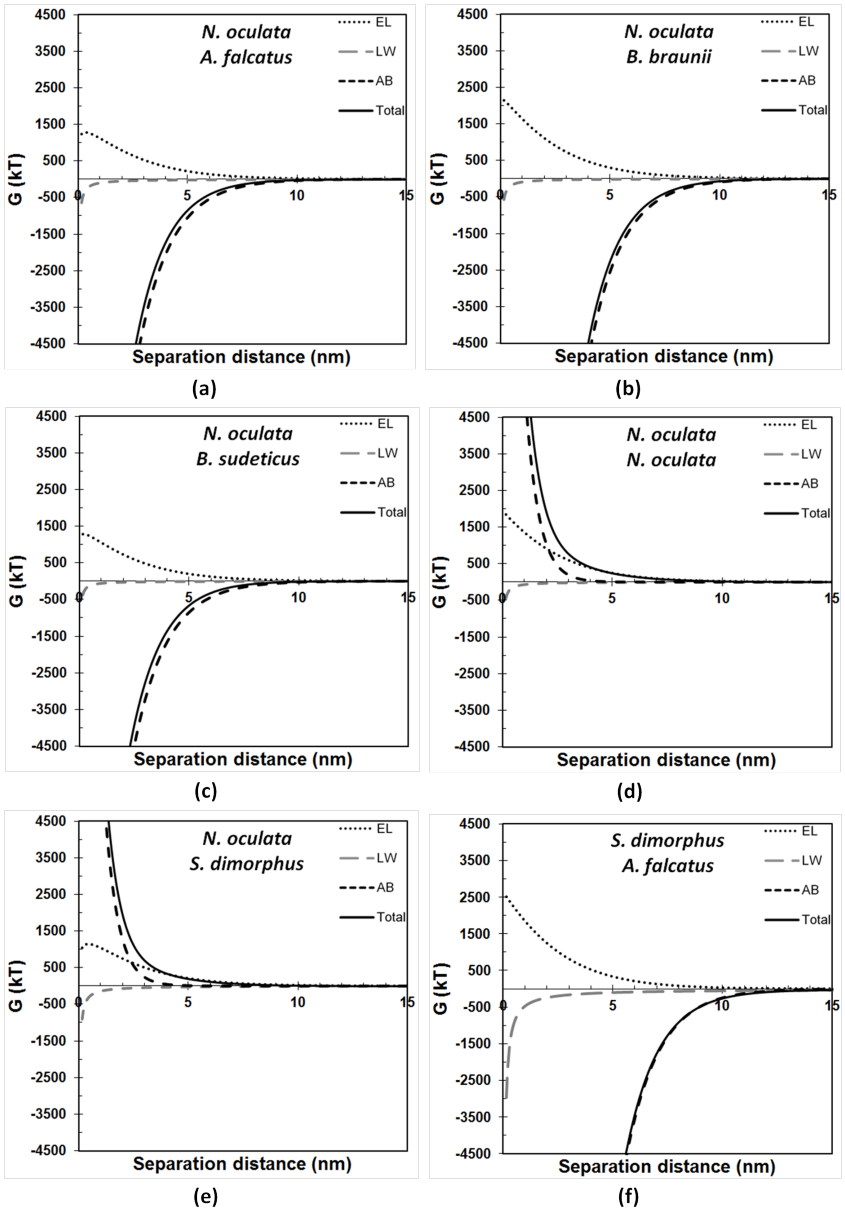

Figure B.13: Energy of interaction for (a) *N. oculata-A. falcatus*, (b) *N. oculata-B. braunii*, (c) *N. oculata-B. sudeticus*, (d) *N. oculata-N. oculata*, (e) *N. oculata-S. dimorphus*, and (f) *S. dimorphus-A. falcatus* systems according to the XDLVO model.

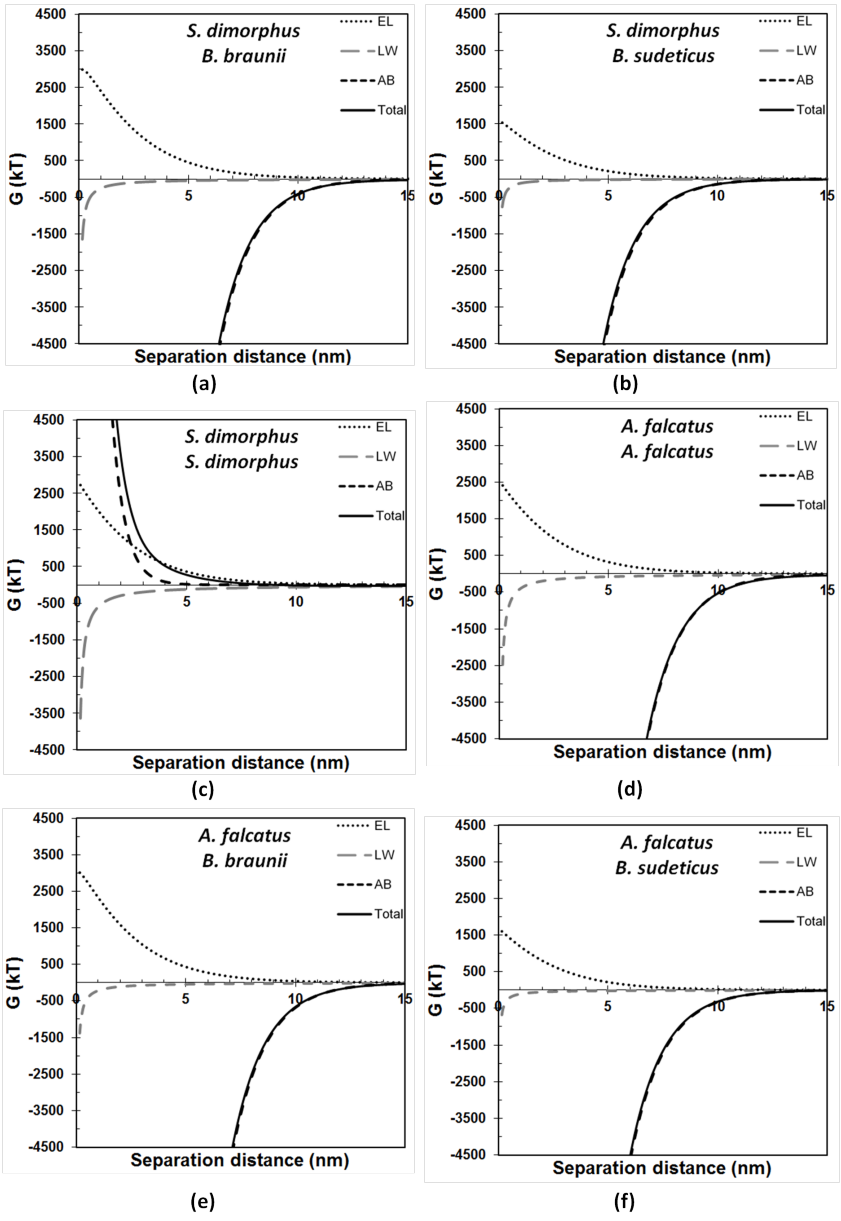

Figure B.14: Energy of interaction for (a) *S. dimorphus-B. braunii*, (b) *S. dimorphus-B. sudeticus*, (c) *S. dimorphus-S. dimorphus*, (d) *A. falcatus-A. falcatus*, (e) *A. falcatus-B. braunii*, and (f) *A. falcatus-B. sudeticus* systems according to the XDLVO model.

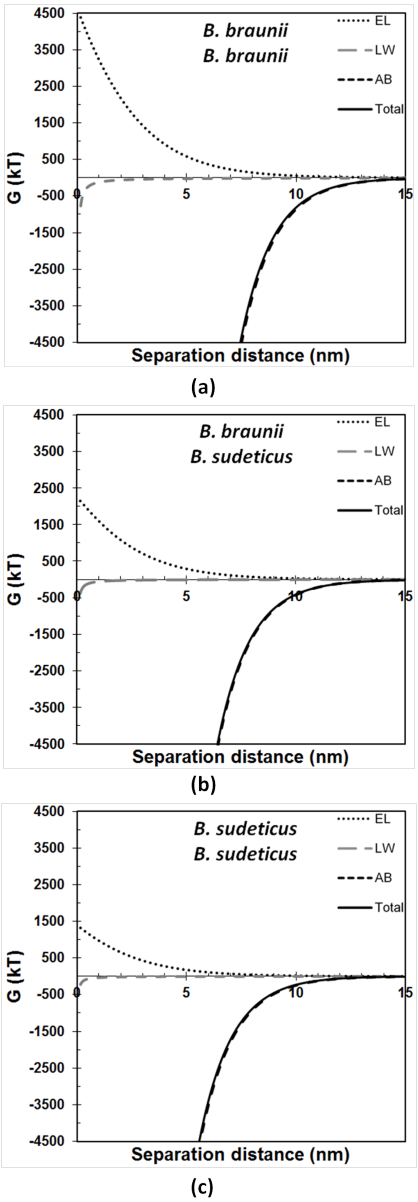

Figure B.15: Energy of interaction for (a) *B. braunii*-*B. braunii*, (b) *B. braunii*-*B. sudeticus*, and (c) *B. sudeticus*-*B. sudeticus* systems according to the XDLVO model.

B.5 Saltwater species-saltwater species interactions

In this section electrostatic (EL), van der Waals (LW), acid base (AB), and total interaction energy of saltwater species-saltwater species systems are presented.

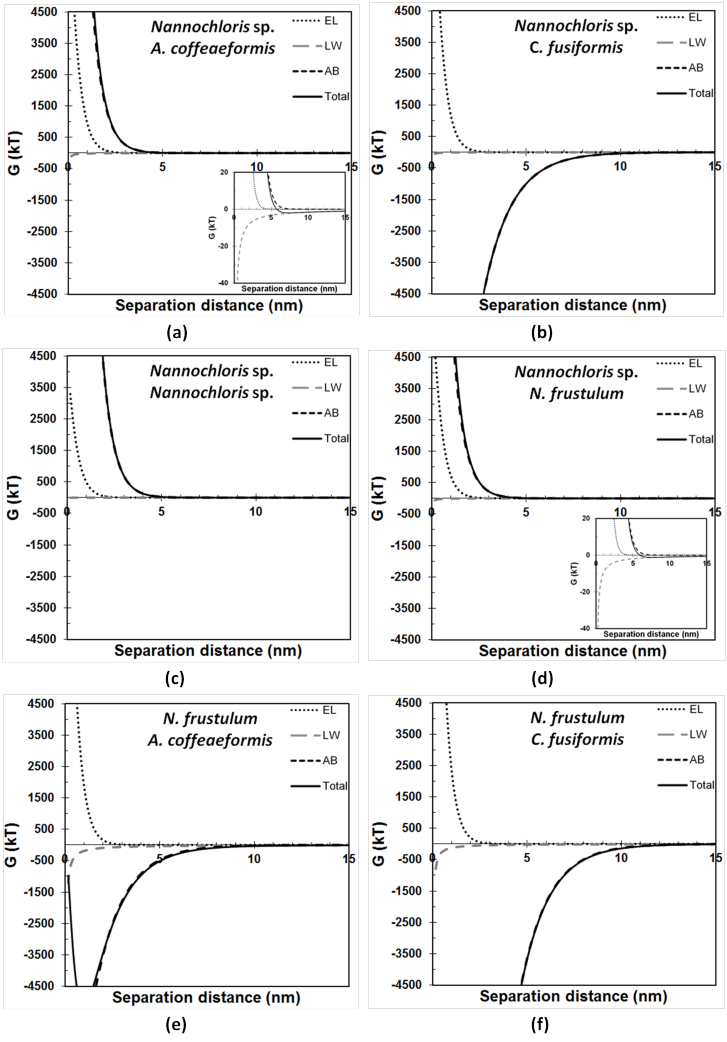

Figure B.16: Energy of interaction for (a) *Nannochloris* sp.-*A. coffeaeformis* and (b) *Nannochloris* sp.-*C. fusiformis*, (c) *Nannochloris* sp.-*Nannochloris* sp., (d) *Nannochloris* sp.-*N. frustulum*, (e) *N. frustulum*-*A. coffeaeformis*, and (f) *N. frustulum*-*C. fusiformis* systems according to the XDLVO model.

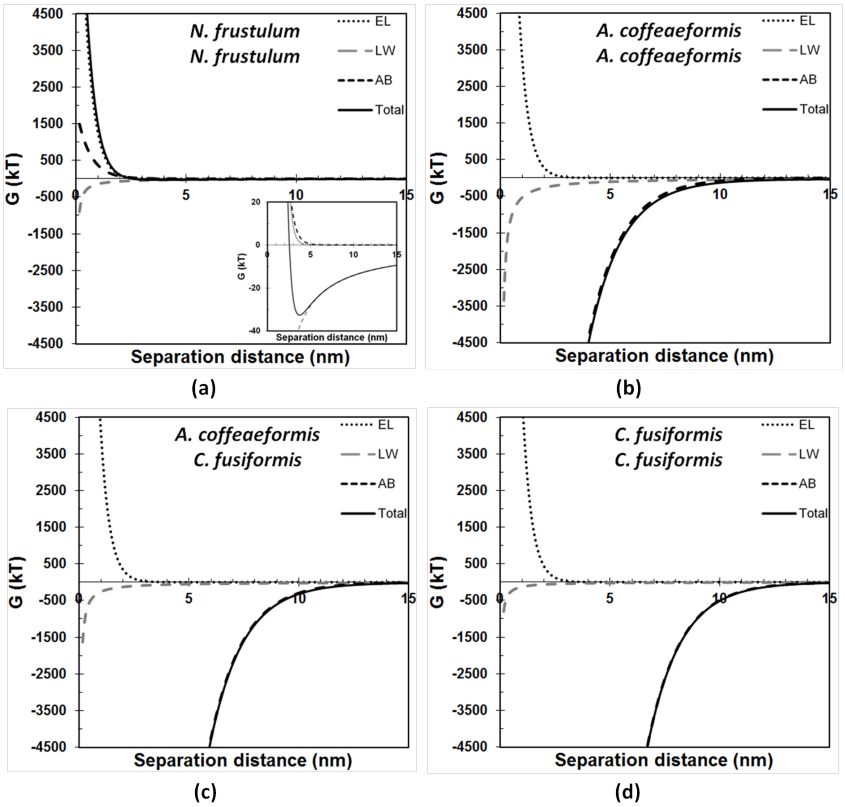

Figure B.17: Energy of interaction for (a) *N. frustulum*-*N. frustulum*, (b) *A. coffeaeformis*-*A. coffeaeformis*, (c) *A. coffeaeformis*-*C. fusiformis*, and (d) *C. fusiformis*-*C. fusiformis* systems according to the XDLVO model.

Appendix C

Results from the Thermodynamic Model

This appendix contains the free energy of co-aggregation and its van der Waals and acid base components for cell to cell interaction between algal species based on the thermodynamic model.

C.1 Freshwater species-freshwater species interactions

In this section free energy of coaggregation of the freshwater algal species are presented.

Table C.1: Interaction energy (in mJ m^{-2}) for *C. vulgaris* interacting with freshwater species according to the thermodynamic model.

Interaction energy between *C. vulgaris* and fresh water species						
		A. fal.	*B. bra.*	*C. vul.*	*B. sud.*	*N. ocu.*
C. vulgaris	ΔG_{LW}	-4.13	-2.34	-4.38	-1.93	-3.56
	ΔG_{AB}	-16.55	-32.66	25.20	-17.25	31.50
	ΔG_{co-agg}	-20.68	-34.99	20.83	-19.18	27.94

Table C.2: Interaction energy (in mJ m^{-2}) for *N. oculata* interacting with freshwater species according to the thermodynamic model.

Interaction energy between *N. oculata* and fresh water species						
		A. fal.	*B. bra.*	*B. sud.*	*N. ocu.*	*S. dim.*
N. oculata	ΔG_{LW}	-3.37	-2.34	-1.93	-3.37	-3.50
	ΔG_{AB}	-11.28	-27.46	-11.62	38.14	27.66
	ΔG_{co-agg}	-14.65	-29.80	-13.55	35.24	24.15

Table C.3: Interaction energy (in mJ m^{-2}) for *S. dimorphus* interacting with freshwater species according to the thermodynamic model.

Interaction energy between *S. dimorphus* and fresh water species						
		A. fal.	*B. bra.*	*B. sud.*	*C. vul.*	*S. dim.*
S. dimorphus	ΔG_{LW}	-4.07	-2.30	-1.89	-4.30	-4.23
	ΔG_{AB}	-25.06	-43.20	-26.30	20.94	15.61
	ΔG_{co-agg}	-29.13	-45.50	-28.19	16.63	11.37

Table C.4: Interaction energy (in mJ m^{-2}) for *A. falcatus* interacting with freshwater species according to the thermodynamic model.

LW, AB comp. and free energy of co-agg. for *A. falcatus* interacting with freshwater algal species				
		A. falcatus	*B. braunii*	*B. sudeticus*
A. falcatus	ΔG_{LW}	-3.90	-2.21	-1.03
	ΔG_{AB}	-60.70	-80.18	-85.10
	ΔG_{co-agg}	-64.60	-82.39	-86.13

Table C.5: Interaction energy (in mJ m^{-2}) for *B. sudeticus* interacting with freshwater species according to the thermodynamic model.

Interaction energy for *B. braunii* & *B. sudeticus* interacting with freshwater algal species			
	B. bra.-B. bra.	*B. bra.-B. sud.*	*B. sud.-B.sud.*
ΔG_{LW}	-1.25	-1.03	-0.85
ΔG_{AB}	-102.00	-85.10	-68.20
ΔG_{co-agg}	-103.25	-86.13	-69.05

C.2 Saltwater species-saltwater species interactions

In this section free energy of coaggregation of the saltwater algal species are presented.

Table C.6: Interaction energy for *Nannochloris* sp. interacting with saltwater algal species.

Interaction energy for *Nannochloris* sp. interacting with saltwater algal species					
		A. coffe.	*C. fusi.*	*Nanno. sp.*	*N. frus.*
Nannochloris sp.	ΔG_{LW}	-0.37	-0.17	-0.03	-0.25
	ΔG_{AB}	29.13	-9.16	117.60	27.58
	ΔG_{co-agg}	28.75	-9.32	117.57	27.32

Table C.7: Interaction energy (in mJ m^{-2}) for *A. coffeaeformis* interacting with saltwater species according to the thermodynamic model.

Interaction energy for *A. coffeaeformis* interacting with saltwater algal species				
		A. coffeaeformis	*C. fusiformis*	*N. frustulum*
A. coffeaeformis	ΔG_{LW}	-4.83	-2.16	-3.31
	ΔG_{AB}	-8.57	-28.88	-2.47
	ΔG_{co-agg}	-13.40	-31.04	-5.78

Table C.8: Interaction energy (in mJ m^{-2}) for *C. fusiformis* and *N. frustulum* interacting with saltwater species according to the thermodynamic model.

Interaction energy for *C. fusiformis* & *N. frustulum* interacting with saltwater algal species			
	C. fusi.-*C. fusi.*	*C. fusi.*-*N. frus.*	*N. frus.*-*N. frus.*
ΔG_{LW}	-0.96	-1.48	-2.26
ΔG_{AB}	-44.16	-17.84	0.98
ΔG_{co-agg}	-45.12	-19.31	-1.28

Bibliography

[1] O. Jorquera, A. Kiperstok, E. Sales, M. Embiruçu, and M. Ghirardi, "Comparative energy life-cycle analyses of microalgal biomass production in open ponds and photobioreactors," *Bioresource Technology*, vol. 101, no. 4, pp. 1406–1413, 2010.

[2] Y. Chisti, "Biodiesel from microalgae," *Biotechnology Advances*, vol. 25, pp. 294–306, 2007.

[3] R. Bos, H. van der Mei, and H. Busscher, "Physico-chemistry of initial microbial adhesive interactions-its mechanisms and methods for study," *FEMS Microbiology Reviews*, vol. 23, pp. 179–230, 1999.

[4] S. Hadjoudja, V. Deluchat, and M. Baudu, "Cell surface characterisation of *Microcystis aeruginosa* and *Chlorella vulgaris*," *Journal of Colloid and Interface Science*, vol. 342, no. 2, pp. 293–299, 2010.

[5] S. Shafiee and E. Topal, "When will fossil fuel reserves be diminished?," *Energy Policy*, vol. 37, no. 1, pp. 181–189, 2009.

[6] M. Salameh, "Can renewable and unconventional energy sources bridge the global energy gap in the 21st century?," *Applied Energy*, vol. 75, no. 1-2, pp. 33–42, 2003.

[7] E. I. A. (U.S.) and U. E. I. Administration, *International Energy Outlook, 2010*. Energy Information Administration, 2010.

[8] S. Solomon, D. Qin, M. Manning, Z. Chen, M. Marquis, K. Averyt, M. Tignor, and H. Miller, "Contribution of working group I to the fourth assessment report of the Intergovernmental Panel on Climate Change, 2007," *IPCC. Cambridge University Press, Cambridge, UK and New York, NY, USA*, 2007.

[9] W. Cline, *The Economics of Global Warming*. Washington, DC: Peterson Institute, 1992.

[10] Q. Hu, M. Sommerfeld, E. Jarvis, M. Ghirardi, M. Posewitz, M. Seibert, and A. Darzins, "Microalgal triacylglycerols as feedstocks for biofuel production: perspectives and advances," *The Plant Journal*, vol. 54, pp. 621–639, 2008.

[11] O. Pulz, "Photobioreactors: production systems for phototrophic microorganisms.," *Applied Microbiology and Biotechnology*, vol. 57, pp. 287–293, 2001.

[12] N. Uduman, Y. Qi, M. Danquah, G. Forde, and A. Hoadley, "Dewatering of microalgal cultures: A major bottleneck to algae-based fuels," *Journal of Renewable and Sustainable Energy*, vol. 2, p. 012701, 2010.

[13] L. Brennan and P. Owende, "Biofuels from microalgae-A review of technologies for production, processing and extractions of biofuels and co-

products," *Renewable and Sustainable Energy Reviews*, vol. 14, pp. 557–577, 2010.

[14] C. U. Ugwu, H. Aoyagi, and H. Uchiyama, "Photobioreactors for mass cultivation of algae," *Bioresource Technology*, vol. 99, no. 10, pp. 4021–4028, 2008.

[15] M. Borowitzka, "Commercial production of microalgae: Ponds, tanks, tubes and fermenters," *Journal of Biotechnology*, vol. 70, pp. 313–321, 1999.

[16] E. Stephens, I. Ross, J. Mussgnug, L. Wagner, M. Borowitzka, C. Posten, O. Kruse, and B. Hankamer, "Future prospects of microalgal biofuel production systems," *Trends in Plant Science*, vol. 15, no. 10, pp. 554–564, 2010.

[17] R. Hase, H. Oikawa, C. Sasao, M. Morita, and Y. Watanabe, "Photosynthetic production of microalgal biomass in a raceway system under greenhouse conditions in sendai city," *Journal of Bioscience and Bioengineering*, vol. 89, no. 2, pp. 157–163, 2000.

[18] A. Carvalho, L. Meireles, and F. Malcata, "Microalgal reactors: A review of enclosed system designs and performances," *Biotechnology Progress*, vol. 22, no. 6, pp. 1490–1506, 2006.

[19] C. Gudin and C. Therpenier, "Bioconversion of solar energy into organic chemicals by microalgae," *Advances in Biotechnological Processes*,

vol. 226, pp. 497–509, 1957.

[20] J. Sheehan, T. Dunahay, J. Benemann, and P. Roessler, "A look back at the U.S. department of energy's aquatic species program: Biodiesel from algae," Tech. Rep. NREL/TP-580-24190, National Renewable Energy Laboratory, 1998.

[21] J. Yang, M. Xu, X. Zhang, Q. Hu, M. Sommerfeld, and Y. Chen, "Life cycle analysis on biodiesel production from microalgae: water footprint and nutrients balance," *Bioresource Technology*, vol. 102, pp. 159–165, 2011.

[22] A. Singh, P. Nigam, and J. Murphy, "Mechanism and challenges in commercialisation of algal biofuels," *Bioresource Technology*, vol. 102, pp. 26–34, 2011.

[23] S. Suh and C. Lee, "Photobioreactor engineering: Design and performance," *Biotechnology and Bioprocess Engineering*, vol. 8, pp. 313–321, 2003.

[24] N. Eriksen, "The technology of microalgal culturing," *Biotechnology letters*, vol. 30, no. 9, pp. 1525–1536, 2008.

[25] M. Morweiser, O. Kruse, B. Hankamer, and C. Posten, "Developments and perspectives of photobioreactors for biofuel production," *Applied Microbiology and Biotechnology*, vol. 87, pp. 1291–1301, 2010.

[26] J. Benemann and W. Oswald, "Systems and economic analysis of microalgae ponds for conversion of CO_2 to biomass," Tech. Rep. DE-FG22-93PC93204, U.S. Department of Energy, 1996.

[27] Y. Lee, "Microalgal mass culture systems and methods: Their limitation and potential," *Journal of Applied Phycology*, vol. 13, pp. 307–315, 2001.

[28] E. Molina Grima, E. Belarbi, F. Acien Fernandez, A. Robles Medina, and Y. Chisti, "Recovery of microalgal biomass and metabolites: process options and economics.," *Biotechnology Advances*, vol. 20, pp. 491–515, 2003.

[29] G. Gutzeit, D. Lorch, A. Weber, M. Engels, and U. Neis, "Bioflocculent algal-bacterial biomass improves low-cost wastewater treatment.," *Water science and technology*, vol. 52, no. 12, p. 9, 2005.

[30] H. Oh, S. Lee, M. Park, H. Kim, H. Kim, J. Yoon, G. Kwon, and B. Yoon, "Harvesting of *Chlorella vulgaris* using a bioflocculant from *Paenibacillus* sp. AM49," *Biotechnology Letters*, vol. 23, no. 15, pp. 1229–1234, 2001.

[31] A. Lee, D. Lewis, and P. Ashman, "Microbial flocculation, a potentially low-cost harvesting technique for marine microalgae for the production of biodiesel," *Journal of Applied Phycology*, vol. 21, no. 5, pp. 559–567, 2009.

[32] J. Jones, C. Lee, J. Wang, and M. Poenie, "Use of anion exchange resins for one-step processing of algae from harvest to biofuel," *Energies*, vol. 5,

no. 7, pp. 2608–2625, 2012.

[33] S. Salim, M. Vermuë, and R. Wijffels, "Ratio between autoflocculating and target microalgae affects the energy-efficient harvesting by bioflocculation," *Bioresource Technology*, 2012.

[34] C. Akin, A. Maka, S. Patel, J. Conrad, and J. Benemann, "Removal of CO_2 from flue gases by algae," Tech. Rep. DOE/PC/92521–T97, U.S. Department of Energy, 1993.

[35] C. Bailliez, C. Largeau, and E. Casadevall, "Growth and hydrocarbon production of *Botryococcus braunii* immobilized in calcium alginate gel," *Applied Microbiology and Biotechnology*, vol. 23, no. 2, pp. 99–105, 1985.

[36] G. Kremer, D. J. Bayless, M. Vis, M. Prudich, K. Cooksey, and J. Muhs, "Enhanced practical photosynthetic CO_2 mitigation," Tech. Rep. DE-FC26-00NT40932, U.S. Department of Energy, 2006.

[37] P. Zemke, B. Wood, D. Dye, D. Bayless, and J. Muhs, "Economic analysis of a vertical sheet algal photobioreactor for biodiesel production," in *Energy Sustainability*, (Long Beach, California), pp. 815–819, 2007.

[38] M. B. Johnson and Z. Wen, "Development of an attached microalgal growth system for biofuel production," *Applied Microbiology and Biotechnology*, vol. 85, pp. 525–534, 2010.

[39] J. Cao, W. Yuan, Z. Pei, T. Davis, Y. Cui, and M. Beltran, "A preliminary study of the effect of surface texture on algae cell attachment

for a mechanical-biological energy manufacturing system," *Journal of Manufacturing Science and Engineering*, vol. 131, p. 064505, 2009.

[40] L. Christenson and R. Sims, "Rotating algal biofilm reactor and spool harvester for wastewater treatment with biofuels by-products," *Biotechnology and Bioengineering*, 2012.

[41] A. Ansari, S. Gill, G. Lanza, and W. Rast, *Eutrophication: Causes, Consequences and Control*. New York: Springer, 2011.

[42] J. Noue, G. Laliberte, and D. Proulx, "Algae and wastewater," *Journal of Phycology*, vol. 4, pp. 247–254, 1992.

[43] G. Tchobanoglous, F. Burton, and H. Stensel, *Wastewater Engineering Treatment and Reuse*. New York, NY: Mc Graw Hill, 2003.

[44] A. Guzzon, A. Bohn, M. Diociaiuti, and P. Albertano, "Cultured phototrophic biofilms for phosphorus removal in wastewater treatment," *Water Research*, vol. 42, no. 16, pp. 4357–4367, 2008.

[45] J. Hoffmann, "Wastewater treatment with suspended and nonsuspended algae," *Journal of Phycology*, vol. 34, no. 5, pp. 757–763, 1998.

[46] R. Craggs, P. McAuley, and V. Smith, "Wastewater nutrient removal by marine microalgae grown on a corrugated raceway," *Water Resource*, vol. 31, pp. 1701–1707, 1997.

[47] W. Mulbry, S. Kondrad, C. Pizarro, and E. Kebede-Westhead, "Treatment of dairy manure effluent using freshwater algae: Algal productivity and recovery of manure nutrients using pilot-scale algal turf scrubbers," *Bioresource Technology*, vol. 99, pp. 8137–8142, 2008.

[48] J. Shi, B. Podola, and M. Melkonian, "Removal of nitrogen and phosphorus from wastewater using microalgae immobilized on twin layers: an experimental study," *Journal of Applied Phycology*, vol. 19, no. 5, pp. 417–423, 2007.

[49] A. Wilkie and W. Mulbry, "Recovery of dairy manure nutrients by benthic freshwater algae," *Bioresource Technology*, vol. 84, no. 1, pp. 81–91, 2002.

[50] R. Craggs, W. Adey, K. Jenson, M. St John, F. Bailey Green, and W. Oswald, "Phosphorus removal from wastewater using an algal turf scrubber," *Water Science and Technology*, vol. 33, no. 7, pp. 191–198, 1996.

[51] W. Adey, C. Luckett, and K. Jensen, "Phosphorus removal from natural waters using controlled algal production," *Restoration Ecology*, vol. 1, pp. 29–39, 1993.

[52] S. Chinnasamy, A. Bhatnagar, R. Hunt, and K. Das, "Microalgae cultivation in a wastewater dominated by carpet mill effluents for biofuel applications," *Bioresource Technology*, vol. 101, no. 9, pp. 3097–3105, 2010.

[53] K. Park, B. Lim, and K. Lee, "Growth of microalgae in diluted process water of the animal wastewater treatment plant.," *Water Science and Technology*, vol. 59, no. 11, pp. 2111–2116, 2009.

[54] A. Ruiz-Marin, L. Mendoza-Espinosa, and T. Stephenson, "Growth and nutrient removal in free and immobilized green algae in batch and semi-continuous cultures treating real wastewater," *Bioresource Technology*, vol. 101, no. 1, pp. 58–64, 2010.

[55] C. Gonzalez, J. Marciniak, S. Villaverde, C. Leon, and P. Garcia, "Efficient nutrient removal from swine manure in a tubular biofilm photobioreactor using algae-bacteria consortia," *Water Science and Technology (UK)*, vol. 58, no. 1, pp. 95–102, 2008.

[56] G. Hodaifa, M. Martínez, and S. Sánchez, "Daily doses of light in relation to the growth of *Scenedesmus obliquus* in diluted three-phase olive mill wastewater," *Journal of Chemical Technology and Biotechnology*, vol. 84, no. 10, pp. 1550–1558, 2009.

[57] N. Mallick, "Biotechnological potential of immobilized algae for wastewater n, p and metal removal: a review," *Biometals*, vol. 15, no. 4, pp. 377–390, 2002.

[58] I. Woertz, A. Feffer, T. Lundquist, and Y. Nelson, "Algae grown on dairy and municipal wastewater for simultaneous nutrient removal and lipid production for biofuel feedstock," *Journal of Environmental Engineering*, vol. 135, p. 1115, 2009.

[59] M. E. Martinez, S. Sánchez, J. Jiménez, F. El Yousfi, and L. Muñoz, "Nitrogen and phosphorus removal from urban wastewater by the microalga *Scenedesmus obliquus*," *Bioresource Technology*, vol. 73, no. 3, pp. 263–272, 2000.

[60] J. An, S. Sim, J. Lee, and B. Kim, "Hydrocarbon production from secondarily treated piggery wastewater by the green alga *Botryococcus braunii*," *Journal of Applied Phycology*, vol. 15, no. 2, pp. 185–191, 2003.

[61] J. Park and R. Craggs, "Wastewater treatment and algal production in high rate algal ponds with carbon dioxide addition," *Water Science and Technology*, vol. 61, no. 3, pp. 633–639, 2010.

[62] S. Sawayama, T. Minowa, Y. Dote, and S. Yokoyama, "Growth of the hydrocarbon-rich microalga *Botryococcus braunii* in secondarily treated sewage," *Applied Microbiology and Biotechnology*, vol. 38, no. 1, pp. 135–138, 1992.

[63] S. Sawayama, S. Inoue, and S. Yokoyama, "Continuous culture of hydrocarbon-rich microalga *Botryococcus braunii* in secondarily treated sewage," *Applied Microbiology and Biotechnology*, vol. 41, no. 6, pp. 729–731, 1994.

[64] L. Gonzalez, R. Canizares, and S. Baena, "Efficiency of ammonia and phosphorus removal from a Colombian agroindustrial wastewater by the microalgae *Chlorella vulgaris* and *Scenedesmus dimorphus*," *Bioresource Technology*, vol. 60, no. 3, pp. 259–262, 1997.

[65] M. Jimenez-Perez, P. Sanchez-Castillo, O. Romera, D. Fernandez-Moreno, and C. Perez-Martinez, "Growth and nutrient removal in free and immobilized planktonic green algae isolated from pig manure," *Enzyme and Microbial Technology*, vol. 34, no. 5, pp. 392–398, 2004.

[66] C. Randall, J. Barnard, and H. Stensel, *Design and retrofit of wastewater treatment plants for biological nutrient removal.* CRC Press, Lancaster, PA, 1992.

[67] P. Lau, N. Tam, and Y. Wong, "Wastewater nutrients N and P removal by carrageenan and alginate immobilized *Chlorella vulgaris*," *Environmental Technology*, vol. 18, no. 9, pp. 945–951, 1997.

[68] P. Chevalier and J. de la Noue, "Wastewater nutrient removal with microalgae immobilized in carrageenan," *Enzyme and Microbial Technology*, vol. 7, no. 12, pp. 621–624, 1985.

[69] E. Kebede-westhead, C. Pizarro, W. Mulbry, and A. Wilkie, "Production and nutrient removal by periphyton grown under different loading rates of anaerobically digested flushed dairy manure," *Journal of Phycology*, vol. 39, no. 6, pp. 1275–1282, 2003.

[70] W. Mulbry, S. Kondrad, and J. Buyer, "Treatment of dairy and swine manure effluents using freshwater algae: fatty acid content and composition of algal biomass at different manure loading rates," *Journal of Applied Phycology*, vol. 20, pp. 1079–1085, 2008.

[71] S. Mehta and J. Gaur, "Use of algae for removing heavy metal ions from wastewater," *Critical Reviews in Biotechnology*, vol. 25, pp. 113–152, 2005.

[72] B. Volesky, "Detoxification of metal-bearing effluents: biosorption for the next century," *Hydrometallurgy*, vol. 59, pp. 203–216, 2001.

[73] F. A. Al-Rub, M. El-Naas, and I. Ashour, "Biosorption of nickel on blank alginate beads, free and immobilized algal cells," *Process Biochemistry*, vol. 39, pp. 1767–1773, 2004.

[74] S. Liehr, H. Chen, and S. Lin, "Metals removal by algal biofilms," *Water Science and Technology*, vol. 30, pp. 59–68, 1994.

[75] Y. Li, Y. Gao, X. Li, J. Yang, and G. Que, "Influence of surface free energy on the adhesion of marine benthic diatom *Nitzschia closterium* MMDL533," *Colloids and Surfaces B: Biointerfaces*, vol. 75, pp. 550–556, 2010.

[76] M. Callow and R. Fletcher, "The influence of low surface energy materials on bioadhesion a review," *International Biodeterioration and Biodegradation*, vol. 34, pp. 333–348, 1994.

[77] M. Callow, *Biofilms: Recent advances in their study and control*. Amsterdam, Neitherlands: Harwood Academic Publishers, 2005.

[78] J. Finlay, M. Callow, L. Ista, G. Lopez, and J. Callow, "Influence of surface wettability on the adhesion strength of settled spores of the green

alga *Enteromorpha* and the diatom *Amphora*," *Integrative and Comparative Biology*, vol. 42, pp. 1116–1122, 2002.

[79] K. Becker, "Exopolysaccharide production and attachment strength of bacteria and diatoms on substrates with different surface tensions," *Microbial Ecology*, vol. 32, pp. 23–33, 1996.

[80] R. Holland, T. Dugdale, R. Wetherbee, A. Brennan, J. Finlay, J. Callow, and M. Callow, "Adhesion and motility of fouling diatoms on silicone elastomer," *Biofouling*, vol. 20, pp. 323–329, 2004.

[81] S. Schilp, A. Kueller, A. Rosenhahn, M. Grunze, M. Pettitt, M. Callow, and J. Callow, "Settlement and adhesion of algal cells to hexa(ethylene glycol)-containing self-assembled monolayers with systematically changed wetting properties," *Biointerphases*, vol. 2, pp. 143–150, 2007.

[82] M. Stanley and J. Callow, "Whole cell adhesion strength of morphotypes and isolates of *Phaeodactylum tricornutum (Bacillariophyceae).*," *European Journal of Phycology*, vol. 42, pp. 191–197, 2007.

[83] R. Sekar, V. Venugopalan, K. Satpathy, K. Nair, and V. Rao, "Laboratory studies on adhesion of microalgae to hard surfaces," *Hydrobiologia*, vol. 512, pp. 109–116, 2004.

[84] C. Van Oss, *The properties of water and their role in colloidal and biological systems*. Buffalo, N.Y.: Academic Press, 2008.

[85] P. Hiemenz, *Principles of colloid and surface chemistry*, vol. 14. New York, NY: CRC, 1997.

[86] J. Azeredo, J. Visser, and R. Oliveira, "Exopolymers in bacterial adhesion: interpretation in terms of DLVO and XDLVO theories," *Colloids and Surfaces B: Biointerfaces*, vol. 14, pp. 141–148, 1999.

[87] P. Facchini, A. Neumann, and F. DiCosmo, "Thermodynamic aspects of plant cell adhesion to polymer surfaces," *Applied Microbiology and Biotechnology*, vol. 29, pp. 346–355, 1988.

[88] A. Vilinska and K. Rao, "Surface thermodynamics and extended DLVO theory of *Acidithiobacillus ferrooxidans* cell adhesion on pyrite and chalcopyrite," *The Open Colloid Science Journal*, vol. 2, pp. 1–14, 2009.

[89] P. Sharma and K. H. Rao, "Adhesion of *Paenibacillus polymyxa* on chalcopyrite and pyrite:surface thermodynamics and extended DLVO theory," *Colloids and Surfaces B: Biointerfaces*, vol. 29, pp. 21–38, 2003.

[90] H. Erbil, *Surface Chemistry of Solid and Liquid Interfaces*. Malden, MA: Blackwell Publishing, 2006.

[91] M. Hermansson, "The DLVO theory in microbial adhesion," *Colloids and Surfaces B: Biointerfaces*, vol. 14, pp. 105–119, 1999.

[92] C. van Oss, "Long-range and short-range mechanisms of hydrophobic attraction and hydrophilic repulsion in specific and aspecific interactions," *Journal of Molecular Recognition*, vol. 16, pp. 177–190, 2003.

[93] C. Van Oss, *Interfacial forces in aqueous media*. New York, N.Y.: Marcel Dekker, 1994.

[94] C. Chrysikopoulos and V. Syngouna, "Attachment of bacteriophages MS2 and ϕX174 onto kaolinite and montmorillonite: Extended-DLVO interactions," *Colloids and Surfaces B: Biointerfaces*, 2011.

[95] M. Staal, R. Thar, M. Kuhl, M. Van Loosdrecht, G. Wolf, J. De Brouwer, and J. Rijstenbil, "Different carbon isotope fractionation patterns during the development of phototrophic freshwater and marine biofilms," *Biogeosciences*, vol. 4, no. 4, pp. 613–626, 2007.

[96] F. Incropera, D. Dewitt, T. Bergman, and A. Lavine, *Fundamentals of Heat and Mass Transfer*. Hoboken, NJ: John Wiley & Sons, 2007.

[97] P. Stewart, "Diffusion in biofilms," *Journal of Bacteriology*, vol. 185, no. 5, pp. 1485–1491, 2003.

[98] H. Riber and R. Wetzel, "Boundary-layer and internal diffusion effects on phosphorus fluxes in lake periphyton," *Limnology and Oceanography*, vol. 32, no. 6, pp. 1181–1194, 1987.

[99] Z. Lewandowski and H. Beyenal, *Fundamentals of Biofilm Research*. Boca Raton, FL: CRC Press, 2005.

[100] J. Sperling and R. Grunewald, "Batch culturing of thermophilic benthic algae and phosphorus uptake in a laboratory stream model," *Limnology and Oceanography*, pp. 944–949, 1969.

[101] L. Whitford and G. Schumacher, "Effect of a current on respiration and mineral uptake in *Spirogyra* and *Oedogonium*," *Ecology*, vol. 45, no. 1, pp. 168–170, 1964.

[102] M. Lock and P. John, "The effect of flow patterns on uptake of phosphorus by river periphyton," *Limnology and Oceanography*, vol. 24, no. 2, pp. 376–383, 1979.

[103] L. Whitford and G. Schumacher, "Effect of current on mineral uptake and respiration by a fresh-water alga," *Limnology and Oceanography*, vol. 6, no. 4, pp. 423–425, 1961.

[104] C. McIntire, "Some effects of current velocity on periphyton communities in laboratory streams," *Hydrobiologia*, vol. 27, no. 3, pp. 559–570, 1966.

[105] B. Biggs, D. Goring, and V. Nikora, "Subsidy and stress responses of stream periphyton to gradients in water velocity as a function of community growth form," *Journal of Phycology*, vol. 34, no. 4, pp. 598–607, 1998.

[106] N. Poff, N. Voelz, J. Ward, and R. Lee, "Algal colonization under four experimentally-controlled current regimes in high mountain stream," *Journal of the North American Benthological Society*, vol. 9, no. 4, pp. 303–318, 1990.

[107] M. Ghosh and J. Gaur, "Current velocity and the establishment of stream algal periphyton communities," *Aquatic Botany*, vol. 60, no. 1,

pp. 1–10, 1998.

[108] M. Oemke and T. Burton, "Diatom colonization dynamics in a lotic system," *Hydrobiologia*, vol. 139, no. 2, pp. 153–166, 1986.

[109] M. Lamb and L. R.L., "Effects of current velocity on the physical structuring of diatom (Bacillariophyceae) communities," *OHIO Journal of Science*, vol. 87, no. 3, pp. 72–78, 1987.

[110] J. Marks and L. Lowe, "The independent and itneractive effects of snail grazing and nutrient enrichment on structuring periphyton communities," *Hydrobiologia*, vol. 185, pp. 9–17, 1987.

[111] B. Peterson, L. Deegan, J. Helfrich, J. Hobbie, M. Hullar, B. Moller, T. Ford, A. Hershey, A. Hiltner, G. Kipphut, M. A. Lock, D. Fiebig, V. McKinley, M. Miller, J. Vestal, and G. R. Ventullo, "Responses of a tundra river to fertilization," *Ecology*, vol. 74, pp. 653–672, 1993.

[112] K. Lohman, J. Jones, and C. Baysinger-Daniel, "Experimental evidence for nitrogen limitation in a northern Ozark stream," *Journal of the North American Benthological Society*, vol. 10, pp. 14–23, 1991.

[113] H. Hillebrand, M. Kahlert, A. Haglund, U. Berninger, S. Nagel, and S. Wickham, "Control of microbenthic communities by grazing and nutrient supply," *Ecology*, vol. 83, pp. 2205–2219, 2002.

[114] S. Long, S. Humphries, and P. Falkowski, "Photoinhibition of photosynthesis in nature," *Annual review of plant biology*, vol. 45, no. 1, pp. 633–662, 1994.

[115] C. Brindley, F. Acien, and J. Fernandez-Sevilla, "The oxygen evolution methodology affects photosynthetic rate measurements of microalgae in well-defined light regimes," *Biotechnology and Bioengineering*, vol. 106, no. 2, pp. 228–237, 2010.

[116] M. Kuhl, C. Lassen, and N. Revsbech, "A simple light meter for measurements of PAR (400 to 700 nm) with fiber-optic microprobes: application for P vs. Eo measurements in a microbial mat," *Aquatic Microbial Ecology*, vol. 13, pp. 197–207, 1997.

[117] A. Miron, A. Gomez, F. Camacho, E. Grima, and Y. Chisti, "Comparative evaluation of compact photobioreactors for large-scale monoculture of microalgae," *Progress in Industrial Microbiology*, vol. 35, pp. 249–270, 1999.

[118] M. Kuhl, R. Glud, H. Ploug, and N. Ramsing, "Microenvironmental control of photosynthesis and photosynthesis coupled respiration in an epilithic cyanobacterial biofilm," *Journal of Phycology*, vol. 32, no. 5, pp. 799–812, 1996.

[119] R. Stevenson, M. Bothwell, and R. Lowe, *Algal ecology: freshwater benthic ecosystems*. California, USA: Academic Press, 1996.

[120] N. Revsbech, B. Jorgensen, T. Blackburn, and Y. Cohen, "Microelectrode studies of the photosynthesis and O_2, H_2S, and pH profiles of a microbial mat," *Limnology and Oceanography*, vol. 28, no. 6, pp. 1062–1074, 1983.

[121] I. Gomez, F. Lopez-Figueroa, N. Ulloa, V. Morales, C. Lovengreen, P. Huovinen, and S. Hess, "Patterns of photosynthesis in 18 species of intertidal macroalgae from southern Chile," *Marine Ecology Progress Series*, vol. 270, pp. 103–116, 2004.

[122] J. Wootton and M. Power, "Productivity, consumers, and the structure of a river food chain," *Proceedings of the National Academy of Sciences of the United States of America*, vol. 90, no. 4, p. 1384, 1993.

[123] H. Boston and W. Hill, "Photosynthesis-light relations of stream periphyton communities," *Limnology and oceanography*, vol. 36, no. 4, pp. 644–656, 1991.

[124] J. Graham, C. Lembi, H. Adrian, and D. Spencer, "Physiological responses to temperature and irradiance in *Spirogyra* (ZYGNEMATALES, CHAROPHYCEAE)," *Journal of Phycology*, vol. 31, no. 4, pp. 531–540, 1995.

[125] W. Hill, M. Ryon, and E. Schilling, "Light limitation in a stream ecosystem: responses by primary producers and consumers," *Ecology*, vol. 76, no. 4, pp. 1297–1309, 1995.

[126] A. Banerjee, R. Sharma, Y. Chisti, and U. Banerjee, "*Botryococcus braunii*: a renewable source of hydrocarbons and other chemicals.," *Critical Reviews in Biotechnology*, vol. 22, pp. 245–279, 2002.

[127] E. Molina Grima, F. Acin Fernndez, F. Garca Camacho, and Y. Chisti, "Photobioreactors: light regime, mass transfer, and scaleup," *Journal of Biotechnology*, vol. 70, pp. 231–247, 1999.

[128] C. Dayananda, R. Sarada, M. Rani, T. Shamala, and G. Ravishankar, "Autotrophic cultivation of *Botryococcus braunii* for the production of hydrocarbons and expolysaccharides in various media," *Biomass Bioenergy*, vol. 31, pp. 87–93, 2007.

[129] A. R. Rao, C. Dayananda, R. Sarada, T. R. Shamala, and G. A. Ravishankar, "Effect of salinity on growth of green alga *Botryococcus braunii* and its constituents," *Bioresource Technology*, vol. 98, no. 3, pp. 560–564, 2007.

[130] J. Folch, M. Lees, and G. Sloane-Stanley, "A simple method for the isolation and purification of total lipides from animal tissues," *Journal of Biological Chemistry*, vol. 226, pp. 497–509, 1957.

[131] USDOE, "Microalgae culture collection 1984-1985." U.S. Department of Energy Technical Report, DE-AC02-83CH10093, 1984.

[132] J. Sa, A. Pe, M. Fuentes, G. Acie, and J. Guerrero, "Biomass nutrient profiles of the microalga *Porphyridium cruentum*," *Food Chemistry*,

vol. 70, pp. 345–353, 2000.

[133] T. M. Mata, A. A. Martins, and N. S. Caetano, "Microalgae for biodiesel production and other applications: A review," *Renewable and Sustainable Energy Reviews*, vol. 14, pp. 217–232, 2010.

[134] M. Griffiths and S. Harrison, "Lipid productivity as a key characteristic for choosing algal species for biodiesel production," *Journal of Applied Phycology*, vol. 21, no. 5, pp. 493–507, 2009.

[135] P. Vasudevan and M. Briggs, "Biodiesel production current state of the art and challenges," *Journal of Industrial Microbiology and Biotechnology*, vol. 35, pp. 421–430, 2008.

[136] J. Flora, M. Suidan, P. Biswas, and G. Sayles, "Modeling algal biofilms: Role of carbon, light, cell surface charge, and ionic species," *Water Environment Research*, vol. 67, no. 1, pp. 87–94, 1995.

[137] A. Richmond, "Open systems for the mass production of photoautotrophic microalgae outdoors: physiological principles," *Journal of Applied Phycology*, vol. 4, no. 3, pp. 281–286, 1992.

[138] L. Rodolfi, G. Chini Zittelli, N. Bassi, G. Padovani, N. Biondi, G. Bonini, and M. Tredici, "Microalgae for oil: strain selection, induction of lipid synthesis and outdoor mass cultivation in a low-cost photobioreactor," *Biotechnology and Bioengineering*, vol. 102, no. 1, pp. 100–112, 2009.

[139] W. Dodds, B. Biggs, and R. Lowe, "Photosynthesis-irradiance patterns in benthic microalgae variations as a function of assemblage thickness and community structure," *Journal of Phycology*, vol. 35, no. 1, pp. 42–53, 1999.

[140] T. Murphy and H. Berberoğlu, "Temperature fluctuation and evaporative loss rate in an algae biofilm photobioreactor," *Journal of Solar Energy Engineering*, vol. 134, p. 011002, 2012.

[141] V. Gupta, W. Johnson, P. Shafieian, H. Ryu, A. Alum, M. Abbaszadegan, S. Hubbs, and T. Rauch-Williams, "Riverbank filtration: comparison of pilot scale transport with theory," *Environmental Science and Technology*, vol. 43, no. 3, pp. 669–676, 2009.

[142] M. Madigan and J. Martinko, *Brock biology of microorganisms*. Upper Saddle River, NJ: Pearson Prentice Hall, 2006.

[143] D. Woods and R. Fletcher, "Studies on the strength of adhesion of some common marine fouling diatoms," *Biofouling*, vol. 3, pp. 287–303, 1991.

[144] W. Mulbry and A. Wilkie, "Growth of benthic freshwater algae on dairy manures," *Journal of Applied Phycology*, vol. 13, pp. 301–306, 2001.

[145] C. Pizarro, E. Kebede-Westhead, and W. Mulbry, "Nitrogen and phosphorus removal rates using small algal tufts grown with dairy manure," *Journal of Applied Phycology*, vol. 14, pp. 469–473, 2002.

[146] G. Schumacher and I. Sekoulov, "Improving the effluent of small wastewater treatment plants by bacteria reduction and nutrient removal with an algal biofilm," *Water Science and Technology*, vol. 48, pp. 373–380, 2003.

[147] A. Ozkan, K. Kinney, L. Katz, and H. Berberoglu, "Reduction of water and energy requirement of algae cultivation using an algae biofilm photobioreactor," *Bioresource Technology*, vol. 114, pp. 542–548, 2012.

[148] R. Andersen, *Algal culturing techniques*. Burlington, MA: Academic Press, 2005.

[149] H. Busscher, A. Weerkamp, H. van der Mei, A. van Pelt, H. de Jong, and J. Arends, "Measurement of the surface free energy of bacterial cell surfaces and its relevance for adhesion," *Applied and Environmental Microbiology*, vol. 48, pp. 980–983, 1984.

[150] W. Rasband, "ImageJ." U.S. National Institute of Health, Bethesda, Maryland, USA, http://rsb.info.nih.gov/ij/, 1997-2011.

[151] D. Shaw, *Introduction to Colloid and Surface Chemistry*. London, United Kingdom: Butterworth, 1980.

[152] T. Luxbacher, "Electrokinetic characterization of flat sheet membranes by streaming current measurement," *Desalination*, vol. 199, no. 1-3, pp. 376–377, 2006.

[153] F. Fairbrother and H. Mastin, "Studies in electroendosmosis," *Journal of the Chemical Society*, vol. 125, pp. 2319–2330, 1924.

[154] B. Kirby and E. Hasselbrink Jr., "Zeta potential of microfluidic substrates: 1. Theory, experimental techniques, and effects on separations," *Electrophoresis*, vol. 25, no. 2, pp. 187–202, 2004.

[155] H. Busscher and H. van der Mei, "Microbial adhesion in flow displacement systems," *Clinical Microbiology Reviews*, vol. 19, pp. 127–141, 2006.

[156] S. Bayoudh, A. Othmane, F. Bettaieb, A. Bakhrouf, H. Ouada, and L. Ponsonnet, "Quantification of the adhesion free energy between bacteria and hydrophobic and hydrophilic substrata," *Materials Science and Engineering: C*, vol. 26, no. 2-3, pp. 300–305, 2006.

[157] Q. Chen, C. Boothroyd, G. Tan, N. Sutanto, A. Soutar, and X. Zeng, "Silica coating of nanoparticles by the sonogel process," *Langmuir*, vol. 24, no. 3, pp. 650–653, 2008.

[158] L. Evans and K. Hoagland, eds., *Algal Biofouling*. Amsterdam, The Netherlands: Elsevier, 1986.

[159] R. Henderson, S. Parsons, and B. Jefferson, "Successful removal of algae through the control of zeta potential," *Separation Science and Technology*, vol. 43, no. 7, pp. 1653–1666, 2008.

[160] K. Strevett and G. Chen, "Microbial surface thermodynamics and applications," *Research in Microbiology*, vol. 154, no. 5, pp. 329–335, 2003.

[161] R. Hecky, K. Mopper, P. Kilham, and E. Degens, "The amino acid and sugar composition of diatom cell-walls," *Marine Biology*, vol. 19, no. 4, pp. 323–331, 1973.

[162] A. Latala, M. Nedzi, and P. Stepnowski, "Toxicity of imidazolium and pyridinium based ionic liquids towards algae. *Chlorella vulgaris*, *Oocystis submarina* (green algae) and *Cyclotella meneghiniana*, *Skeletonema marinoi* (diatoms)," *Green Chemistry*, vol. 11, no. 4, pp. 580–588, 2009.

[163] E. Keijbets, J. Chen, E. Dickinson, and J. Vieira, "Surface energy investigation of chocolate adhesion to solid mould materials," *Journal of Food Engineering*, vol. 92, no. 2, pp. 217–225, 2009.

[164] L. Boulangé-Petermann, A. Doren, B. Baroux, and M. Bellon-Fontaine, "Zeta potential measurements on passive metals," *Journal of colloid and interface science*, vol. 171, no. 1, pp. 179–186, 1995.

[165] P. Benes and M. Paulenova, "Surface charge and adsorption properties of polyethylene in aqueous solutions of inorganic electrolytes. i. streaming potential measurement," *Colloid and Material Science*, vol. 251, pp. 766–771, 1973.

[166] R. Shimizu and N. Demarquette, "Evaluation of surface energy of solid polymers using different models," *Journal of Applied Polymer Science*,

vol. 76, no. 12, pp. 1831–1845, 2000.

[167] M. Van Loosdrecht, J. Lyklema, W. Norde, G. Schraa, and A. Zehnder, "The role of bacterial cell wall hydrophobicity in adhesion.," *Applied and Environmental Microbiology*, vol. 53, no. 8, pp. 1893–1897, 1987.

[168] M. Van Loosdrecht, J. Lyklema, W. Norde, G. Schraa, and A. Zehnder, "Electrophoretic mobility and hydrophobicity as a measured to predict the initial steps of bacterial adhesion.," *Applied and Environmental Microbiology*, vol. 53, no. 8, pp. 1898–1901, 1987.

[169] R. Henderson, S. Parsons, and B. Jefferson, "The impact of algal properties and pre-oxidation on solid–liquid separation of algae," *Water Research*, vol. 42, no. 8, pp. 1827–1845, 2008.

[170] B. Zippel and T. Neu, "Growth and structure of phototrophic biofilms under controlled light conditions," *Water Science and Technology*, pp. 203–209, 2005.

[171] B. Wigglesworth-Cooksey, H. van der Mei, H. Busscher, and K. Cooksey, "The influence of surface chemistry on the control of cellular behavior: studies with a marine diatom and a wettability gradient," *Colloids and Surfaces B: Biointerfaces*, vol. 15, no. 1, pp. 71–80, 1999.

[172] A. Franchi and C. OMelia, "Effects of natural organic matter and solution chemistry on the deposition and reentrainment of colloids in porous

media," *Environmental Science and Technology*, vol. 37, no. 6, pp. 1122–1129, 2003.

[173] J. Park, R. Craggs, and A. Shilton, "Recycling algae to improve species control and harvest efficiency from a high rate algal pond," *Water Research*, 2011.

[174] G. Bitton, K. Marshall, *et al.*, *Adsorption of microorganisms to surfaces.* New York, USA: John Wiley and Sons, Inc., 1980.

[175] W. Strumm and J. Morgan, *Aquatic chemistry: chemical equilibria and rates in natural waters.* New York, USA: Wiley Interscience, 1996.

[176] H. Butt and M. Kappl, *Surface and interfacial forces.* Wiley-VCH Verlag GmbH & Co. KGaA.

[177] F. Zhang, L. Cheng, X. Xu, L. Zhang, and H. Chen, "Screening of biocompatible organic solvents for enhancement of lipid milking from *Nannochloropsis* sp.," *Process Biochemistry*, 2011.

[178] H. Dalton and R. Brand-Hardy, "Nitrogen: the essential public enemy," *Journal of Applied Ecology*, vol. 40, no. 5, pp. 771–781, 2003.

[179] D. Cordell, J. Drangert, and S. White, "The story of phosphorus: Global food security and food for thought," *Global Environmental Change*, vol. 19, no. 2, pp. 292–305, 2009.

[180] Y. Jo, J. Oh, and J. Yoo, "Environmental characterization of periphyton community," *Journal of Ocean University of China (English Edition)*, vol. 5, no. 4, pp. 305–310, 2006.

[181] P. Metzger and C. Largeau, "*Botryococcus braunii*: a rich source for hydrocarbons and related ether lipids," *Applied Microbiology and Biotechnology*, vol. 66, pp. 486–496, 2005.

[182] C. van Oss, M. Chaudhury, and R. Good, "Interfacial Lifshitz-van der Waals and polar interactions in macroscopic systems," *Chemical Review*, vol. 88, pp. 927–941, 1988.